The effect of addition of ceria on platinum supported on carbon materials in the hydrogenation of ethylene

By

Audacity Maringa

A dissertation submitted to the Faculty of Science, University of the Witwatersrand, Johannesburg, in fulfillment for the degree of Master of Science.

Supervisors: Professor M.S. Scurrell

Professor N.J. Coville

June, 2011

DECLARATION

I declare that this dissertation, which I submit for the Degree of Master of Science in the University of the Witwatersrand, Johannesburg, is apart from the recognized assistance of my supervisor, Professor M.S Scurrell, my own work. It has not been submitted before for any degree, diploma or examination in any other institution.

_____ On this _____ day of _____ 2010

(Candidate)

_____ On this _____ day of _____ 2010

(Supervisor)

DEDICATION

I dedicate this work to my beloved one, Josphine, my parents, my sisters (Alice, Nyaradzo and Polite) and brother Peter.

ACKNOWLEDGEMENTS

I would like to thank the following people and organizations for their support and assistance towards the success of this project:

- Professor M.S Scurrell, Professor N.J Coville for their outstanding supervision during the course of this study
- Dr Amit Deshmukh for guidance and support during the course of the project
- The CATOMAT group for company and the support that you provided
- The Microscopy and Microanalysis Unit for the microscopy analysis
- The University of the Witwatersrand and National Research Foundation (NRF) PGM Flagship for the financial support.
- Special thanks to my beloved one, Josphine, and my family for their support
- Finally I thank Jehovah for making it possible

PRESENTATIONS AND PUBLICATIONS

Oral presentations

Audacity Maringa, Michael S. Scurrell, Neil J. Coville, *The effect of ceria addition onto platinum supported on carbon materials in the hydrogenation of ethylene*. PGM seminar, University of Western Cape, Cape Town, South Africa, September 2010.

Poster presentations

Audacity Maringa, Michael S. Scurrell, Neil J. Coville, *The effect of ceria addition onto platinum supported on carbon materials*, Cross Faculty Symposium, University of the Witwatersrand, Johannesburg, South Africa, October 2010.

Audacity Maringa, Michael S. Scurrell, Neil J. Coville, *The effect of ceria addition onto platinum supported on carbon materials*. South African Chemical Institute (SACI), University of the Witwatersrand, Johannesburg, South Africa, February 2011.

Attendances

- PGM seminar, University of Western Cape, Cape Town, South Africa, July 2009.
- CATSA conference, Cape Town, South Africa, November 2009
- South African Nanotechnology Initiative (SANI), Nanoscience Young Researcher Symposium (NYRS), University of Johannesburg, Johannesburg, South Africa, May 2010.
- SACI Young Chemists Symposium, North West University, Potchefstroom, South Africa, October 2010

Publications

Audacity Maringa, Michael S. Scurrell, Deshmukh Amit, Neil J. Coville, Hydrogenation of ethylene using Pt-CeO_2/C catalysts. (**To be submitted**)

ABSTRACT

This study reports the synthesis of carbon materials (carbon nanotubes (CNTs), coiled carbon nanofibers (CCNFs) and carbon spheres (CSs)) using the chemical vapour deposition (CVD) method. The as-synthesized carbon materials were functionalized using nitric acid in order to introduce functional groups and improve the hydrophilic behavior of the carbon materials. Both the as-synthesized and functionalized carbon materials were characterized by TEM, TGA, Raman and FTIR spectroscopy. The presence of functional groups was confirmed by alkalimetry titration and IR spectroscopy data. Ceria (synthesized using the sol-gel method), activated carbon (AC) and titania (P25) were other catalysts supports used and their morphologies were determined by TEM.

Platinum was deposited on the various supports to give Pt loadings of 0.5, 1 and 5 % using the polyol method. It was found that small Pt particle sizes were obtained with average particle sizes of 1.8, 2.3, 2.6, 2.9, 2.7 and 1.6 nm for Pt/CCNF, Pt/CNT, Pt/CS, Pt/AC, Pt/CeO_2 and Pt/TiO_2 respectively at 0.5 % Pt loading. Pt was also deposited on the CeO_2/CM supports (5 % and 10 % CeO_2 loadings) to make Pt-CeO_2/CM catalysts. The Pt supported catalysts were characterized by TEM, EDS, XRD, TPR, BET and TGA.

The platinum supported catalysts were tested for the hydrogenation of ethylene. The effect of functionalization of the carbon materials was determined. Pt/functionalized carbon materials had better activity than Pt/as-synthesized carbon materials. On the effects of supports; Pt/TiO_2 showed the best activity compared to Pt/CCNF, Pt/CNT, Pt/CS, Pt/AC, Pt/CeO_2 and this was attributed to the small Pt sizes formed on TiO_2 (Pt mean size was 1.6 nm). An interesting feature in this study was the higher activity of the Pt-CeO_2/CM as compared to Pt/CM. This was due to the effect of ceria in preserving the surface area of Pt by suppressing sintering. The effect of increasing the ratio of hydrogen to ethylene was investigated and the findings indicated that all the ethylene was converted to ethane. This was attributed to the fact that at a high hydrogen concentration, the rate of formation of the carbon deposit is slow and the rate of hydrogenation is high. No carbon deposits are thus expected on the Pt catalyst particles. It was found that an increase in the Pt loading resulted in an increase in the rate of reaction.

TABLE OF CONTENTS

		Page number
Declaration		ii
Dedication		iii
Acknowledgement		iv
Presentations and publications		v
Abstract		vi
Table of content		vii
List of figures		xii
List of tables		xv
List of abbreviation		xvi
CHAPTER ONE		1
INTRODUCTION		1
1.1	Background	1
1.2	Motivation	2
1.3	Objectives of the project	3
1.4	Outline of the dissertation	4
CHAPTER TWO		7
LITERATURE REVIEW		7
2.1	Introduction	7
2.2	Unsupported catalysts	7
2.2.1	Raney nickel	8
2.2.2	Adams' catalyst	9
2.3	Supported catalysts	9
2.3.1	Role of support	9
2.3.2	Desirable characteristic of a support	10

2.3.3	Why supported catalysts?	10
2.4	Carbon supports for hydrogenation reactions	10
2.4.1	Carbon nanotubes	11
2.4.2	Carbon nanofibers	13
2.4.3	Carbon spheres	15
2.4.4	Carbon helices	16
2.4.5	Activated carbon	17
2.5	Metal oxides as support	18
2.5.1	Ceria	18
2.5.2	Titania	20
2.6	Combination of ceria and carbon materials	20
2.7	Preparation methods for supported catalysts	21
2.7.1	Low temperature chemical precipitation	21
2.7.2	Deposition precipitation	21
2.7.3	Colloidal methods	22
2.7.4	Sol-Gel method	22
2.7.5	Impregnation	23
2.7.6	Microemulsions	23
2.7.7	Electrochemical deposition	24
2.7.8	Microwave heating	25
2.8.0	Hydrogenation of ethylene	25
2.8.1	Why hydrogenate ethylene	26
2.8.2	Studies undertaken using ethylene hydrogenation	26
2.9.0	Mechanism of ethylene hydrogenation	27
2.9.1	Horiuti-Polanyi mechanism	27
2.9.2	Twigg mechanism	28
2.9.3	Jenkins-Rideal mechanism	29
2.10	Hydrogen adsorption and surface migration	29
2.11	Summary	31

CHAPTER THREE 37

EXPERIMENTAL METHODS 37

3.1 Introduction 37
3.2 Materials and chemicals 37
3.3 Synthesis of carbon materials 37
3.3.1 Catalyst preparation for CNTs 38
3.3.2 Synthesis of CNTs 38
3.3.3 Catalyst preparation for CCNFs 39
3.3.4 Synthesis of CCNFs 39
3.3.5 Purification of CCNFs 39
3.3.6 Synthesis of carbon spheres 40
3.3.7 Summary of the carbon materials synthesis procedures 40
3.4 Functionalization of carbon materials 40
3.4.1 Oxidation of carbon materials 40
3.5 Synthesis of ceria 41
3.6 Synthesis of the supported platinum catalyst 41
3.6.1 Synthesis of platinum supported on carbon materials 41
3.6.2 Synthesis of platinum supported on oxides 42
3.6.3 Synthesis of Pt-CeO_2/CM 42
3.7 Characterization techniques used in this study 43
3.7.1 Transmission electron microscopy 43
3.7.2 Thermal gravimetric analysis 44
3.7.3 Ultraviolet-Visible spectrophotometry 44
3.7.4 Raman spectroscopy 44
3.7.5 Temperature programmed reduction 45
3.7.6 X-ray diffraction 45
3.7.7 Brunauer-Emmett-Teller N_2 adsorption (Surface area) 46
3.7.8 Fourier transform infrared spectroscopy 46
3.7.9 Inductively coupled plasma atomic spectra emission spectroscopy 46

3.8	Hydrogenation reactions	46
3.8.1	Experimental set up	47
CHAPTER FOUR		50
RESULTS AND DISCUSSION		50
4.1	Introduction	50
4.2.1	TEM analysis of the carbon materials	50
4.2.1.2	Purification of CCNFs	51
4.2.1.3	Analysis of the functionalized carbon materials	52
4.2.1.4	Thermal gravimetric analysis of the carbon materials	56
4.2.1.5	Raman spectra of the carbon materials	58
4.2.1.6	Infrared spectroscopy	60
4.2.1.7	Surface area and pore volume measurements	62
4.2.2	Characterization of ceria by TEM	62
4.2.3	Characterization of activated carbon and titania by TEM	63
4.3	Analysis of the Pt supported catalysts	64
4.3.1	Mechanism of polyol synthesis	64
4.3.2	Formation of Pt: UV-vis spectroscopy	65
4.4	0.5% Pt loaded catalysts.	65
4.4.1	TEM analysis for the 0.5% Pt loaded on to the as-synthesized CMs	66
4.4.2	TEM analysis for the 0.5% Pt loaded catalysts (polyol method)	67
4.4.3	Determination of presence of Pt in the catalyst.	70
4.4.4	Surface area and pore volume measurements of 0.5% Pt catalysts	71
4.5	1% Pt loaded catalysts	71
4.5.1	Microwave versus conventional heating	74
4.6	5% Pt loaded catalysts	74
4.6.1	Effect of loading on the particles size	77
4.6.2	Temperature programmed reduction	77

4.6.3 X-ray diffraction studies on Pt supported catalysts 80
4.6.4 Particle size from XRD 82
4.7 Ceria supported on carbon materials 83
4.7.1 XRD profile of ceria supported on carbon materials 84
4.7.2 Platinum deposited onto CeO_2/CM 85
4.8 Catalytic activity 87
4.8.1 Effect of functionalization 87
4.8.2 Effect of metal loading 90
4.8.3 Effects of increasing the ratio of H_2:C_2H_4 91
4.9 Effect of catalyst supports 91
4.9.1 Effect of adding ceria on the Pt/CM catalyst 93
4.9.2 Effect of temperature 94
4.9.3 Effect of ceria loading 95

CHAPTER FIVE 99

CONCLUSION AND RECOMMENDATIONS 99

5.1 Introduction 99
5.2.1 Carbon materials 99
5.2.2 Ceria 100
5.2.3 Titania and activated carbon 100
5.3 Deposition of platinum 100
5.4 Hydrogenation activities of the Pt supported catalysts 101
5.5 Recommendations for future work 102

LIST OF FIGURES

CHAPTER TWO

Figure 2.1:	The Raney process, in which a nickel/aluminium alloy is prepared by fusion and subsequently the Al is dissolved by NaOH, leaving a Ni sponge.	8
Figure 2.2:	Image of a MWNT showing different graphene sheets rolled together.	12
Figure 2.3:	Schematic representation of different stacking shapes of graphene sheets of CNF. P-CNF: platelet carbon nanofibers	14
Figure 2.4:	Mechanism of CNF synthesis	14
Figure 2.5:	Coiled carbon nanotubes with pentagon-heptagon rings	16
Figure 2.6:	Horiuti-Polanyi mechanism for hydrogenation of ethylene	28
Figure 2.7:	Twigg mechanism of ethylene hydrogenation	29
Figure 2.8:	Possible extremes in hydrogen adsorption	30
Figure 2.9:	Removal of carbonaceous deposit by reaction of spillover hydrogen, leading to restoration of catalytic site	31

CHAPTER THREE

Figure 3.1:	A schematic CVD setup for carbon material synthesis	38
Figure 3.2:	Schematic representation of the hydrogenation reaction set up	47

CHAPTER FOUR

Figure 4.1:	TEM images of the as synthesized (a) CCNFs (b) CSs (c) CNTs	51
Figure 4.2:	TEM images of the HF treated CCNFs (a) uncoiled fibers and (b) coiled fibers	52
Figure 4.3:	Different oxygen-containing surface groups on the carbon materials	53
Figure 4.4:	TEM image of CCNFs functionalized at 100 ^{o}C for 3 h	54

Figure 4.5:	TEM images of (a) CNTs (b) CCNFs (c) CSs functionalized by reflux at 50 ^{o}C for 12 h.	55
Figure 4.6a:	TGA profile of CCNFs before and after purification	57
Figure 4.6b:	TGA profile of the as-synthesized and functionalized CNTs	57
Figure 4.6c:	TGA profile of the as-synthesized and functionalized CSs	58
Figure 4.7:	Comparison of the Raman spectra of functionalized and as-synthesized (a) CCNFs, (b) CNTs and (c) CSs.	59
Figure 4.8:	IR spectra of (A) CCNFs , (B) CNTs and (C) CSs with (a) as-synthesized (b) functionalized samples are shown in all the three figures	61
Figure 4.9:	TEM image of ceria	63
Figure 4.10:	TEM images of (a) AC and (b) titania	63
Figure 4.11:	Schematic representation of the mechanism behind the polyol synthesis method	64
Figure 4.12:	UV-Vis spectra of Pt	65
Figure 4.13:	Pt loaded to the as-synthesized (a) CCNFs, (b) CNTs and (c) CSs	67
Figure 4.14:	Filtrates obtained from (a) Pt/CCNF, (b) Pt/CNT and Pt/CS	67
Figure 4.15:	TEM images and size distributions of 0.5% Pt supported on (a) and (b) CCNF; (c) and (d) CCNF; (e) and (f) CNT; (g) and (h) CS; (i) and (j) AC; (k) and (l) CeO_2; (m) and (n) TiO_2.	69
Figure 4.16:	EDS spectra of Pt/CCNF	70
Figure 4.17:	TEM images and size distributions of 1% Pt supported on (a) and (b) CCNF prepared by conventional heating and the rest were prepared by microwave heating; (c) and (d) CCNF; (e) and (f) CNT; (g) and (h) CS; (i) and (j) AC; (k) and (l) CeO_2; (m) and (n) TiO_2	73
Figure 4.18:	TEM images and size distributions of 5% Pt supported on (a) and (b) CCNFs prepared by conventional heating and the rest were prepared by microwave heating; (c) and (d) CCNFs; (e) and (f) CNTs; (g) and (h) CSs; (i) and (j) AC; (k) and (l) CeO_2; (m) and (n) TiO_2.	77
Figure 4.19:	TPR profile of (a) Pt/CS, (b) Pt/CCNF and (c) Pt/CNT	78
Figure 4.20:	TEM image of Pt/CCNF (a) before and (b) after TPR analysis	79

Figure 4.21:	H_2-TPR profile of Pt/CeO_2 and CeO_2	79
Figure 4.22:	XRD patterns of (a) CCNF and Pt/CCNF, (b) CS and Pt/CS and (c) CNT and Pt/CNT	80
Figure 4.23:	XRD patterns of (a) AC and Pt/AC, (b) CeO_2 and Pt/CeO_2 and (c) TiO_2 and Pt/TiO_2	81
Figure 4.24:	TEM images of (a) CeO_2/CCNF, (b) CeO_2/CS and (c) CeO_2/CNT	83
Figure 4.25:	TGA profile of 5% and 10% loading of ceria on CCNF.	84
Figure 4.26:	XRD patterns of (a) CeO_2/CCNF, (b) CeO_2, (c) CeO_2/CNT and (d) CeO_2/CS	85
Figure 4.27:	TEM images of (a) Pt-CeO_2/CCNF (b) Pt-CeO_2/CNT and (c) Pt-CeO_2/CS	86
Figure 4.28:	EDS spectra of Pt-CeO_2/CCNF	86
Figure 4.29:	Ethylene conversion over Pt supported on (a) as-synthesized CCNFs and (b) functionalized CCNFs at 30 ^oC	88
Figure 4.30a:	TEM images of the Pt/as-synthesized CCNFs (a) before and (b) after hydrogenation of ethylene	88
Figure 4.30b:	TEM images of (a) before and (b) after hydrogenation of ethylene using Pt/functionalized CCNF	89
Figure 4.31:	Effect of Pt loading on the conversion of ethylene, (a) 0.5%, (b) 1%, (c) 5%	90
Figure 4.32:	Effects of the supports on the conversion of ethylene.	92
Figure 4.33:	Effect of adding ceria to the Pt/CM catalyst.	93
Figure 4.34:	Cartoon showing a possible mechanism for suppression of Pt sintering.	94
Figure 4.35:	TEM image of Pt-CeO_2/CCNF	94
Figure 4.36:	Effect of temperature on ethylene conversion over 0.5% Pt/CCNF.	95
Figure 4.37:	TEM image of (a) before and (b) after hydrogenation of ethylene	95
Figure 4.38:	Effect of ceria loading.	96
Figure 4.39:	TEM image of 1% Pt-10% CeO_2/CCNF	96

LIST OF TABLES

Page number

CHAPTER THREE

Table 3.1: Summary of the carbon materials synthesis conditions 40

CHAPTER FOUR

Table 4.1a: Yield of CMs remaining after reflux for 3 h at 100 ^{o}C 53

Table 4.1b: Yield of CMs remaining after reflux for 12 h at 50 ^{o}C 53

Table 4.2: Estimates of the acid groups on the carbon materials (50 ^{o}C/12 h) 56

Table 4.3: Raman data for as-synthesized and acid-treated CCNF and CNTs 60

Table 4.4: Surface area and pore volume of the catalyst supports 62

Table 4.5: Summary table of the mean particle size of catalyst with different Pt loading. 70

Table 4.6: Pt loading in the catalysts obtained from ICP AES analysis 71

Table 4.7: Comparison of the results obtained using different heating method 74

Table 4.8: Summary table of the mean particle size of catalyst with different Pt loading. 82

Table 4.9: Ceria loading obtained using TGA 84

Table 4.10: Pt loading in the catalysts 87

Table 4.11: Conversion rates of the 1% Pt supported for the as-synthesized and functionalized CNTs and CSs in 300 mins 89

Table 4.12: Conversion of ethylene using different loadings of Pt on CNTs and CSs 91

Table 4.13: Effect of increasing flow rate of H_2:C_2H_4. ($H_2/C_2H_4 = 5$) 91

LIST OF ABBREVIATIONS

AC:	Activated carbon
a.u:	Arbitrary unit
BET:	Brunauer-Emmett-Teller
ca:	approximately
CCNF(s):	Coiled carbon nanofiber(s)
CNT(s):	Carbon nanotube(s)
CM(s):	Carbon material(s)
CS(s):	Carbon sphere(s)
CVD:	Chemical vapor deposition
DNA:	Deoxyribonucleic acid
DWNT(s):	Double walled nanotube(s)
EAS:	Electrochemical active surface
EDS:	Energy dispersion spectroscopy
EG:	Ethylene glycol
f-CNFs:	fishbone carbon nanofibers
FID:	Flame ionization detector
FTIR:	Fourier-transform infrared spectroscopy
g:	Grams
GC:	Gas chromatography
h:	Hour
ICP-AES:	Inductively coupled plasma atomic spectra emission spectroscopy
I_D/I_G:	Ratio of the intensity of D- and G-band
IUPAC:	International Union of Pure and Applied Chemistry
mEq:	milliequivalent
mins:	minutes
mL:	milliliter
mol:	Mole
MWNT(s):	Multi walled nanotube(s)
nm:	Nanometers

p-CNFs:	platelet carbon nanofibers
r-CNFs:	ribbonlike carbon nanofibers
SWNT(s):	Single walled nanotube(s)
TCD:	Thermal conductivity detector
TEM:	Transmission electron microscope
TGA:	Thermal gravimetric analysis
THF:	Tetrahydrofuran
TPR:	Temperature programmed reduction
TWC:	Three way catalyst
UV-vis:	Ultra violet-visible spectroscopy
WGS:	Water gas shift
XRD:	X-ray diffraction

CHAPTER ONE

INTRODUCTION

1.1 Background

Hydrogenation is the addition of molecular hydrogen to an unsaturated hydrocarbon. Unsaturated hydrocarbons possess either double bonds or triple bonds as found in alkenes and alkynes respectively. The importance of hydrogenation is seen in the petrochemical industry where compounds in crude oil containing multiple bonds are converted to saturated compounds before use in gasoline.[1] The unsaturated compounds are not wanted because they are unstable and burn in air with a smoky flame.[2] A typical olefin saturation reaction is shown below.

$$C_6H_{12} + H_2 \rightarrow C_6H_{14}$$

Hydrogenation is also essential in the fine chemicals and pharmaceutical industries, for example, in the production of sorbitol from glucose. Sorbitol is a sweetener in "sugar free" food products intended for diabetics and is used as a starting material for vitamin synthesis.[3] In the food industry hydrogenation is used to convert vegetable oils to margarine .[4] A typical example is the conversion of oleic acid to stearic acid,[5] which is shown below.

$$CH_3(CH_2)_7CH{=}CH(CH_2)_7COOH + H_2 \rightarrow CH_3(CH_2)_7CH_2CH_2(CH_2)_7COOH$$

Hydrogenation is a process which can be performed by either heterogeneous or homogeneous catalysts.[6] Heterogeneous catalysis is a two phase reaction in which the catalyst is a solid (either a finely divided metal such as platinum, palladium and nickel or supported metals such as palladium on activated carbon) and the reactants are gaseous or liquid substances (hydrogen gas and an unsaturated hydrocarbon). In homogeneous catalysis, the reaction occurs in one phase. Typically organometallic complexes of ruthenium, rhodium and iridium are used. In this project, hydrogenation using a novel heterogeneous carbon supported catalyst was used.

Heterogeneous catalysts used for hydrogenation reactions are based on transition metals. These are classified as base metals (Ni, Cu and Co) and platinum group metals (Pt, Pd, Rh,

Ru, Ir).[7] The platinum group metals were selected for use over the base metals because they are more active and thus require milder conditions and a smaller amounts of catalyst. The disadvantage of the platinum group metals is that they are more costly. Platinum was selected because of its outstanding ability to catalyze the hydrogenation of alkenes. In contrast with palladium, isomerization and double bond migration almost never occur when platinum is used.[8]

The hydrogenation of ethylene is one of the most common reactions used in organic chemistry. It was first studied by Sabatier and Senderens in an effort to understand this simple alkene hydrogenation reaction.[9] The hydrogenation of ethylene was used to understand the mechanism of the reaction with the assumption that the data would apply to more complicated alkenes. For example, the principle involved in this reaction was used to understand the catalytic hydrogenation of unsaturated vegetable oils used in the production of margarine.[10] In this project the hydrogenation of ethylene was used as a test reaction to study the effect of different catalyst supports on catalytic performance.

1.2 Motivation

Platinum is one of the most expensive platinum group metals. The role of platinum is attributed to its excellent chemical and physical properties. For instance, its resistance to oxidation and its ability to withstand high temperatures in the catalytic converters used in cars make Pt very useful.[11] In 2006 the platinum demand by application was 50.4% for use as an autocatalyst in vehicles.[12] It is very important to use such a precious metal very effectively and efficiently. Use of unsupported platinum in catalysis is very wasteful as only the outer layer will be involved in the reaction and the bulk will not used. Supported platinum will also reduce sintering and poisoning of the catalyst. The platinum nanoparticles can be dispersed evenly on a support thus increasing the surface area which in turn will increase the rate of the reaction. Carbon materials (CMs) come in many morphologies ranging from fullerenes to graphenes. In this project the CMs used include carbon nanofibers (CNFs), carbon nanospheres (CNSs) and carbon nanotubes (CNTs). CMs have been selected as the support because of their unique chemical and physical properties. The properties include their inertness and their ability to resist acidic or alkaline conditions. The catalysts used in the study will be as denoted as Pt/CM.

Some examples of the use of Pt or Pd supported on CM have been described in the literature. Pt/CNF has been reported to have a better activity when compared to platinum on activated

carbon (Pt/AC) and platinum on alumina (Pt/Al_2O_3) for the hydrogenation of toluene.[13] High activity and selectivity were obtained using a 2% Pt/CNT catalyst in the selective hydrogenation of citral.[14] Functionalized carbon microsphere supported palladium has been shown to be effective in the hydrogenation of ethylene.[15]

Despite the good activity of the Pt/CM catalysts, the reports have suggested that sintering is a major problem leading to catalyst deactivation. It has been suggested that the addition of ceria to a Pt catalyst could reduce sintering.[16] Ceria has been reported to be useful in the catalytic converters of vehicles where it stabilizes the precious metals (and alumina) against sintering and particle growth.[17] Pt/ceria has been found effective in the selective hydrogenation of α,β unsaturated aldehydes.[18] Combining the beneficial aspects of CMs and ceria could yield a good catalyst for hydrogenation reactions. These catalysts are denoted as Pt-CeO_2/CM. A Pt-CeO_2/C catalyst has been studied in the citral hydrogenation reaction.[19] The results indicate that the presence of ceria was beneficial. The beneficial effect is brought about by interaction between ceria and Pt, forming a Pt-O-Ce bond which acted as an anchor to suppress sintering.[16] In this work, further investigations of the beneficial effects of ceria in the hydrogenation of ethylene were studied. To fulfil this goal, ceria was added to the different Pt/CM catalysts.

1.3 Objective of the project

The main aim of this project is to study the effect of the addition of ceria to the Pt/CM catalytic system for the hydrogenation of ethylene. The objectives of this study include:

1. To synthesize carbon materials (CNT, CNS, CNF) using the chemical vapour deposition (CVD) method.
2. To synthesize and characterize platinum supported on the carbon materials.
3. To synthesize Pt on CeO_2/CM, Pt on ceria, Pt on activated carbon and Pt on titania to provide comparative data.
4. To study the hydrogenation of ethylene by varying the active catalysts.

This study will then provide results that will allow for the evaluation of the Pt/CM catalysts as potential olefin hydrogenation catalysts.

1.4 Outline of the dissertation

The outline of the dissertation is given below:

Chapter 1 (*Introduction*) – This Chapter gives an insight, motivation and objectives of the study.

Chapter 2 (*Literature review*) - A review of the literature pertaining to carbon materials, ceria, titania and activated carbon as catalyst support in the hydrogenation reactions is given. A brief discussion of the metals involved in hydrogenation reactions is also included.

Chapter 3 (*Experimental*) - The experimental procedures and all analytical techniques that were used in this study are presented and described in this chapter.

Chapter 4 (*Results and discussions*) - The results obtained in this study, together with their discussion and interpretation are presented in this Chapter.

Chapter 5 (*Conclusions*) – Conclusions are drawn from the results obtained in this project.

References

1. http://science.jrank.org/pages/3465/Hydrogenation-Hydrogenation-in-industry.html (accessed 15 November 2010)
2. http://www.faqs.org/faqs/autos/gasoline-faq/part1/ (accessed 15 November 2010)
3. K. van Gorpa, E. Boermana, C.V. Cavenaghib, P.H. Berbena, Catal. Today 52 (1999) 349-361
4. http://www.isco.com/WebProductFiles/Applications/105/Application_Notes/Catalytic_Hydrogenation.pdf (accessed 15 November 2010)
5. http://www.elmhurst.edu/~chm/vchembook/558hydrogenation.html (accessed 15 November 2010)
6. Morrison, Boyd, Organic Chemistry, Prentice-Hall International, (1992) 324-325
7. H. F. Rase, Handbook of Commercial catalysts, CRS press, USA (2000) 108-109
8. G.Ertl, H. Knozinger, J. Weitkamp, Handbook of heterogeneous catalysis, Wiley, Germany, volume 5 (1997) 2192-2193
9. J. Horiuti and K. Miyahara, Hydrogenation of Ethylene on Metallic Catalysts, NSRDS-NBS, (1968) 13-14
10. http://www.tutorvista.com/chemistry/hydrogenation-of-ethene (accessed 15 November 2010)
11. http://www.chemistryexplained.com/elements/L-P/Platinum.html (accessed 15 November 2010)
12. http://www.unctad.org/infocomm/anglais/platinum/uses.htm (accessed 15 November 2010)
13. M. Zhou, G. Lin, H. Zhang, Chin. J. Catal. 28 (2007) 210-211
14. E. Asedegbega-Nieto, A. Guerrero-Ruiz, I. Rodriguez-Ramos, Carbon 44 (2006) 804-805
15. K. C. Mondal, L. M. Cele, M. J. Witcomb, N. J. Coville, Catal. Commun. 9 (2008) 494–498
16. H. Shinjoh, M. Hatanaka, Y. Nagai, T. Tanabe, N. Takahashi, T. Yoshida, Y. Miyake, Top Catal. 52 (2009) 1967–1971
17. A.F. Diwell, R.R. Rajaram, H.A. Shaw, T.J. Truex, Studies in Surface Science and Catalysis, 71 (1991) 139-152
18. J. Silvestre-Albero, F. Rodriguez-Reinoso, A. Sepulveda-Escribano, J. Catal. 210 (2002) 127-128

19. J. C. Serrano-Ruiz, A. Sepulveda-Escribano, F. Rodriguez-Reinoso, D. Duprez, J. Mol. Catal. A: Chem. 268 (2007) 227-234

CHAPTER TWO

LITERATURE REVIEW

2.1 Introduction

This chapter focuses on the literature associated with solid catalyst involved in hydrogenation reactions. Solid catalysts can be classified as either unsupported catalysts or impregnated (or supported) catalysts. The different supports used for hydrogenation activities will be discussed. The chapter will conclude with literature associated with the hydrogenation of ethylene.

Heterogeneous catalysts used for hydrogenation reactions are mostly based on transition metals. These are classified as base metals (Ni, Cu and Co) and platinum group metals (Pt, Pd, Rh, Ru, Ir).[1] The platinum group metals are more active as compared to the base metals and require milder conditions and smaller amounts of catalyst as compared to the base metals. The disadvantage of the platinum group metals is that they are more costly and for that reason they are usually supported to reduce the amount of precious metal used. Platinum metal was selected in this dissertation study because of its outstanding ability to catalyze the hydrogenation of alkenes. In contrast with palladium, isomerization and double bond migration in olefins almost never occurs when platinum is used.[2]

Homogeneous catalysts used for hydrogenation reactions are mainly based on the organic complexes of ruthenium, rhodium and iridium. Their mechanism of reaction involves forming active complexes with the reactants that are unstable. The unstable complexes will breakdown to form the product and reform the catalyst. The major drawback of homogeneous catalysts is that they are difficult to separate from the products (and reactants). For this reason heterogeneous catalysts are preferred because of the ease to separate them from the product.

2.2 Unsupported catalysts

Unsupported catalysts are typically made by precipitation, hydrothermal synthesis and fusion. They can be (mixed) metals or oxides and, as their name suggests, the entire catalyst is made of active materials. Raney nickel and Adams' catalyst fall into this category and both are active in the hydrogenation of hydrocarbons.

2.2.1 Raney nickel

Raney nickel was discovered by an American engineer Murray Raney in 1925.[3] He discovered that metal alloy leaching gave a superior hydrogenation catalyst when compared to unleached metal. He made a 50:50 Ni/Al alloy by fusion and then leached out Al with aqueous NaOH. The resulting Ni sponge is the Raney nickel. The synthetic process is shown in Figure 2.1. The advantage of the catalyst is that it is ready for use, requiring no reduction or other activation and has a high surface area. The disadvantage of the catalyst is that high temperature is required for fusion, it is pyrophoric (will ignite instantaneously in air) and therefore it has to be stored under water. It is also a health hazard since acute exposure to Raney Ni may causes irritation of the respiratory tract, nasal cavities and it also causes pulmonary fibrosis if inhaled.[4] Apart from safety concerns, a Raney Ni catalyst can have a slower of rate of reaction and requires high temperatures when compared to the platinum group metal catalysts.[5]

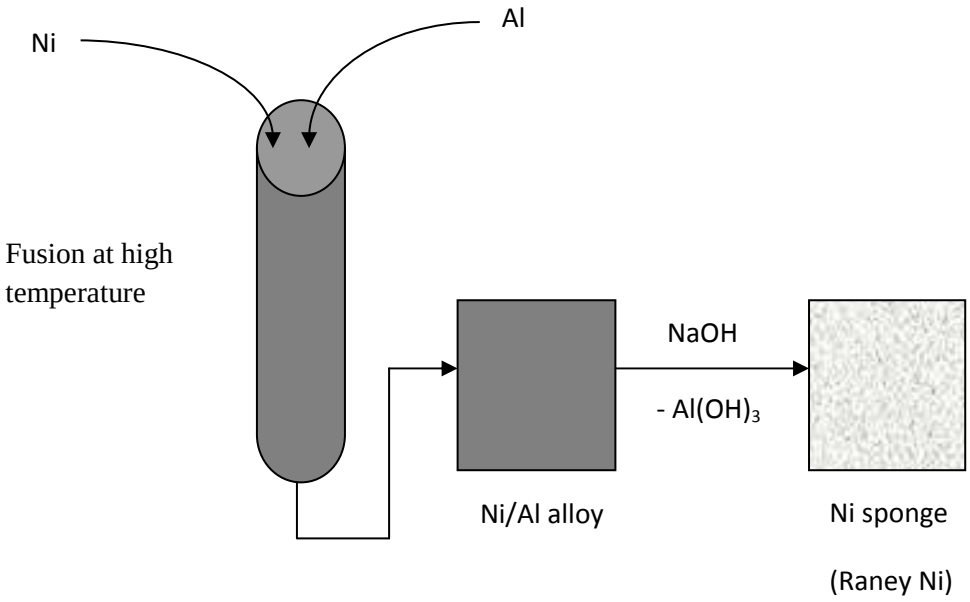

Figure 2.1 The Raney process, in which a nickel/aluminium alloy is prepared by fusion and subsequently the Al is dissolved by NaOH, leaving a Ni sponge.[6]

An example of a reaction catalyzed by Raney Ni is the conversion of benzene to cyclohexane. The reaction is a liquid phase reaction which occurs at a temperature between 200 - 225 ^{o}C and pressure of 50 bar. Li and Xu.[7] have shown that silica-supported Ni–P amorphous catalysts had a higher activity than the Raney Ni catalyst. Liu et al, [8] also cited the lower efficiency and environmental pollution caused by Raney Ni and proposed the use of Ni/CNF (CNF=carbon nanofiber) as an alternative catalyst. A Ni/CNF catalyst presents high activity

in the liquid phase benzene hydrogenation to cyclohexane, and gives 99.5% yield of cyclohexane. In other words a supported catalyst would be preferred to an unsupported catalyst.

2.2.2 Adams' catalyst

Adam's catalyst is made of platinum oxide (PtO_2). Adams' catalyst was discovered by Voorhees and Adams.[9] It was prepared by fusion of chloroplatinic acid (H_2PtCl_6) or ammonium chloroplatinate [$(NH_4)_2PtCl_6$] and sodium nitrate. In the process platinum nitrate is heated to remove nitrogen oxides leaving behind platinum oxide. The equations for the synthesis of PtO_2 are shown below.

$$H_2PtCl_6\ (aq) + 6\ NaNO_3\ (aq) \rightarrow Pt(NO_3)_4\ (s) + 6\ NaCl\ (aq) + 2\ HNO_3\ (aq)$$

$$Pt(NO_3)_4\ (s) \rightarrow PtO_2\ (s) + 4\ NO_2\ (g) + O_2\ (g)$$

An advantage of using the Adams' catalyst is that it is easy to prepare. Brown et al,[10] investigated the hydrogenation of cyclohexene using PtO_2, unsupported Pt and supported Pt. They discovered that the platinum catalyst produced by borohydride reaction caused the absorption of hydrogen to proceed at nearly twice the rate observed with the commercial Adams' catalyst. The supported platinum showed the best activity, an activity 3-4 times that of an unsupported catalyst.

2.3 Supported catalysts

Supported catalysts are commonly used in the case of precious metals or unstable compounds. Here, the active metal precursor is deposited on a porous support. The support can be an oxide (e.g. silica, titania, alumina, ceria and magnesia), or a carbon (activated carbon, carbon nanotubes, carbon spheres and carbon nanofibers). A supported catalyst facilitates the flow of gases through the reactants and diffusion of reactants through the pores to the active phase to enhance the selectivity, retarding the sintering of the active phase and increasing the poison resistance of the metal.[11]

2.3.1 Role of support

The basic role of the support is to maintain the catalytically active phase in a highly dispersed state, stabilization of the active component and enlargement of the specific surface area.[12]

The role of the support is not limited to being a carrier, and it can also contribute to the catalytic activity and can react to some extent with other catalyst ingredients during the manufacturing process. The support can also play a crucial role in terms of providing either acidity or basicity to the reaction.

2.3.2 Desirable characteristic of a support

1. The support material should be inert towards the chemical reaction. The advantage is that it will not interfere with the reaction, but it can affect the shape selectivity due to the pore arrangement. Thus, the effect of addition of a promoter may be studied without interference from the support.
2. Adequate structural properties to allow the transport of gases through the support structure.
3. High surface area and a well-developed porosity are very important for achieving a high dispersion of the active phase in the catalyst.[13]
4. Stability of the support at high temperature.

2.3.3 Why supported catalysts?

- Costs. The active components for a catalytic reaction are often expensive metals (e.g. Pt, Ru, Rh and Re) and through dispersion the cost of catalyst can be minimized.
- Activity. A supported catalyst has a comparable activity to that of unsupported catalyst, which leads to fast reaction rates, short reaction times and maximum throughput, elimination of side products and lowering of purification costs.
- Selectivity. Supported catalysts have a high selectivity towards the desired product. This means they facilitate generation of a maximum yield of a desired product.
- Regenerability helps to keep process costs low.

2.4 Carbon supports for hydrogenation reactions

Carbon materials have been used for a long time in heterogeneous catalysis, because they can act as direct catalysts or more importantly they can satisfy most of the desirable properties required for a catalyst support.[11] Carbon materials are good as catalyst supports owing to their specific properties: they are stable in both acid and basic media, and the carbon can be burnt off, allowing an economic and ecological recovery of the precious catalytic metal.[14]

The interaction of the active phase with the support (carbon) can be modified by pretreatment of the support. However carbon materials cannot be used in reactions that are carried out under the following conditions: hydrogenation at temperatures higher than 427 ^{o}C (methane will be formed) or oxidation above 227 ^{o}C (carbon dioxide will be given off).[13]

The carbon materials can exhibit a range of different pore sizes (micro, meso, and macro) and pore distributions. According to IUPAC, micropores are smaller than 2 nm, mesopores are in the range between 2 and 50 nm, and macropores are larger than 50 nm. The different pores have different effects on catalytic reactions.[13] Micropores show strong adsorption for small molecules. The mesopores allows access of reactants to the active phase of a catalyst. The macropores are useful for the transport of molecules between the liquid phase and the mesopores. Several studies have reported that for liquid-phase hydrogenation reaction, the use of CNT and CNF supports possessing large mesoporosity provides better catalytic activities than an activated carbon, for which mass-transfer limitations are in operation.[13] Mesoporous carbon spheres has been reported to exhibit a high specific activity compared to the monodisperse carbon spheres.[15]

2.4.1 Carbon nanotubes

The discovery of fullerene in 1985 by the Smalley research group at Rice University stimulated the research into other forms of carbon.[16] In 1991 a Japanese scientist Ijima studied the carbons formed by an arc discharge process under a TEM. His findings of carbon nanotubes led to an explosion of other studies in the area.[17] Carbon nanotubes (CNTs) can be thought of as narrow strips of graphene rolled up into seamless tubes.[18] CNTs are allotropes of carbon with a cylindrical nanostructure.

CNTs are classified as single walled nanotubes (SWNTs), double walled nanotubes (DWNTs) and multi walled nanotubes (MWNTs) depending on the number of rolled up graphene layers that they possess. A typical MWNT is shown in Figure 2.2.[19]

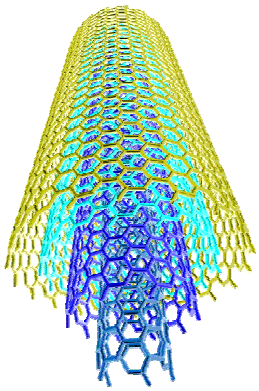

Figure 2.2. Image of a MWNT showing different graphene sheets rolled together.[19]

There are various methods used to synthesize CNTs. The major methods used are arc discharge, laser ablation and chemical vapour deposition (CVD) methods. Arc discharge is the simplest method used to produce CNTs. It involves breaking down the reactant containing carbon by an electric current between two graphite electrodes. A disadvantage is that it is difficult to separate the CNTs from the soot and the residual catalytic metals present in the crude product.[20] Laser ablation involves the laser vaporization of graphite rods e.g. with a 50:50 catalyst mixture of cobalt and nickel at 1200 °C in flowing argon. Its drawbacks include difficulties in purifying and scaling up the CNT production.[20] Chemical vapour deposition (CVD) of hydrocarbons over a metal catalyst is a classical method that has been used for many decades to produce various carbon materials such as carbon fibers and filaments. Large amounts of CNTs can be formed by catalytic CVD of, for example, acetylene over nickel, cobalt and iron catalysts supported on silica, alumina, calcium carbonate and titania. The method is considered to be a low cost, large scale procedure for the synthesis of high quality CNTs using gaseous or liquid hydrocarbons as carbon source. The mechanism of synthesis involves decomposition of the carbon source, followed by dissolution of the carbon phase into metal catalytic nanoparticles and redeposition of carbon on the catalytic surface.[21]

CNTs have been used to support metals in hydrogenation reaction. A 1 % (w/w) platinum catalyst deposited on CNTs was found to be active for the hydrogenation of nitrobenzene.[22] A yield of 90 % aniline was obtained. Pt, Rh and Pt-Rh particles supported by CNTs were effective catalysts for the hydrogenation of benzene at room temperature.[23] Pd/CNT catalysts were found to be active for a cyclooctene hydrogenation reaction.[13] Pan and Wai[24] have reported the hydrogenation of benzene and its derivative at room temperature using a

Rh/CNT catalyst. CNTs supported on palladium catalysts have been reported for the selective hydrogenation of cinnamaldehyde at atmospheric pressure. Ge et al[25] have reported that the Pd/CNT catalyst has a good conversion of 92 % for cinnamaldehyde and 90.8 % selectivity of cinnamaldehyde to hydrocinnamaldehyde. Ju et al[26] have found that depositing a NiP amorphous alloy on CNTs can improve catalytic activity, which is attributed to the dispersion produced by the support, an electron donating effect and the hydrogen storage ability of CNTs. Pt/CNT showed a higher activity in comparison to Pt/AC in the hydrogenation of trans-stilbene.[27] The advantage of Pt/CNT was in avoiding the effect of the diffusion of the reactant and product molecules in the micropores. Yan et al[28] have reported a high catalytic performance of a Pt-Sn-B/CNT catalyst in the liquid phase hydrogenation of chloronitrobenzene. The conversion of chloronitrobenzene could reach 99.9 % and the dechlorination of chloroaniline was less than 1.9 %.

2.4.2 Carbon nanofibers

The history of graphitic carbon nanofibers (CNFs) goes back more than a century. The first patent describing the production of carbon filaments was published in 1889.[29] The fibers were often formed by metal-based catalysts used for the conversion of carbon-containing gases, such as in Fischer-Tropsch syntheses or steam reforming reactions. Their occurrence was considered a nuisance. In the 1980s researchers realised the potentials of the CNFs[30] as unique materials suitable for various applications.

There are three main types of CNFs,[31] which differ in the alignment of the graphene layers: In ribbonlike CNFs (r-CNFs) the graphene layers are parallel to the growth axis. Platelet CNFs (p-CNFs) display graphene layers perpendicular to the growth axis, while herringbone or fishbone CNFs (f-CNFs) have layers stacked obliquely with respect to the growth axis. The schematic diagram for the three types of CNF are shown in Figure 2.3.[32] In general CNFs have a larger diameter than those presented by CNTs.[13]

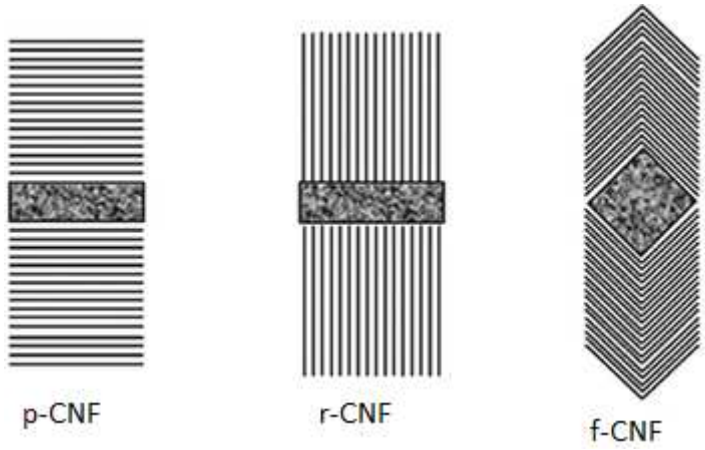

Figure 2.3. Schematic representation of different stacking shapes of graphene sheets of CNF. P-CNF: platelet carbon nanofibers; r-CNF: ribbon-like carbon nanofibers; f-CNF: fishbone carbon nanofibers[32]

The methods of synthesizing the CNFs are similar to those used in CNT synthesis, which include arc discharge, laser ablation and chemical vapour decomposition (CVD). Owing to the low cost and ease of large scale production of CNFs, the CVD method is preferred over other methods. The mechanism of CNF synthesis is shown in Figure 2.4.

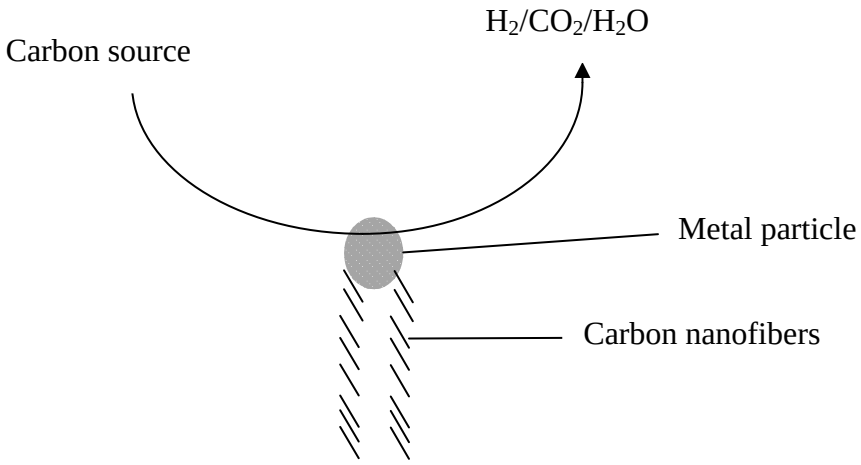

Figure 2.4. Mechanism of CNF synthesis. The first step is the decomposition of carbon-containing gases on the metal surface, followed by carbon atoms dissolving in and diffusing through the bulk of the metal. Lastly the precipitation of carbon in the form of a CNF occurs

CNFs have been used as a catalyst support in a number of reactions. Ni and Pd particles supported by CNFs have shown an excellent selective hydrogenation capacity for crotonaldehyde[33]to crotyl alcohol and cinnamaldehyde[34] to cinnamyl alcohol. Rh

nanoparticles on CNFs are highly active in the liquid-phase hydrogenation of cyclohexene.[35] Liang et al[36] have reported that Pd/CNF has a high activity and stability in the hydrogenation of cyclooctene, presumably as a result of a special metal-support interaction and absence of micropores. Liu et al[8] have reported the high activity of Ni/CNF in the liquid phase hydrogenation of benzene to cyclohexane. The high activity was attributed to the effective surface area, the skeletal structure and the metallic and semi-conductive properties of the CNFs. Among the different types of CNFs supporting platinum, p-CNFs were found to be the best support in the hydrogenation of nitroarenes to aromatic amines.[37] The efficiency of the Pt/p-CNF was attributed to the steric and the electronic effects derived from the interaction between Pt nanoparticles and the p-CNF support. Similar results were obtained by Motoyama and co-workers.[38] they showed that p-CNF was more effective as a support in comparison to other types of CNFs. They used ruthenium in their investigation and they concluded that the Ru/p-CNF catalyst was highly active and reusable for arene hydrogenation reactions. Toebes et al[39] studied the effect of the different concentrations of oxygen-containing surface groups on the CNF support for the hydrogenation of cinnamaldehyde. They found that the activity was strongly dependent on the amount of oxygen in/on the CNF support. The as synthesized Ni/CNF catalysts have been reported to show a very good activity and selectivity for the hydrogenation of chloronitrobenzene to the corresponding chloroanilines.[40]

2.4.3 Carbon spheres

The discovery of fullerenes in 1985 stimulated research effort into carbon materials. This included studies on the well known carbon spheres. Carbon spheres (CSs) have always attracted a lot of attention due to their unique properties and applications.[41] Carbon spheres have similar properties to graphite or fullerene, and they have been used to fabricate diamond films, lubricating materials and special rubber additives.[42] Carbon spheres can be used as electrodes, as a support for catalysts, capsules for magnetic nanoparticles, a template for synthesizing other hollow materials and for the delivery of drugs. Carbon spheres can be hollow or solid.

Carbon spheres can be synthesized using various methods which include chemical vapour deposition, arc plasma techniques, catalyzed reduction and hydrothermal synthesis. Chemical vapour deposition can occur in the presence or absence of a catalyst. Carbon spheres have been obtained by pyrolysis of acetylene at temperature between 900 ^{o}C and 1000 ^{o}C.[43] This

method does not require a catalyst hence there is no catalyst removal step required. In the hydrothermal synthesis method the carbon source is heated in an autoclave.[44] Owing to the advantageous properties of carbon spheres as catalyst supports, several studies have been carried out on different catalytic reactions. Co[45] and Pd[46] nanoparticles supported on carbon spheres have shown high activity for the conversion of ethylene to ethane. Ni/CS catalysts were found to be active in the gas phase hydrogenation of nitrobenzene with aniline formed as the sole product.[47]

2.4.4 Carbon helices

Helical carbon materials such as carbon micro-coils or nano-coils have a relatively long history and have received increasing attention in recent years.[48] Great efforts have recently been made to study single carbon nanofibers[49] and nanotubes[50] because of their coiled morphologies and potential applications. Some of the applications for the carbon helices include nano-scale mechanical springs and electrical inductors.[50] Carbon helices are also ideal candidates for electromagnetic wave adsorbent tunable micro-devices, bioactivators, Li battery electrodes and hydrogen containers.[51] Nano-coils are also interesting in that helices abound in nature e.g. DNA, proteins, etc., and a connection can be made at the nano-scale between carbon based inorganic and organic structures.[52] For application of coils it is necessary to have control over the coil morphology and geometry, which to date has not been adequately achieved. It has been proposed that while the curvature in the case of helically coiled single walled nanotubes could possibly be due to the regular insertion of pentagon-heptagon pairs at the junction, it is however unclear whether a similar mechanism could hold for multi-walled nanotubes. Figure 2.5 shows a coiled carbon nanotube with pentagon-heptagon rings.[53]

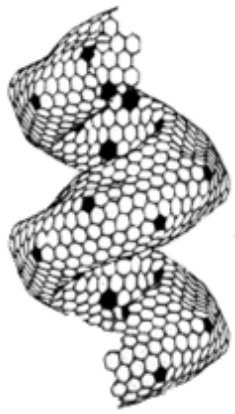

Figure 2.5. Coiled carbon nanotubes with pentagon-heptagon rings.[53]

CVD has been used to synthesize the helical carbon materials. By varying the experimental conditions it was established that it is possible to produce carbon nanostructures with significant structure differences such as straight, curved or helical morphologies. For example, coiled nanocoils with a twisted form can be grown from the Ni/Al_2O_3 catalysed pyrolysis of acetylene.[54]

Not much is known about helical carbon materials as catalyst supports. Li and Zhang[55] have reported the use of helical nano-coiled and micro-coiled carbon fibers as catalyst supports for the electrooxidation of methanol. They concluded that the platinum supported on the helical nano-coiled and micro-coiled carbon fibers exhibited superior electrocatalytic activity and anti-poisoning ability relative to the straight fibers. The use of helical carbon nanofibers as catalyst supports for the hydrogenation reactions is an area of interest as it has not been studied to date.

2.4.5 Activated carbon

Activated carbon (AC) is also known as activated charcoal and it refers to the type of carbon formed from a carbon source which is processed with oxygen in order to increase the number of pores in the product.[56] The highly porous carbon materials with high surface area are used to absorb other substances for example the impurities in sugar[57]. The surface area for an activated carbon is at least 500 m^2g^{-1}.

For the production of activated charcoal, carbon sources (wood, charcoal, peat, lignite, coal and petroleum pitch) are used as the precursors or raw materials. The methodology used for the synthesis of activated charcoal involves either physical reactivation or chemical activation. In the former type, the raw material is activated by using specific gases, whereas in the latter case, the precursor is impregnated with certain chemicals (strong salt, base or acid), which is then carbonized at a lower temperature.[56] One of the limiting factors in chemical activation is the retention of the impregnated substances in the activated carbon product. Chemical activation is preferred over physical activation owing to the lower temperatures and shorter time needed to activate the carbon.

AC has been used as a support for metal catalysts for a very long time. A 2.4 % Pt/AC has been reported to have a toluene conversion of 55 % to give methylcyclohexane.[58] Jiang et al,[59] showed that platinum catalysts supported on activated carbon with high purity, large

surface area, large pore volume and appropriate pore structure exhibited a high activity for the hydrogenation of ortho-nitrochlorobenzene to 2,2′-dichlorohydrazobenzene. Palladium supported catalysts on AC have been used to study the selective hydrogenation of cinnamaldehyde.[60] Cabiac et al[60], reported the presence of hydrocinnamaldehyde and that there was no sign of cinnamyl alcohol formation in the reaction.

2.5 Metal oxides as support

The conventional supports for hydrogenation catalysts include titania, silica, alumina and ceria. These supports have different morphologies and structures. Their influence on the hydrogenation activity varies depending on how they interact with the active phase. Only ceria and titania are discussed below. Ceria will be discussed since its effect on addition to the Pt/C systems is the one that will be examined in this dissertation. Titania was selected in order to compare the carbon supports with a conventional support.

2.5.1 Ceria

Ceria is an oxide of cerium and cerium is the most abundant of the rare earth elements. It is a pale yellow powder with chemical formula CeO_2. CeO_2 is stable at room temperature and atmospheric pressure. It can maintain its structure under intensive reduction at elevated temperatures. Ceria in the fluorite structure exhibits several defects depending on the partial pressure of oxygen. The defect structure is an intrinsic property required for its potential in catalysis, energy conversion etc.[61]

There are various methods used to prepare cerium oxide particles, such as by precipitation, hydrothermal, sol-gel and microemulsion procedures.[62] The sol-gel method has the advantage in that the ceria produced has the following attributes: purity, homogeneity and controlled porosity combined with an ability to form a large surface area at low temperatures.[63]

Monyanon et al[64] prepared ceria using a sol-gel method. Cerium nitrate was used as the source of ceria and urea as a precipitating agent. The mechanism of reaction is as follows: Urea in solution hydrolyses to give hydroxyl ions. Cerium nitrate reacts with hydroxyl ions to give cerium (III) hydroxide. In the presence of atmospheric oxygen, cerium (III) hydroxide is

oxidized to cerium (IV) hydroxide. The cerium (IV) hydroxide is dehydrated to give cerium (IV) oxide (ceria). The chemical equations for ceria formation are shown below:

$CO(NH_2)_2$ (aq) + $3H_2O$ (l)→ CO_2 (g) +$2NH_4^+$ (aq) + $2OH^-$ (aq)

$Ce(NO_3)_3.6H_2O$ (aq) + $3NH_4$+ (aq) + 3OH- → $Ce(OH)_3$ (s) + $3NH_4NO_3$ (aq) + $6H_2O$ (l)

$Ce(OH)_3$ (s) + O_2 (g) + $2H_2O$ (l) → $4Ce(OH)_4$ (s)

$Ce(OH)_4$ -nH_2O (s)→ $CeO_2.xH_2O$ (l) + yH_2O (where x + y = n)

Ceria has unique properties which include high mechanical strength, oxygen ion conductivity and oxygen storage capacity.[65] It is used in fuel cells, optical films, polishing materials, gas sensors, promoting precious metals in the water gas shift (WGS) reaction and it is a crucial component of automotive, three way, emissions-control catalysts.[66] The role of ceria in the three way catalyst (TWCs) of automotives is very attractive and important in utilising efficiently precious metals. Ceria is suggested to: [67]

- Promote the noble metal dispersion
- Increase the thermal stability of the Al_2O_3
- Promote water gas shift and steam reformation reactions
- Favour catalytic activity at the interfacial metal-support sites
- Promote CO removal through oxidation employing lattice oxygen
- Store and release oxygen under lean and rich conditions respectively

Ceria is a good catalyst support. Phenol has been hydrogenated to cyclohexanone at 180 ^oC and under atmospheric pressure on 3 % Pd/CeO_2 and phenol conversion was 80 % (in which about 50 % was cyclohexanone, 35 % cyclohexanol and 15 % cyclohexane).[68] For the conversion of propionitrile to n-proplyamine, a copper-lanthanide oxide catalyst has shown that CeO_2 was more active than the other lanthanide oxides.[69] The selective partial hydrogenation of acetylene to ethylene was reported on Au/CeO_2 in the gas phase at 300 ^oC.[70] The selectivity towards acetylene was 100 %. Ni/CeO_2 catalysts were reported to be effective for the conversion of benzene to cyclohexane at 100 ^oC and the reaction was reported to be stable for at least 20 h.[71] Cerium-based platinum catalysts have been extensively studied for the hydrogenation of crotonaldehyde. On chlorine-free Pt/CeO_2, a crotyl alcohol selectivity has been reported to be 83 % in the hydrogenation of crotonaldehyde.[72]

2.5.2 Titania

Titania is an oxide of titanium. Its chemical formula is TiO_2. It has many crystal forms. These forms include rutile, anatase and brookite.[73] Rutile is the most stable form of titania. Commercial titania (Degussa, P25) typically contains 85 % anatase and 15 % rutile.

Titanium dioxide is a white powder with high opacity, brilliant whiteness, excellent covering power and resistance to colour change. These properties have made it a valuable pigment and opacifier for a broad range of applications in paints, plastic goods, inks and paper.[74] Titania shows photochemical properties, such as high refractive index, excellent transparency in the visible and near infra red region, as well as high performance in the photocatalysis of water splitting and for degradation of organic compounds under UV light irradiation.[75] Also, TiO_2 is a widely used oxide semiconductor material used in dye-sensitized solar cells.

Palladium nanoparticles supported on titania have been used in the hydrogenation of acetylene.[76] These catalysts showed 66.8 % selectivity for ethylene after 10 h. In the hydrogenation of heptyne, Pd/TiO_2 showed a very high selectivity of at least 90 % to heptene.[77]. The hydrogenation of propylene has been studied on Pt/TiO_2, $Pt–Au/TiO_2$ and Pt_2Au_4/TiO_2 catalysts.[78] It is also important to note that TiO_2 has been implicated in strong metal support interactions.[79]

2.6 Combination of ceria and carbon materials

Several studies have been done on the enhancement of the catalytic activities when ceria has been added to metals supported on carbon materials. Most studies have focused on fuel cells. Wang et al[80], reported a comparison between $Pt\text{-}CeO_2$/CNTs and Pt supported on CNT in terms of their electrochemical active surface (EAS) areas, methanol electro-oxidation activity and chronoamperometry. The results indicated that CeO_2 can enhance the catalytic activity of Pt for methanol electro-oxidation with no apparent decrease of EAS. Similar results were also obtained by Xu and Shen[81] for the electrochemical oxidation of ethanol. It was shown that $Pt\text{-}CeO_2/C$ gave a better performance than Pt/C. Compared with Pt/CNT, $Pt–CeO_2$/CNT exhibited higher catalytic activity for methanol electro-oxidation.[82]

In the hydrogenation of citral, $Pt–CeO_2/C$ has been reported to have a good activity.[83] The conversion of citral reached close to 100 %, when the catalyst was reduced at 200 ^oC. The

main products reported were citronellal, unsaturated alcohols (geraniol and nerol) and the saturated alcohol, citronellol. For hydrogenation reactions, not much has been done to examine the effect of adding ceria to a carbon material supported catalyst.

2.7 Preparation methods for supported catalysts

The purpose of this sub-section is to present a general overview of the most common synthetic methods used for fabricating supported catalysts. The methods include low temperature chemical precipitation, deposition precipitation, colloidal, sol-gel, impregnation, microemulsions, electrochemical methods and the microwave heated polyol method. It is important to note that there is no single method which is superior to any other. Methods depend on the end applications of the catalyst and chemicals available.[84]

2.7.1 Low temperature chemical precipitation

Platinum based catalysts can be made by chemical precipitation at low temperature. Supported and unsupported catalyst can be made and the process involves the addition of a reducing agent to a platinum salt solution. Bi-metallic catalysts can be made by co-precipitation of a solution of two metal precursor salts. The precursor salt is reduced to the metallic state and will precipitate out of solution. For supported catalysts, the support is added prior to metal precursor reduction. A typical example is the reduction of hexachloroplatinic acid using sodium borohydride.[85] The advantage of this method is that the preparation occurs under mild conditions i.e. at low temperatures.

2.7.2 Deposition precipitation

Deposition of a precursor of an active component from a solution onto a support can be brought about by chemical reactions. This is done by adding an excess solution of the precursor with respect to the pore volume of the support and using the support in the form of a powder. Deposition precipitation can be realized in a number of ways:

- Increase in solution pH
- Change of valency of the metal ion
- Removal of a stabilizing ligand surrounding the metal ion

A typical example is the synthesis of nickel nanoparticles supported on CNFs. The increase in pH brought about by hydrolysis of urea has led to the deposition of nickel from aqueous solution.

The following reactions are envisaged:

$CO(NH_2)_2$ (aq) + $3H_2O \rightarrow CO_2$ (g) + $2NH_4^+$ (aq) + $2OH^-$ (aq)

Ni^{2+} (aq) + $2OH^-$ (aq) $\rightarrow Ni(OH)_2$ (s)

The nickel hydroxide deposited on the CNF was reduced at elevated temperatures. Ni particles with sizes ranging from 6-8 nm were reported to be obtained by this method.[86] The advantage of the deposition precipitation technique is: its reproducibility, high metal loadings can be achieved, high metal dispersion at high metal loading and a uniform distribution of the active component over the support.

2.7.3 Colloidal methods

The method is similar to the chemical precipitation method. However it involves the addition of a capping agent or protecting agent. A capping agent is a material that prevents agglomeration of the catalyst particles and can be used to control particle size. Common capping agents include ligands, surfactants or polymers. The experimental procedure entails combining the metal source, a reducing agent, support, and a capping agent and mixing the reagents together under appropriate reaction conditions. The colloidal metal particles obtained are stabilized by either steric hindrance or by electrostatic charges. A typical example is the synthesis of Pt/C using the surfactant SB12.[87]

The advantage of using the colloidal method is that a narrow size distribution of metal nanoparticles is obtained. The major drawback is the presence of the protecting agent, which may hinder the catalytic performance of the nanoparticles. The protecting agent can be removed by decomposition at elevated temperatures. Due to a sintering effect the distribution of metal particles are affected by template removal, and can result in lowered catalytic performance.[88]

2.7.4 Sol-Gel method

The sol-gel technique begins with the formation of suspended particles (a sol) that is aged and dried to form a semi-solid suspension of particles in a liquid (a gel), which is finally calcined resulting in formation of a mesoporous solid or powder. There are four distinct steps involved in the sol-gel technique: [89]

1. Formation of the gel
2. Aging to allow fine tuning of the gel

3. Drying to remove the solvent from the gel
4. Calcination to permanently change the physical and chemical properties of the solid

Hu et al[90] reported the synthesis of Pt/Al_2O_3 using the sol-gel technique. The advantage of the sol-gel technique is that it allows the control of size through the aging and calcination steps. This method can be used to produce catalysts with a uniform metal distribution, tuneable particle size, high surface area, and stable dispersion.[90] The major drawback associated with this method is that the catalytic nanoparticles may be buried within the structure rather than within the pores. If the particles are not located near the pores they will not be accessible to reactants and therefore will not generate efficient catalysts.

2.7.5 Impregnation

Impregnation is the most commonly used method to fabricate catalysts. The method involves the impregnation of the support material with the salt solution containing the metal to be deposited. This is followed by a reduction step. The reduction step can either be carried out by liquid phase reduction using borohydride, formic acid and hydrazine as a reducing agent, or gas phase reduction using hydrogen as a reducing agent under elevated temperatures. For example, Zhou et al[91] synthesized Pt nanoparticles supported on XC-72R carbon black using formaldehyde as a reducing agent.

The advantage of the impregnation method is that it is simple and can be used for mass production of supported catalysts. However its drawback is that the metal particles have a large size, a broad size distribution of the catalyst particles and a poor reproducibility.[91]

2.7.6 Microemulsions

Microemulsions are also known as reverse micelles. At high water concentration an emulsion consists of small oil droplets surrounded by a continuous water phase. At a high oil concentration an emulsion consists of small water droplets surrounded by a continuous oil phase. Since most metal precursors are inorganic salts they are soluble in water, hence emulsions made of high oil concentrations are used. Reverse micelles are water-in-oil droplets stabilized by a surfactant. A very commonly used surfactant is sodium bis(2-ethylhexyl)sulfosuccinate (Na(AOT)). The droplets are dispersed randomly in solution and are subject to Brownian motion. They exchange water content and re-form into distinct micelles. The size of the water-in-oil droplets increases with increasing water content. The

droplet size and the resulting particle size can be influenced by the chain length of the stabilizer.

In order to obtain the catalyst nanoparticles, the metal salt is reduced by adding a reducing agent into the microemulsion system. When the nanoparticles are formed, they are deposited onto the support, which is done by adding a solvent such as tetrahydrofuran (THF) in conjunction with the support powder to the microemulsion system. For example, Pt-Ru catalysts can be formed using the microemulsion techniques and have been directly deposited onto carbon black without the need of an emulsion-breaking solvent (such as THF).[92] The advantage of the microemulsion method is the ability to control particle size easily by varying the synthesis conditions. Unfortunately, the catalyst fabrication by microemulsions is costly since expensive surfactants and oils are needed. Furthermore, both surfactants and the oils can have a negative environmental impact.

2.7.7 Electrochemical deposition

Electrochemical deposition occurs at the interface of an electronically conductive substrate and an electrolyte solution containing the salt of the metal to be deposited. There are five stages to the electrochemical deposition of metals:

1. Transport of metal ions in solution to the electrode surface
2. Electron transfer
3. Formation of metal ad-atoms via adsorption
4. Nucleation and growth of metal particles
5. Growth of the three-dimensional bulk metal phase

If growth is stopped at the fourth step it results in the production of nanoparticles and if growth is continued metal films will be produced. Deposition occurs when the substrate has been supplied with sufficient potential to reduce the metal salt to a zero valent state:

$$M^{z+} + ze^{-} \rightarrow M^{0}$$

The electrochemical method has been used to deposit Pt onto carbon substrates at the anode and cathode of fuel cells to improve the Pt utilization and reduce the Pt loading.[93] The advantage of using the electrochemical method is that nanoparticle size can be controlled by controlling the deposition potential and time.

2.7.8 Polyol method

Microwave irradiation through dielectric heating loss is a fast, simple and uniform energy efficient method that has been used to synthesize metal catalysts. The microwave heating process has been used in place of a conventional heating method to produce supported catalysts.[94] For example, in the conventional method, a polyol (most commonly ethylene glycol) solution containing the metal salt is refluxed at 160 ^{o}C for 3 h to decompose the polyol to yield an in situ generated reducing species for the reduction of the metal ions to their elemental state.[88] The fine metal produced can be captured by the support material suspended in the solution. For the microwave method, a polyol solution containing the metal salt is put into a microwave oven and heated.[94] A typical synthesis can be outlined as follows:[94] an aqueous solution of H_2PtCl_6 is mixed with ethylene glycol and the pH of the solution adjusted by the addition of KOH. Then, the purified CNTs are uniformly dispersed in the mixed solution by ultrasound. After a period of microwave heating, the resulting CNTs are filtered and the residue washed with acetone. The residue is then dried at 100 ^{o}C overnight in a vacuum oven.

The pH value of the Pt precursor solution is an important factor for the preparation of Pt/CNT catalysts by the polyol process. Li et al[95] found out that at a lower pH range (pH 3.6-5.8), the Pt nanoparticles are agglomerated and not well dispersed on the CNT surface. On the other hand a more uniform dispersion of Pt nanoparticles were formed in the pH range 7.4-9.2. The proposed mechanism to explain the pH effect during the formation of the Pt nanoparticles in ethylene glycol solution is:

$$CH_2OHCH_2OH\ (l) \rightarrow CH_3CHO\ (l) + H_2O\ (l)$$

$$2CH_3CHO\ (l) + (PtCl_6)^{2-}\ (aq) + 6OH^-\ (aq) \rightarrow 2CH_3COO^-\ (aq) + Pt\ (s) + 6Cl^-\ (aq) + 4H_2O\ (l)$$

The acetate formed can act as a stabilizer by forming a chelate-type complex via the acetyl groups. The polyol method is very attractive as it is a simple and straightforward method to synthesize catalysts.

2.8 Hydrogenation of ethylene

The hydrogenation of ethylene involves the addition of molecular hydrogen to ethylene to yield ethane. The reaction is exothermic such that temperature control is essential.

The equation for the formation of ethane is shown below:

$$C_2H_4\,(g) + H_2\,(g) \rightarrow C_2H_6\,(g)$$

The reaction occurs in the presence of a catalyst. Most of the catalysts used contain transition metals or transition metal oxides. The hydrogenation catalysts frequently used are grouped into two types; base metals (Ni, Cu and Co) and platinum group metals (Pt, Pd, Rh, Ru and Ir). The advantage of the base metals is that they are cheap compared to the platinum group metals. However they require high temperature and pressure in their operation. The platinum group metals on the other hand can be used under milder conditions and small amounts of catalyst are used.

2.8.1 Why hydrogenate ethylene?

Ethylene hydrogenation has been selected to evaluate the catalytic properties of various catalysts because the reaction is structure insensitive[96] and occurs at low temperature, yielding only one product ethane.[97] Structure insensitivity implies that the activity of ethylene hydrogenation is independent of the catalyst particle morphology. In other words the particle size of the catalyst does not affect the activity of the reaction. Somorjai[98] described structure insensitivity as a reaction in which the kinetics (rate, activation energy) are the same for a crystal surface, dispersed particles, films and metal foils. The difference in rate will be associated with different supports. The other advantage of using ethylene is that it has a high reaction rate when forming ethane.

2.8.2 Studies undertaken using ethylene hydrogenation

Hydrogenation of ethylene has been used as a probe reaction in many studies. The hydrogenation of ethylene has received much attention and a full understanding of its chemistry provides information about hydrogenation, exchange, dehydrogenation and isomerization of more complicated alkenes.[99] For example, the principle involved in a hydrogenation reaction has been used to understand the catalytic hydrogenation of unsaturated vegetable oils used in the production of margarine.[100]

Park and co-workers[101] used the hydrogenation of ethylene to investigate the catalytic behaviour induced by supporting nickel on three different types of graphite nanofibers. In the process they managed to evaluate the potential of graphite nanofibers as a support medium and also the impact of the orientation of the graphite platelets on the catalytic activity and selectivity of the metal.

Ethylene hydrogenation has been studied as a probe reaction by Gao et al[102] using MoAl alloy films to allow the straightforward comparison between the chemistry on the alloy, the carbide and oxycarbide phases. They reported that molybdenum oxycarbide materials were inactive for the hydrogenation of ethylene because of site blockage by oxygen on the surface of the catalyst.

Grunes et al, [103] described the hydrogenation of ethylene as structure insensitive and used it to determine in situ the active metal surface area of a platinum nanoparticle array model catalyst. It has been reported that ethylidyne, di-σ bonded ethylene, and π-bonded ethylene were present during the ethylene hydrogenation reaction.[104] Of interest was the fact that ethylene hydrogenation occurs at the same rate regardless of whether ethylidyne is present or absent.

Several other studies have been conducted using the hydrogenation of ethylene which include reports on the activity of oxides (e.g. zinc oxide[105]), determining optimum conditions[106] and the effect of particle size[107] using Ni catalysts, kinetic studies (for example using a Pt (111) surface[108]), and the activity of supported Pt catalysts[109].

2.9 Mechanism of ethylene hydrogenation

There are three main mechanisms that have been used to describe the hydrogenation of ethylene. These include the Horiuti-Polanyi mechanism, the Twigg mechanism and the Jenkins-Rideal mechanism.

2.9.1 Horiuti-Polanyi mechanism

The Horiuti-Polanyi mechanism[110] states that the adsorption of ethylene occurs on the surface of a transition metal (for example Pt) by using one of the carbon-carbon double bonds. This is followed by hydrogenation with atomic hydrogen (formed from the dissociatively adsorbed molecular hydrogen) through an ethyl intermediate to ethane. The ethane is finally desorbed into the gas phase. The illustration of the Horiuti-Polanyi mechanism is shown in Figure 2.6.

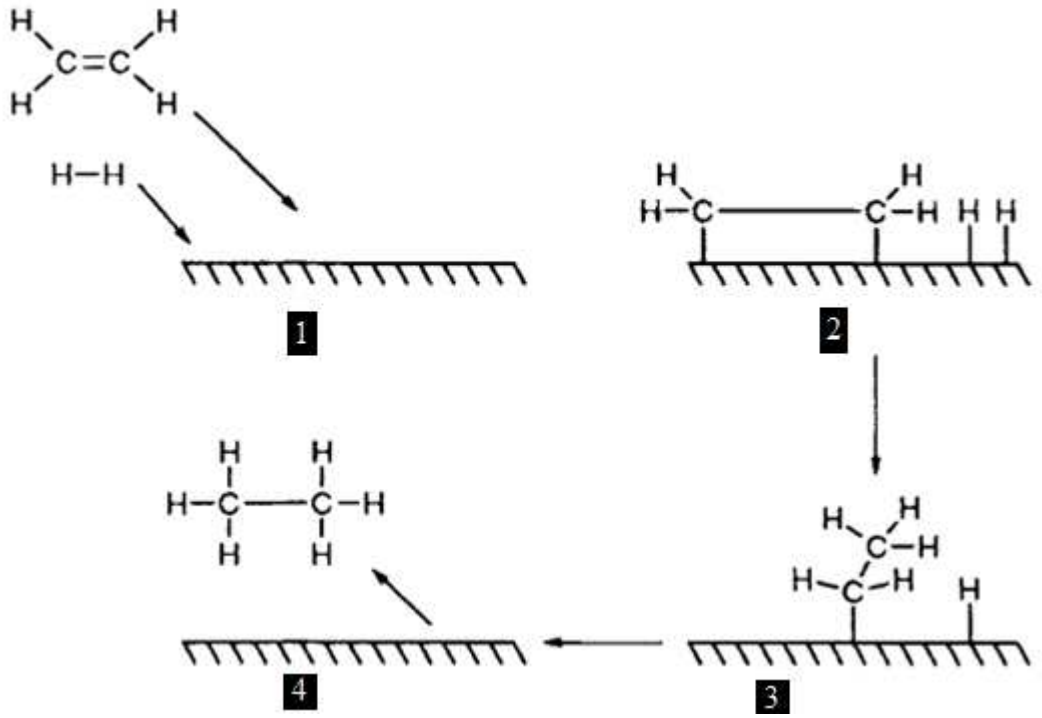

Figure 2.6. Horiuti-Polanyi mechanism for hydrogenation of ethylene. (1) Diffusion of ethylene and hydrogen to the metal surface. (2) Ethylene and hydrogen adsorption on the metal surface. Hydrogen dissociates on the surface to form hydrogen atoms. (3) One of the surface hydrogen atoms reacts with adsorbed ethylene to form surface ethyl. (4) The other hydrogen atom reacts with the ethyl radical bound on the surface to form ethane. Ethane desorbs from the catalyst surface.[99]

2.9.2 Twigg mechanism

The Twigg mechanism[111] suggests that the hydrogen molecules are first dissociated into atoms on the catalytic surface through reaction with ethylene and hydrogenation takes place after the addition of another hydrogen atom. The Twigg mechanism is shown in Figure 2.7.

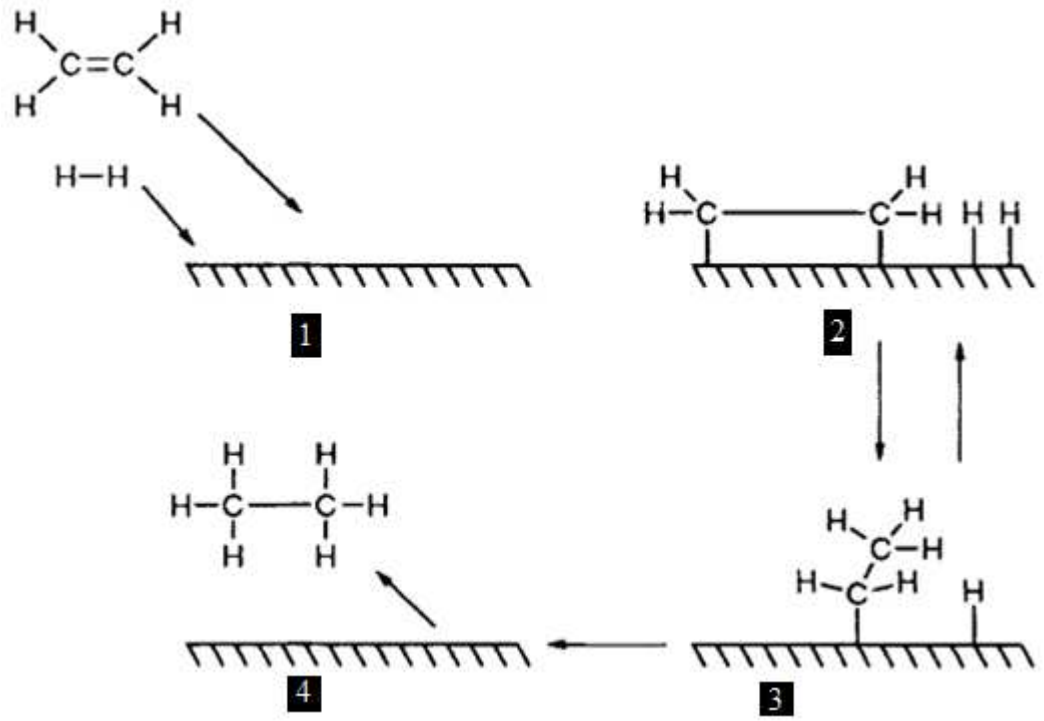

Figure 2.7. Twigg mechanism of ethylene hydrogenation. (1) Diffusion of ethylene to the catalyst surface. (2) Ethylene is adsorbed on the catalyst surface. (3) Adsorbed ethylene reacts with hydrogen to give an ethyl group and adsorbed hydrogen atom. (4) The ethyl radical bound on the catalyst surface react with adsorbed hydrogen atom to form ethane which desorbs from the Ni surface.[111]

2.9.3 Jenkins-Rideal mechanism

The Jenkins-Rideal mechanism[112] proposes that the gas phase ethylene reacts with adsorbed hydrogen to produce ethane. The first step in the mechanism involves hydrogen being chemisorbed on to the surface of the catalyst. The second step is the reaction between bulk ethylene with adsorbed hydrogen to produce ethane. The third step entails the flow of ethane out of the reaction zone.

2.10 Hydrogen adsorption and surface migration

During hydrogenation reactions, molecular hydrogen diffuses to the catalyst surface where it is adsorbed. After adsorption on the metal surface, it dissociates to form hydrogen atoms. The hydrogen atoms can migrate into the metal crystallite and in some cases react with the metal to form metal hydrides. The metal surface in which hydrogen has penetrated may be less reactive, since rearrangement of the surface is required to release the hydrogen atoms. The difficulties that may arise in releasing a hydrogen atom during a reaction are shown in Figure 2.8.

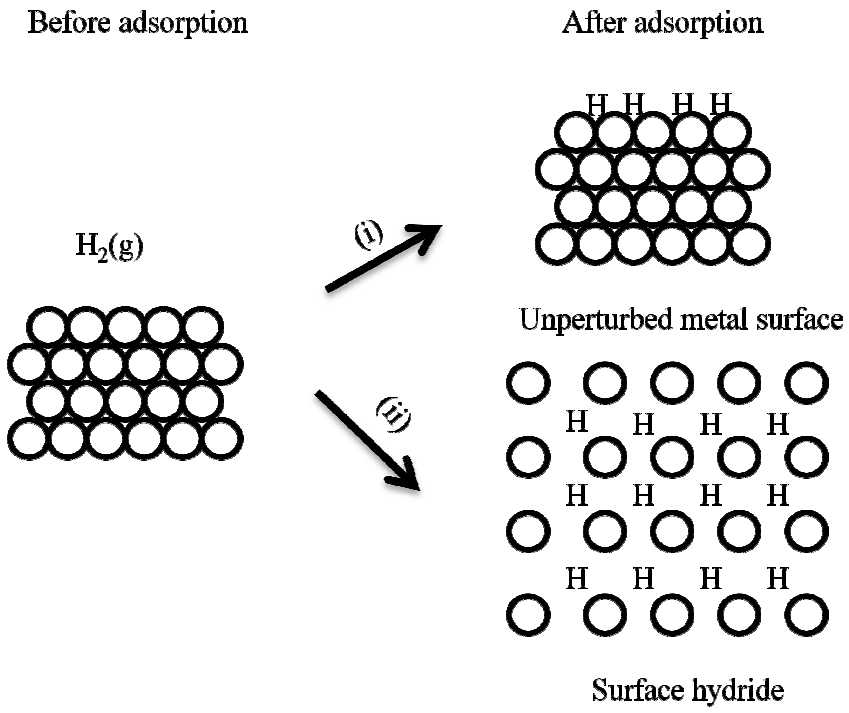

Figure 2.8. Possible extremes in hydrogen adsorption. (i) Hydrogen is adsorbed without a chemical reaction. (ii) Hydrogen reacts with the metal surface to form a hydride.[1]

For the hydrogenation activity, Figure 2.8 (i) is preferred as the atoms of hydrogen would be available for reaction. Surface migration of atomic hydrogen is a phenomenon of great interest, for it appears to have a significant effect on catalysis in some reactions.[113] The process has been called spillover when it involves surface diffusion from the metallic site to the support (C, Al_2O_3, SiO_2). Hydrogen spillover has been observed in Pt/ZrO_2, Pt/SiO_2 and Pt/TiO_2 systems.

In hydrogenation, the supported metal may adsorb and activate hydrogen whilst the support may adsorb the substance to be hydrogenated and the reaction may proceed on the support surface as a result of hydrogen spillover. For example the increase in the rate of ethylene hydrogenation on Pt/SiO_2 catalyst diluted with SiO_2 or Al_2O_3 has been attributed to hydrogen spillover.[113]

It has been shown that the hydrogenation of pent-1-ene to pentane by hydrogen adsorbed on Pt/SiO_2 was very fast at 100 ^oC.[113] It has been suggested that at first the hydrogenation is effected by the hydrogen adsorbed on Pt and later it is effected by the spillover hydrogen adsorbed on SiO_2.

Beside an increase in the rate of activity, hydrogen spillover offers other advantages which include:

- The hydrogen participating in the spillover can also interact with organic deposits and can ensure the removal of coke[114] as shown in Figure 2.9.
- Hydrogen spillover can also promote an increase in the rate of adsorption of hydrogen

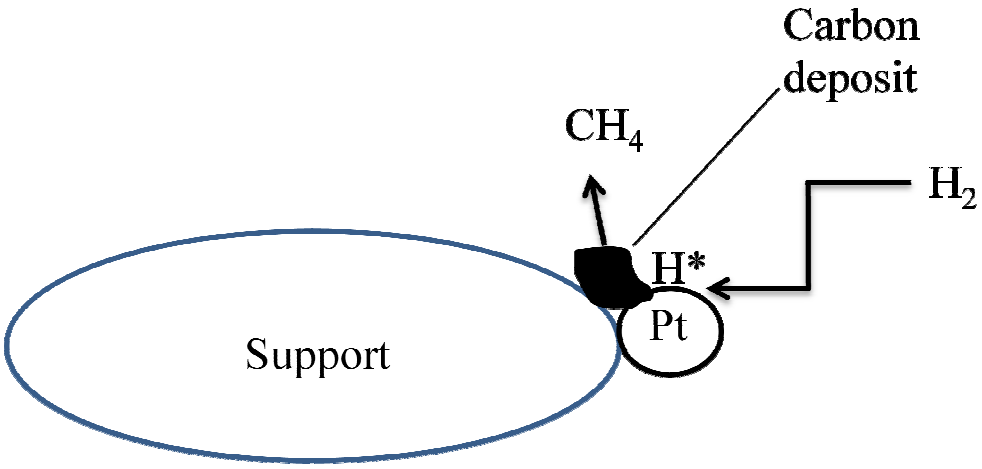

Figure 2.9. Removal of carbonaceous deposit by reaction of spillover hydrogen, leading to restoration of catalytic site.

2.11 Summary

From the literature cited in the preceding sections, it is clear that they are many factors which affect hydrogenation reactions. The different supports possess different morphologies which in turn will result in different catalytic activities. The hydrogenation of ethylene has been used as a probe reaction because of its simplicity and also to determine the possible mechanism of the hydrogenation reaction of more complicated alkenes. It is also important to note that during hydrogenation, hydrogen adsorption and surface migration can also occur and may have a negative effect if the hydrogen reacts with the metal surface.

References

1. H. F. Rase, Handbook of Commercial Catalysts, CRS press, USA (2000) 108-112
2. G.Ertl, H. Knozinger, J. Weitkamp, Handbook of heterogeneous catalysis, Wiley, Germany, 5 (1997) 2192
3. D. S. Tarbell, A. T. Tarbell, J. Chem. Edu. 54 (1977) 26-28
4. http://fscimage.fishersci.com/msds/96307.htm (accessed 11 November 2010)
5. http://www.tititudorancea.com/z/hydrogenation.htm (accessed 11 November 2010)
6. G. Rothenberg, Catalysis: Concept and Green Applications, Wiley. Germany, (2008) 137-138
7. H. Li, Y. Xu, Mater. Lett. 51 (2001) 101–107
8. P. Liu, H. Xie, S. Tan, K. You, N. Wang, H. Luo, React. Kinet. Catal. Lett. 97 (2009) 101–108
9. V. Voorhees, R. Adams, J. Amer. Chem. Soc. 44 (1922) 1397
10. H. C. Brown, C. A. Brown, 22 (1966) 149-164
11. F. Rodríguez-Reinoso, Carbon 36 (1998) 159-175
12. D. J. Suh, T. Park, S. Ihm, Ind. Eng. Chem. Res. 31 (1992) 1849-1856
13. P. Serp, J. Fugueiredo, Carbon Materials for Catalysis, Wiley, USA, (2009) 132-538
14. M. A. Fraga, E. Jordao, M. J. Mendes, M. M. A. Freitas, J. L. Faria, J. L. Figueiredo, J. Catal. 209 (2002) 355–364
15. J. Chen, N. Xia, T. Zhou, S. Tan, F. Jiang, D. Yuan, Int. J. Electrochem. Sci. 4 (2009) 1063 - 1073
16. Kroto, H. W., Heath .J. R., O'Brien S. C., Curl R. F., and R. E., Nature 318 (1985) 162-163.
17. S. Ijima, Nature 354 (1991) 56-58.
18. A. Jorio, G. Dresselhaus, M. S. Dresselhaus, Carbon Nanotubes, Springer, New York (2008) 5-6
19. http://www.reade.com/supersite/610 (accessed 25 November 2010)
20. http://www.azonano.com/details.asp?ArticleID=1561 (accessed 25 November 2010)
21. K. B. Kouravelou, S.V. Sotirchos, Rev. Adv. Mater. Sci. 10 (2005) 243-248
22. C. Li, Z. Yu, K. Yao, S. Ji, J. Liang J. Mol. Catal. A 226 (2005) 101-105
23. B. Yoon, H. Pan, C. M. Wai, J. Phys. Chem. C 113 (2009) 1520–1525
24. H. Pan, C. M. Wai, J. Phys. Chem. C, 113 (2009) 19782–19788
25. C. Ge, Y. Li, J. Zhao, R. Zhou, Indian. J. Chem. 49A (2010) 281-282
26. Y. Ju, F. Li, J. Natur. Gas. Chem. 15 (2006) 313-318

27. T. Onoe, S. Iwamoto, M. Inoue, Catal. Comm. 8 (2007) 701–706
28. X. Yan, J. Sun, Y. Fang, Z. Xu, W. Wang, Front. Chem. China, 1 (2006) 41-44
29. T.V. Hughes and C.R. Chambers, US Patent 405,480 (1889).
30. J.W. Geus and J.W. Linowski, US Patent 4,855,091 (1989).
31. N. M. Rodriguez, A. Chambers, R. T. K. Baker, Langmuir 11 (1995) 3862-3866
32. Y. A. Zhu, Z. J. Sui, T. J. Zhao, Y. Dai, Z. M. Cheng, W. K. Yuan, Carbon 43 (2005) 1694–1699
33. F. Salman, C. Park, R.T.K. Baker, Catal. Today 53 (1999) 385-386.
34. C. Pham-Huu, N. Keller, G. Ehret, L.J. Charbonniere, R. Ziessel and M.J. Ledoux, J. Mol. Catal. A 170 (2001) 155-156.
35. T.G. Ros, D.E. Keller, A.J. van Dillen, J.W. Geus, D.C. Koningsberger, J. Catal. 211 (2002) 85-86
36. C. Liang, W. Xia, M. Berg, Y. Wang, H. Soltani-Ahmadi, O. Schlűter, R. A. Fischer, M. Muhler, Chem. Mater. 21 (2009) 2360-2366
37. M. Takasaki, Y. Motoyama, K. Higashi, S. Yoon, I. Mochida, H. Nagashima, Organic Lett. 10 (2008) 1601-1604
38. M. Takasaki, Y. Motoyama, K. Higashi, S. Yoon, I. Mochida, H. Nagashima, J. Asian. Chem. 2 (2007) 1524-1533
39. M. L. Toebes, T. A. Nijhuis, J. Hájek, J. H. Bitter, A. J. van Dillen, D. Y. Murzin, K. P. de Jong, Chem. Eng. Sci. 60 (2005) 5682 – 5695
40. C. Wang, J. Qiu, C. Liang, L. Xing, X. Yang, Catal. Comm. 9 (2008) 1749–1750
41. F. Wang, L. Pang, Y. Jiang, B. Chen, D. Lin, N. Lun, H. Zhu, R. Liu, X. Meng, Y. Wang, Y. Bai, L. Yin Mater. Lett. 63 (2009) 2564–2566
42. J. Miao, D. Hwang, K. Narasimhulu, P. Lin, Y. Chen, S. Lin, L. Hwang, Carbon 42 (2004) 813–822
43. S.D. Mhlanga, N.J. Coville, S.E. Iyuke, A.S. Afolabi, A.S. Abdulkareem, N. Kunjuzwa, J. Exp. Nanoscience 5 (2010) 40–51
44. M, Li, Q. Wu, M. Wen, J. Shi, Nanoscale Res. Lett. 4 (2009) 1365–1370
45. S.D. Mhlanga, K.C. Mondal, N. Naidoo, N. Kunjuzwa, M.J. Witcomb, N. J. Coville S. Afr. J. Sci. 105 (2009) 304-308
46. K.C. Mondal, L.M. Cele, M.J. Witcomb, N.J. Coville Cat. Comm. 9 (2008) 494–498.
47. A. Márquez, S. Gil, A. Romero, J. Valverde, S. Gómez-Quero, M. A. Keane, Appl. Catal. A 363 (2009) 188-198
48. Q. Liu, Z. Cui, Z. Ma, S. Bian, W. Song, J. Phys. Chem. C 111 (2007) 12420-12424

49. S. Motojima, Y. Itoh, S. Asakura, H. Iwanaga, J. Mater. Sci. 30 (1995) 5049-5055
50. W. Wang, K. Yang, J. Gaillard, P. R. Bandaru, A. M. Rao, Adv. Mater. 20 (2008) 179–182
51. J. Liu, X. Zhang, Y. Zhang, X. Chen, J Zhu, Mater. Res. Bull 38 (2003) 261-267
52. P. R. Bandaru, C. Daraio, K. Yang, A. M. Rao, J. Appl. Phys. 101 (2007) 094307-4
53. H. Hou, Z. Jun, F. Weller, A. Greiner, Chem. Mater. 15 (2003) 3170-3175
54. X. Chen, S. Yang, K. Takeuchi, T. Hashishin, H. Iwanaga, S. Motojiima, Dia. Rel. Mater 12 (2003) 1836–1840
55. L. Zhang, F. Li, Electrochimica Acta 55 (2010) 6695–6702
56. http://www.buzzle.com/articles/activated-charcoal-benefits.html (accessed 25 November 2010)
57. http://ifcext.ifc.org/ifcext/sustainability.nsf/AttachmentsByTitle/gui_sugar_WB/$FILE/sugar_PPAH.pdf (accessed 15 December 2010)
58. H. Kong, M. Zhou, G. Lin, H. Zhang, Catal. Lett. 135 (2010) 83–90
59. C. Jiang, H. Yin, Z. Chen, J. Zhejiang. Univ. SCI. B. 6 (2005) 378-381
60. A. Cabiac, G. Delahay, R. Durand, P. Trens, B. Coq, D. Plee, Carbon 45 (2007) 3–10
61. Q. Yuan, H. Duan, L. Li, L. Sun, Y. Zhang, C. Yan, J. Col. Inter. Sci. 335 (2009) 151–167
62. M. Yan, W. Wei, N. Zuoren, J. Rar. Earths 25 (2007) 53-57
63. R. D. Gonzalez, T. Lopez, R. Gomez, Catal. Today 35 (1997) 293-317.
64. S. Monyanon, S. Pongstabodee, A. Luengnaruemitchai, J. Pow. Source 163 (2006) 547-554
65. Z. Yang, K. Zhou, X. Liu, Q. Tian, D. Lu, S. Yang, Nanotechnology 18 (2007) 185606-185610
66. Q. Yuan, H. Duan, L. Li, L. Sun, Y. Zhang, C. Yan, J. Col. Inter. Sci. 335 (2009) 151–167
67. J. Kaspar, P. Fornasiero, M. Grazionl, Catal. Today. 50 (1999) 285-298.
68. S. Velu, M.P. Kapoor , S. Inagaki, K. Suzuki, Appl. Catal. A. 245 (2003) 317–331
69. J. Branco, D. Ballivet-Tkatchenko, A. Pires de Matos, J. Mol. Catal. A 307 (2009) 37–42
70. Y. Azizi, C. Petit, V. Pitchon, J. Catal. 256 (2008) 338– 344.
71. S. Chettibi, R. Wojcieszak, E. H. Boudjennad, J. Belloni, M. M. Bettahar, N. Keghouche, Catal. Today 113 (2006) 157– 165.
72. M. Abid, V. Paul-Boncour, R. Touroude , Appl. Catal. A 297 (2006) 48–59

73. J. Park, C. Lee, K. Jung, D. Jung, Bull. Korean Chem. Soc. 30 (2009) 402-404
74. http://www.chemlink.com.au/titanium.htm (accessed 30 November 2010)
75. http://www.electrochem.org/meetings/scheduler/abstracts/214/0342.pdf (accessed 30 November 2010)
76. J. Hong, W. Chu, M. Chen, X. Wang, T. Zhang, Catal. Commun. 8 (2007) 593–597
77. O. Mekasuwandumrong, S. Phothakwanpracha, B. Jongsomjit, A. Shotipruk, J. Panpranot, Catal. Lett. 136 (2010) 164–170
78. L. B. Ortiz-Soto, J. R. Monnier, M. D. Amiridis, Catal. Lett. 107 (2006) 13-17
79. J. Cunningham, G. H. Al-Sayyed, Surf. Sci. 169 (1986) 289-298
80. J. Wang, J. Xi, Y. Bai, Y. Shen, J. Sun, L. Chen, W. Zhu, X. Qiu, J. Pow. Sour. 164 (2007) 555–560
81. C. Xu, P. Shen, J. Pow. Sour. 142 (2005) 27–29
82. D. Guo, S. Cui, H. Sun, J. Nanopart. Res. 11 (2009) 707–712
83. J. C. Serrano-Ruiz, A. Sepulveda-Escribano, F. Rodriguez-Reinoso, D. Duprez, J. Mol Catal A: Chem. 268 (2007) 227-234
84. J. Zhang, PEM fuel cell electrocatalysts and catalyst layers, Springer, Canada, (2009) 447-448
85. J. Zeng, J. Y. Lee, J. Chen1, P. K. Shen, S. Song, Fuel Cells 7 (2007) 285–290
86. J.H. Bitter, M.K. van der Lee, A.G.T. Slotboom, A.J. van Dillen, K.P. de Jong, Catal. Lett. 89 (2003) 139-142
87. X. Wang, I-M. Hsing, Electrochim. Acta 47 (2002) 2981–2987.
88. H. Oh, J. Oh, Y. Hong, H. Kim, Electrochim. Acta 52 (2002) 7278-7285
89. T. Teranishi, M. Hosoe, T. Tanaka, M. Miyake, J. Phys. Chem. B. 229 (1999) 3818-3819
90. L. Hu, K. A. Boateng, J. M. Hill, J. Mol. Catal. A 259 (2006) 51-60
91. Z. Zhou, W. Zhou, S. Wang, G. Wang, L. Jiang, H. Li, G. Sun, Q. Xin, Catal. Today (2004) 523-528
92. L. Xiong, A. Manthiram, J. Solid State Ionics 176 (2005) 385–392
93. H. Kim, N. P. Subramanian, B. N. Popov, J. Pow. Source 138 (2004) 14–24
94. W. Chen, J. Zhao, J. Y. Lee, Z. Liu, Mater. Chem. Phys. 91 (2005) 124–129
95. X. Li, W. Chen, J. Zhao, W. Xing, Z. Xu, Carbon 43 (2005) 2168–2174
96. Y. H. Romdhane, B. Bellamy, V. De Gouveia, A. Masson, App. Surf. Sci. 31 (1988) 383-401

97. R. D. Cortright, S. A. Goddard, J. E. Rekoske, J. A. Dumesic, J. Catal. 127 (1991) 342--353
98. G. A. Somorjai, Catal. Lett. 7 (1990) 169-182
99. P. S. Cremer, G. A. Somorjai, J. Chem. Soc. Faraday Trans, 91 (1995) 3671-3677
100. http://www.tutorvista.com/chemistry/hydrogenation-of-ethene (accessed 15 November 2010)
101. C. Park, R. T. K. Baker, J. Phys. Chem. B. 102 (1998) 5168-5177
102. F. Gao, Y. Wang, W.T. Tysoe, J. Mol. Catal. A. Chem. 249 (2006) 111–122
103. J. Grunes, J. Zhu, E. A. Anderson, G. A. Somorjai, J. Phys. Chem. B 106 (2002) 11463-11468
104. P. S. Cremer, X. Su, Y. R. Shen, G. A. Somorjai, J. Am. Chem. Soc. 118 (1996) 2942-2949
105. http://pubs.acs.org/doi/pdf/10.1021/j100845a036 (accessed 15 November 2010)
106. S. Sato, K. Miyahara, 1. Res. Inst. Catal. 13 (1965) 10-19
107. J. W. Fulton, O. K. Crosser, A.I.Ch.E J. 11 (1965) 513-520
108. F. Zaera, G. A. Somorjai, J. Am. Chem. Soc. 106 (1984) 2288-2293
109. J. C. Schlatter, M. Boudart, J. Catal. 24 (1972) 482-492
110. J. Horiuti, M. Polanyi, Trans. Faraday Soc,.30 (1934) 1164-1172
111. G. H. Twigg, Disc. Farad. Soc. 8 (1950) 152-159
112. G.I. Jenkins, E. Rideal, J. Chem. Soc. (1955) 2490-2500
113. V. V. Rozanov, O. V. Krylov, Russian Chem. Rev. 66 (1997) 107-119
114. G. M. Pajonk, S. J Teichner, G. J Germain, Eds., Spillover of Adsorbed Species, Elsevier, Amsterdam (1983) 100-101

CHAPTER THREE

EXPERIMENTAL

3.1 Introduction

This chapter presents the detailed synthesis of carbon materials used in the study and the procedure used to deposit platinum onto the carbon materials, ceria and titania. The characterization techniques used in this project are also discussed. Finally, a discussion of the hydrogenation reactions performed using different platinum supported catalysts is given.

3.2 Materials and chemicals

All the chemicals used in this project were reagent grade. Solvents were obtained in high purity from the suppliers unless otherwise mentioned. The carbon materials (carbon nanotubes (CNTs), coiled carbon nanofibers (CCNFs) and carbon spheres (CS)) were synthesized in the laboratory using the chemical vapour deposition (CVD) method. Activated carbon and titania (Sigma Aldrich) were used without further purification. Ceria was synthesized in the laboratory using the sol-gel technique.

3.3 Synthesis of carbon materials

There are three major synthetic methods that are used to synthesis carbon materials. These methods include laser ablation, arc discharge and chemical vapour deposition (CVD). CVD has been selected for use in this study because it generates materials with a high purity and can be scaled up for mass production. The carbon materials were synthesized using the CVD method. A schematic experimental setup for CVD growth is shown in Figure 3.1. The growth process involves heating a catalyst material to high temperature in the tube furnace followed by passing hydrocarbon gas through the tube reactor for a period of time. The carbon materials grown over the catalyst were collected upon cooling the system to room temperature. Some key parameters in carbon material growth are the hydrocarbon, as well as the catalyst and temperature.

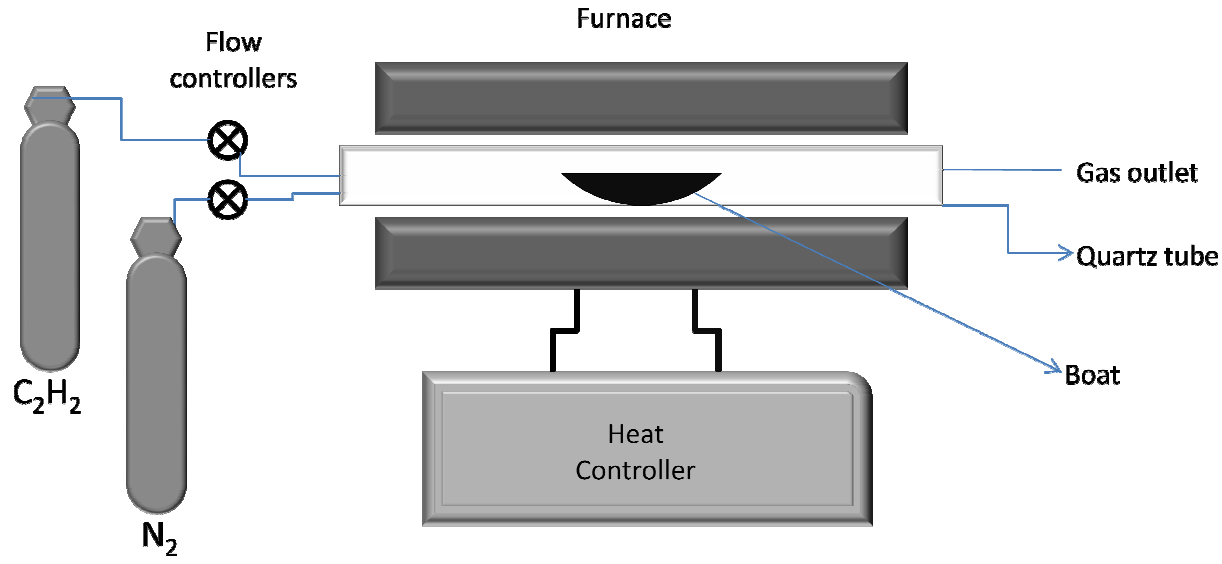

Figure 3.1. A schematic CVD setup for carbon material synthesis.

3.3.1 Catalyst preparation for CNTs[1]

The synthesis of carbon nanotubes was performed using the catalytic chemical vapour deposition technique. The catalyst used for the synthesis was Fe/Co supported on $CaCO_3$. For the preparation of a 5 % Fe-Co supported catalyst, the selected Fe and Co precursors ($Fe(NO_3)_3.9H_2O$ and $Co(NO_3)_2.6H_2O$) were dissolved in water (25 mL) to make a 50:50 precursor solution. The solution was then added dropwise to 10 g of support ($CaCO_3$) and stirred for at least an hour at room temperature. The mixture was then filtered and the slurry was allowed to semi-dry at room temperature for 30 minutes. The catalyst was then placed in an oven at 120 ^oC for 12 h and calcined at 400 ^oC for 16 h in air.

3.3.2 Synthesis of CNTs[1]

The carbon nanotubes were obtained by the catalytic decomposition of acetylene over the supported Fe-Co/$CaCO_3$ catalyst. The furnace was electronically controlled such that the heating rate, reaction time, reaction temperature and gas flow rate were accurately maintained as desired. In a typical synthesis protocol, 1 g of Fe-Co/$CaCO_3$ catalyst was uniformly spread on a small quartz boat that was placed at the centre of a horizontal furnace. The furnace was heated at 10 ^oC/min under the flow N_2 (40 mL/min) to 700 ^oC. After reaching the desired temperature of 700 ^oC, the flow of N_2 was increased to 240 mL/min and acetylene was introduced at a flow rate of 90 mL/min for 1 h. Thereafter the flow of acetylene was stopped and the reactor was cooled under N_2 at 40 mL/min to ambient temperatures. The small quartz

boat was then removed from the reactor and the product was collected along with the catalyst.

3.3.3 Catalyst preparation for CCNFs[2]

The catalytic system used for CCNF synthesis involved copper supported on TiO_2. For the preparation of 5% copper supported catalysts, the selected copper precursor ($Cu(NO_3)_2 \cdot 3H_2O$, Sigma-Aldrich) was dissolved in distilled water to form a homogeneous solution (0.262 M). The solution was then added dropwise (5 mL/min) to the support powder (TiO_2, Degussa P25, Sigma-Aldrich) under stirring to form a suspension. After 90 minutes of stirring the suspension was heated to 60 °C and isothermal evaporation under stirring was then carried out. The resulting product (Cu/TiO_2) was finally ground and sieved using a 500 μm mesh sieve. The catalyst was then placed in an oven at 100 °C for 12 h and calcined at 400 °C for 16 h in air.

3.3.4 Synthesis of CCNFs[2]

The coiled carbon nanofibers were obtained by the catalytic decomposition of acetylene over the supported copper catalyst following the same path as of CNTs synthesis. The furnace was electronically controlled such that the heating rate, reaction temperature and gas flow rate were accurately maintained as desired. In a typical run, approximately 0.8 g of catalyst material was uniformly spread onto a small quartz boat, and placed in the centre of a horizontal furnace. The catalyst was then activated by heating at 10 °C/min in H_2 at 100 mL/min to a temperature of 250 °C. At 250 °C acetylene at a flow rate of 100 mL/min was introduced for 1 h. Thereafter the flow of acetylene was stopped and the reactor was cooled under H_2 to ambient temperature. The resultant material was then harvested for characterization and stored for later use.

3.3.5 Purification of CCNFs

The CCNFs produced were mixed with the residual titania from the catalyst (Cu/TiO_2). Hydrofluoric acid (HF) was used to remove the titania. In a typical purification process, 100 mL of 40% HF (the operation was carried in a fume hood) was placed into a 250 mL plastic beaker and 0.5 g of CCNFs was added. The mixture was sonicated for 5 minutes. Thereafter the mixture was left in the fume hood for 12 h. The mixture was then separated using a filter paper and washed with distilled water until the pH of the filtrate was around 7. The HF treated CCNFs were then dried in an oven at 120 ^{o}C for 12 h.

3.3.6 Synthesis of carbon spheres[3]

The carbon spheres were obtained by decomposition of acetylene at high temperatures. The furnace (vertical) was electronically controlled such that the heating rate, reaction temperature and gas flow rate were accurately maintained as desired. The furnace was heated at 10 °C/min in Ar at 100 mL/min to a temperature of 900 ^{o}C. At 900 ^{o}C acetylene was introduced for 1 h. Thereafter the flow of acetylene was stopped and the reactor was cooled under Ar at 100 mL/min to ambient temperature. The product was then harvested for characterization and stored for later use.

3.3.7 Summary of the carbon materials synthesis procedures

Table 3.1 shows the reaction conditions used for the synthesis of the different carbon materials.

Table 3.1: Summary of the carbon materials synthesis conditions

Carbon Materials	**CNTs**	**CCNFs**	**CSs**
Temperature	700 ^{o}C	250 ^{o}C	900 ^{o}C
Catalyst	Co-Fe/$CaCO_3$	Cu/TiO_2	No catalyst
Carbon source	Acetylene	Acetylene	Acetylene

3.4 Functionalization of carbon materials

The chemical structure of CMs consists mainly of carbon atoms and as such, they do not contain any functional groups. Chemical functionalization therefore plays an essential role in tailoring the properties and application versatility of CMs.[4] Most of the functional groups are formed by oxidation of the carbon materials. Oxidation can be carried out in the gas phase using oxygen, ozone and carbon dioxide, or in the liquid phase using strong acids such as nitric acid, sulphuric acid or other oxidizing agents, such as NaOCl, H_2O_2, $KMnO_4$, $K_2Cr_2O_7$ and OsO_4.[5] In this project functionalization was performed using nitric acid.

3.4.1 Oxidation of carbon materials

Prior to oxidation of the carbon materials, polyaromatic compounds were extracted for 12 h using 100 mL of toluene in a Soxhlet apparatus. During the Soxhlet extraction, the

hydrophobic graphite particles were dispersed and removed from the carbon materials. The thimble containing the residual carbon materials was collected and vacuum-dried at 333 K for 12 h.[6] The purified carbon materials were oxidized with concentrated nitric acid at temperatures of 50 ^{o}C (for 12 h) and 100 ^{o}C (for 3 h). In a typical oxidation process, 1 g of CNTs was placed in a 250 mL round bottom flask containing 100 mL of concentrated nitric acid. The mixture was sonicated for 15 minutes in a ultrasonic bath at room temperature. The mixture was then stirred for 12 h at a temperature of 50 ^{o}C. Thereafter the mixture was diluted with distilled water and filtered using a Büchner funnel and filter paper (MN 615, 110 mm). The CNTs were then washed several times with water until the filtrate had a pH of approximately seven. Finally the CNTs were dried in an oven at 120 ^{o}C for 12 h.

The amount of functional groups (hydroxyl, carboxyl, carbonyl, etc) attached to the walls of the CMs were estimated by using an alkalimetry titration method. In this method, the oxidized CMs were suspended in a NaCl (0.1 mol dm^{-3}) electrolyte. Ion exchange occurs between the cations of the electrolyte and the active hydrogen of the functional groups leading to hydrogen ions being evolved. The change of the pH of the suspension during the addition of the titrant is due to the progressive dissociation of acidic groups. The quantities of strong acids detected correspond to the acid group dissociated in solution of pH less than 7. Stronger acids with pK_a less than 7 mainly comprise of carboxylic acids and these can be titrated using a very weak base such as $NaHCO_3$.

3.5 Synthesis of ceria[7]

Ceria was prepared by a sol-gel method. Cerium nitrate solution with a concentration of 0.1 M was mixed with a 0.4 M urea solution. The mixture was aged at 100 ^{o}C for 50 hours. The precipitate that formed was washed with water and ethanol. Ceria was then dried overnight at 100 ^{o}C and then calcined at 300 ^{o}C for 2 h.

3.6 Synthesis of the supported platinum catalyst

Platinum was deposited on the various supports (carbon materials, ceria and titania) using the polyol method.

3.6.1 Synthesis of platinum supported on carbon materials (Pt/CM)[8]

The synthesis was done using the microwave assisted polyol synthesis. Before the Pt/CM was synthesized, UV-vis spectroscopy was used to follow the formation of Pt from

hexachloroplatinic acid. The method used ethylene glycol as both a solvent and reducing agent. The method was chosen because it is a straightforward, inexpensive catalytic synthesis method of low toxicity. In the method, the CCNFs (0.2 g) were dispersed in 50 mL of ethylene glycol solution. The CCNFs in solution were sonicated for 15 minutes until all agglomerates were broken down and dispersed evenly. The solution was mechanically stirred for 30 minutes and 0.21 mL of 0.05 M H_2PtCl_6 was added dropwise and the solution was further stirred for 3 hours to ensure that the precursor ions would be distributed evenly throughout the solution and dispersed evenly on the support. The mixture was then irradiated in a microwave oven (input power 810 W) for 4 minutes with on–off cycle (60 s on – 120 s off). For comparison, the mixture was refluxed for 3 h using an oil bath at a temperature of 160 ^oC. The product was filtered and washed with acetone and distilled water. The residue (Pt/C) was then dried at 120 ^oC for 12 h.

3.6.2 Synthesis of platinum supported on oxides

The Pt/CeO_2 and Pt/TiO_2 were prepared by reduction of H_2PtCl_6 on CeO_2 and TiO_2 supports. The method is similar to the synthesis used to produce Pt/CM catalysts. Ceria and titania were used instead of the carbon nanomaterial.

3.6.3 Synthesis of Pt-CeO_2/CM[9]

The Pt-CeO_2/CM was prepared using the polyol process. The appropriate amount of cerium nitrate, H_2PtCl_6, and sodium acetate were added into a solution of ethylene glycol. The mixture was uniformly mixed with a carbon nanomaterial by sonication. The resultant mixture was irradiated in the microwave oven (input power 810 W) for 4 minutes with on–off cycle (60 s on – 120 s off). Afterwards the suspension was filtered and the residue was washed with acetone and deionized water. The solid products were dried at 120 ^oC for 12 h in an oven.

The Pt-CeO_2/CM catalysts were also synthesized by making CeO_2/CM first and then depositing platinum on the support (CeO_2/CM). The CeO_2/CM was synthesized by the polyol method. Cerium nitrate and sodium acetate were added to a beaker containing 50 mL of ethylene glycol. The mixture was then mixed for 30 minutes and CM was added into the mixture. Stirring was done for 3 h. The resultant mixture was irradiated in the microwave oven (input power 810 W) for 4 minutes with on–off cycle (60 s on – 120 s off). Afterwards

the suspension was filtered and the residue was washed with acetone and deionized water. The solid products were dried at 120 ^{o}C for 12 h in an oven.

The solid product (0.2 g) was dispersed in 50 mL of ethylene glycol solution. CeO_2/CM in ethylene glycol solution was sonicated for 15 minutes until all agglomerates were broken down and dispersed evenly. The solution was mechanically stirred for 30 minutes and 0.21 ml of 0.05M H_2PtCl_6 was added dropwise and the solution was further stirred for 3 hours to ensure that the precursor ions would be scattered throughout the solution and dispersed evenly. The mixture was then irradiated using a microwave oven (input power 810 W) for 4 minutes with on–off cycle (60 s on – 120 s off). The product was filtered and washed with acetone and distilled water. The residue (Pt-CeO_2/CM) was then dried at 120 ^{o}C for 12 h.

3.7 Characterization techniques used in this study

The following techniques were used to characterise the supports and the catalysts: transmission electron microscopy (TEM) equipped with energy dispersion X-ray (EDX) capabilities, thermal gravimetric analysis (TGA), ultraviolet-visible spectrophotometry (UV-Vis), Raman spectroscopy, temperature programmed reduction (TPR), X-ray diffraction (XRD), Brunauer-Emmett-Teller N_2 adsorption (BET), Fourier transform infrared (FTIR) spectroscopy and inductively coupled plasma atomic spectra emission spectroscopy (ICP-AES)

3.7.1 Transmission electron microscopy

Transmission electron microscopy (TEM) is a technique that is used to confirm the morphology of the materials. The beam of light is able to pass through the sample and the transmitted electrons produce an image of the sample. TEM is a useful tool and is used extensively for the characterization of organic and inorganic materials. In this study, the TEM analysis (FEI Tecnai G2 Spirit electron microscope at 120 kV) was used to determine the aggregate morphology, particle size and particle size distribution of either the support or the catalyst. The EDX was used to obtain the composition of the catalyst.

A small quantity of a sample to be analyzed was placed in a glass vial containing 5 mL of methanol. The mixture was then sonicated for 15 minutes to give a homogeneous suspension of the sample in the solvent. A drop of the suspension was then spread on a carbon copper grid (200 mesh) and allowed to dry at room temperature. The grid was then mounted onto an exchange rod and placed into the TEM chamber and was ready for viewing.

3.7.2 Thermal gravimetric analysis

Thermal gravimetric analysis (TGA) is a technique that is used to study the changes in a sample with variation in heating temperature. The changes are usually associated with weight loss resulting from dehydration or decomposition of the sample as the temperature increases. The weight loss can also arise from the formation of physical and chemical bonds that can lead to the release of volatile compounds. In this study, the material's thermal stability was studied using a Perkin Elmer Thermogravimetric Analyzer (TGA 4000).

About 0.05 g of the sample was used for the thermal gravimetric analysis. The sample was placed into a high temperature alumina cup that was supported on an analytical balance located in the furnace chamber. The balance was zeroed, and the sample was heated from ambient temperature to 900 ^{o}C at the rate of 10 ^{o}C per minute. The weight loss with increase in temperature was automatically recorded. The TGA curve plots the TGA signal, converted to percent weight change on the Y-axis against the temperature on the X-axis.

3.7.3 Ultraviolet-visible spectrophotometry

UV-vis spectrophotometry is used to determine the absorption or transmission of UV-vis light (180 to 820 nm) by a sample.[10] It is applicable to qualitative and quantitative determination of many organic and inorganic compounds in a solution. Compounds analysed by this technique must have chromophores (covalently bonded but unsaturated groups such as NO_2, C=C and C=O) that absorb electromagnetic radiation in the ultraviolet and visible region of the spectrum. The amount of energy absorbed is directly proportional to the concentration of the compound in the solution.

Samples were placed in a cuvette that was 1 cm wide and 4.5 cm long. The cuvette was then placed in the instrument and absorbances were measured. Water was used as a reference sample and also to re-zero the instrument. Spectra were then plotted of absorbance against wavelength using a Analytikjena, Specord 50 instrument.

3.7.4 Raman spectroscopy

Raman spectroscopy is used in chemistry and other branches of science to study vibrational, rotational and other low frequency modes in a sample. After a sample has been illuminated with a laser beam, some monochromatic radiation is scattered. The scattered light has

different energies depending on the type of molecular vibrations present in the sample. The backscattering radiation allows one to determine the structure and quality of the sample.[11]

A Jobin-Yvon T64000 Raman spectrometer was used to measure the vibrations in the sample. It was operated in a single mode with 600 lines/mm grating. A 514.5 nm line of the argon ion laser was used as the source of excitation. Laser light was focused on to the sample using a 20x objective lens of an Olympus microscope. The scattered light was collected in a backscattering configuration and was detected using a nitrogen cooled charge coupled detector.

3.7.5 Temperature programmed reduction

Temperature-programmed reduction (TPR) is a widely used tool used for the characterization of metal oxides, mixed metal oxides, and metal oxides dispersed on support.[12] The TPR method yields quantitative information of the reducibility of the oxide's surface, as well as the heterogeneity of the reducible surface. TPR is a method in which a reducing gas mixture flows over a sample. A thermal conductivity detector (TCD) is used to measure changes in the thermal conductivity of the gas stream. The TCD signal is then converted to the concentration of active gas using a level calibration

TPR experiments on the prepared catalysts were carried out using an ASAP 2020 Micrometrics analyzer in a 5 % H_2/Ar gas mixture. Samples were pretreated with Ar at 150 ^oC for 2 h. The hydrogen consumption was recorded with a TCD cell while the sample was linearly heated from 50 to 800 ^oC at 10 ^oC/min.

3.7.6 X-ray diffraction

Powder XRD is the most widely used X-ray diffraction technique to find the crystallization and morphology of materials. As the name suggests, the sample is usually in a powder form, consisting of fine grains of single crystalline material to be studied.[13] The term 'powder' means that crystalline domains are randomly oriented in the sample. Therefore when the 2-D diffraction pattern is recorded, it shows concentric rings of scattering peaks corresponding to the various d spacings in the crystal lattice. The positions and the intensities of the peaks are used for identifying the underlying structure (or phase) of the material. This phase identification is important because the material properties are highly dependent on its structure. A D8 Bruker X-ray diffractometer was used for the analysis.

3.7.7 Brunauer-Emmett-Teller N_2 adsorption (Surface area analysis)

Brunauer-Emmett-Teller N_2 adsorption (BET) is a technique that is used to measure surface area, pore volume and pore size distributions of a sample. The BET analysis was carried out using an automated gas adsorption analyser (Tristar 3000 V6.05)

Samples were degassed using a Micrometrics Flow Prep 060 Sample Degas System at 120 ^{o}C for 12 h prior to nitrogen adsorption. The BET surface area was calculated based on the adsorption data in the relative pressure range of 0.001-0.20.

3.7.8 Fourier transform infrared spectroscopy

Fourier transform infrared (FTIR) spectroscopy is one of the most important tools used to identify functional groups present in a molecule or compound. FTIR spectroscopy provides information about the chemical bonding or molecular structure of materials. It can be utilized to quantify components of an unknown mixture. It can be applied to the analysis of solids, liquids, and gases.

FTIR measurements were performed using a Bruker-Tensor 27-ATR FTIR spectrometer in the range from 4000-400 cm^{-1}. The FTIR spectra were recorded at room temperature when the infrared light was passed through the sample.

3.7.9 Inductively coupled plasma atomic spectra emission spectroscopy

Inductively coupled plasma atomic spectra emission spectroscopy (ICP-AES) is a very important tool which is used to determine the percentage loading of platinum. The samples for ICP-AES analysis were digested in an microwave oven for 2 h with aqua regia in order to collect platinum ions in solution. Then, the aliquots of solution were diluted to 50 mL using distilled water and analyzed using inductively coupled argon plasma emission spectrometer, (GENESIS ICP-AES SPECTRO Analytical Instruments)

3.8 Hydrogenation reactions

Hydrogenation reactions were used in this study to determine the effect of adding ceria on to platinum supported on carbon materials. In the process, the effect of various supports was also determined.

3.8.1 Experimental set up

The catalytic hydrogenation reactions were performed at atmospheric pressure by passing continuously, a gas feed containing 5 % hydrogen in argon or a 5 % ethylene in argon stream over the catalyst (100 mg) packed in a fixed bed steel micro-reactor. The micro-reactor was fitted with a thermocouple for controlling temperature. Inside the micro-reactor, there is a frit, which allows a passage of the gases from the micro reactor to the gas chromatograph (GC). During a hydrogenation reaction, the frit is covered with quartz wool in order to keep the catalyst in place. The sample size (amount of catalyst used) was 0.1 g. The experimental set up is shown in Figure 3.2.

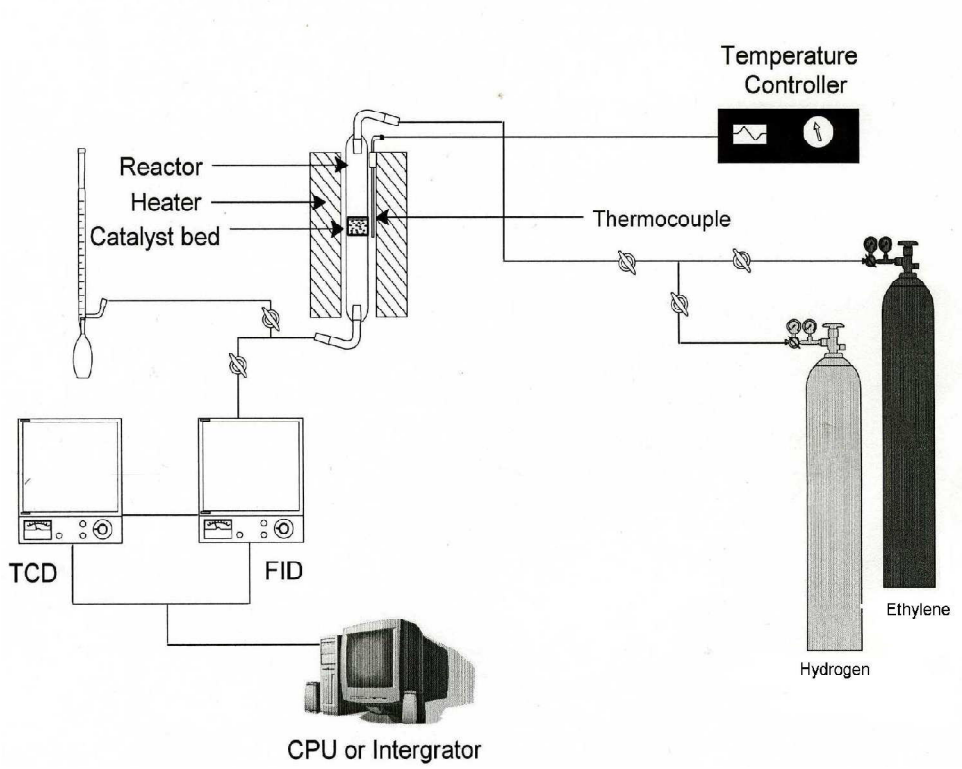

Figure 3.2. Schematic representation of the hydrogenation reaction set up

Gas chromatography (GC) was used to characterize the products of the hydrogenation of ethylene. The use of the GC is to separate volatile components of a reaction mixture prior to GC analysis. The separated components were detected by the GC detectors. The most common detectors used for gas chromatography are the flame ionization detector (FID) and the thermal conductivity detector (TCD). Both are sensitive to a wide range of components and both work over a wide range of temperatures. TCD can be used to detect any component

other than the carrier gas as long as the thermal conductivities are different from the carrier gas. The TCD used a Porapak Q column.

The conditions of the GC: the column temperature was 80 ^{o}C, injector temperature was 200 ^{o}C and the detector temperature was 100 ^{o}C. The carrier gas was Argon with a pressure of 100 Kpa.

The following investigations were conducted in the project: the effect of increasing the temperature, flow rate of gases, metal loading and the ratio of hydrogen to ethylene. The conversion of ethylene to ethane was calculated as follows:

$$\text{Conversion (t)} = \frac{([C_2H_4\,(0)]-[C_2H_4\,(t)])}{[C_2H_4\,(0)]} \times 100\ \%$$

Where (t) is the time at which the conversion was taken and (0) is the initial time.

References

1. E. Couteau, K. Hernadi, J. W. Seo, L. Thien-Nga, C. Miko, R. Gaal, L. Forro, Chem. Phys. Lett. 378 (2003) 9–17
2. A. Shaikjee, N.J. Coville, Mater. Chem. Phys. 125 (2011) 899–907
3. S.D. Mhlanga, N.J. Coville, S.E. Iyuke, A.S. Afolabi, A.S. Abdulkareem, N. Kunjuzwa, J. Exp. Nanoscience 5 (2010) 40–51
4. S.B. Dibyendu, D. Rama, N. Zhang, J. Xie, V.K. Varadan, D. Lai, G.N. Mathur, Smart Mater. Struct. 13 (2004) 1263-1267
5. F. Rodríguez-Reinoso, Carbon 36 (1998) 159-175
6. E. R. Alvizo-Paez, J. M. Romo-Herrera, H. Terrones, M. Terrones, J. Ruiz-Garcia, J. L.Hernandez-Lopez, Nanotechnology 19 (2008) 1-9
7. S. Monyanon, S. Pongstabodee, A. Luengnaruemitchai, J. Pow. Source 163 (2006) 547-554
8. X. Li, W. Chen, J. Zhao, W. Xing, Z. Xu, Carbon 43 (2005) 2168–2174
9. J. Zhao, W. Chen, Y. Zheng, Mat. Chem. Phys. 111 (2009) 591-595
10. http://www.ptli.com/testlopedia/tests/UV-VIS-SPEC.asp (accessed 23 June 2009)
11. L. A. Lyon, C. D. Keating, A. P. Fox, B. E. Baker, L. He, S. R. Nicewarner, S. P. Mulvaney, M. J. Natan, Anal. Chem. 70 (1998) 341-361
12. www.vscht.cz/kat/download/lab_tpr_eng.doc (accessed 23 June 2009)
13. http://www.mrl.ucsb.edu/mrl/centralfacilities/xray/xray-basics/index.html#x2 (accessed 23 June 2009)

CHAPTER FOUR

RESULTS AND DISCUSSION

4.1 Introduction

This chapter presents the results obtained from the various experiments performed in this study. This includes the characterization of the carbon materials (CMs) as well as the platinum supported on the CMs and oxides (CeO_2 and TiO_2). Finally, the results for the hydrogenation of ethylene using the different platinum supported catalysts are discussed.

4.2.1 TEM analysis of the carbon materials

The carbon materials [coiled carbon nanofibers (CCNFs), carbon spheres (CS) and carbon nanotubes (CNTs)] were synthesized using the chemical vapour deposition method as described in **Chapter 3**. The as-synthesized CMs were characterized by transmission electron microscopy (TEM) and the results are shown in Figure 4.1. It was observed that the as-synthesized CMs (Figure 4.1 a and c) had some impurities which were suspected to be the remains of the catalysts used in their synthesis. There were no impurities observed in the TEM image of the CSs (Figure 4.1 b) as the synthesis was done in the absence of a catalyst.

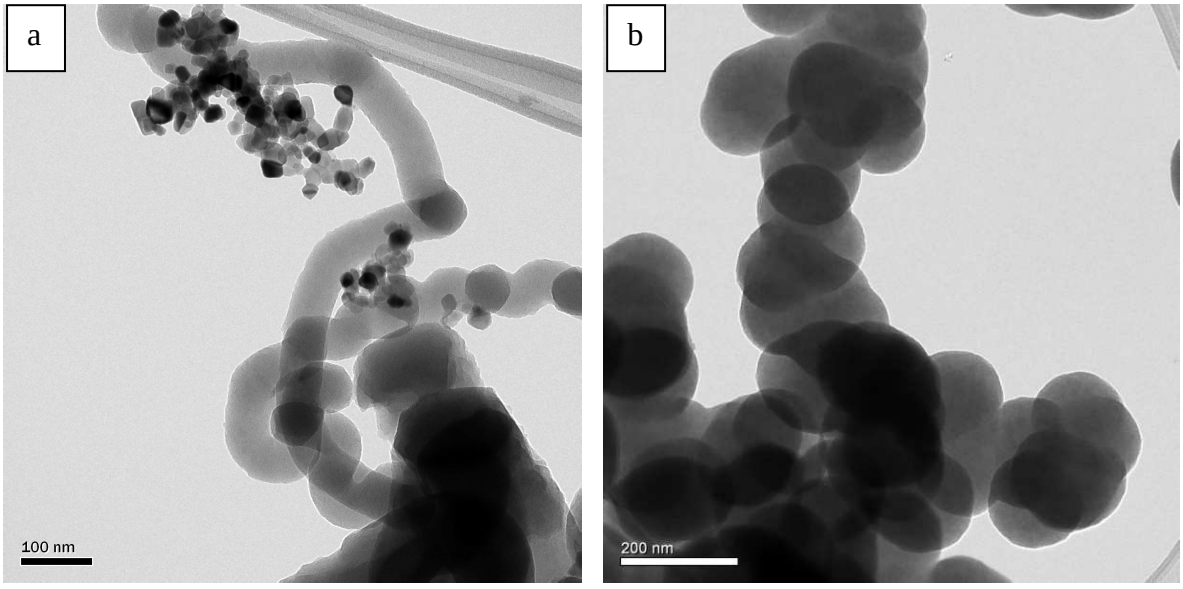

Figure 4.1: TEM images of the as synthesized (a) CCNFs (b) CSs (c) CNTs

4.2.1.2 Purification of CCNFs

The CMs produced in this study were investigated as catalyst supports. A catalyst works best in the absence of impurities. The CCNFs were believed to be contaminated by titania which was used as a catalyst support for the Cu/TiO_2 catalyst. Hydrofluoric acid (HF) was used to remove the residual titania and its advantage is that it does not react with CCNFs. The probable reaction that takes place is as follows:

$$4HF\ (aq) + TiO_2\ (s) \rightarrow TiF_4\ (aq) + 2H_2O\ (l)$$

Therefore the TiF_4 produced in solution would be removed by filtration and the CCNF would remain as a residue. The HF treated CCNFs were characterized by TEM in order to verify the disappearance of the titania residue on the CCNFs. Figure 4.2 shows the TEM images for the HF treated CCNFs. It was observed from TEM images that all the TiO_2 was successfully removed by HF. Of interest is the fact that the morphology of the CCNFs were not affected by the HF treatment though it cannot be observed from TEM if the properties of the CCNF were affected by the HF treatment. Figure 4.2 shows that the material contains both coiled and uncoiled fibers. The estimated ratio of coils to uncoiled fibers is 60/40.

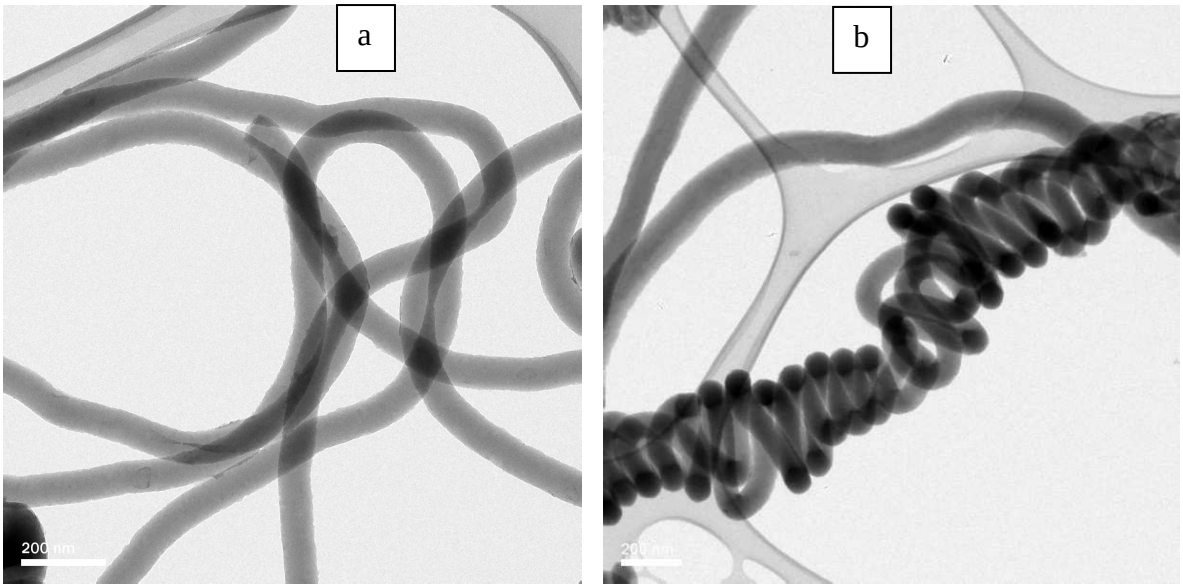

Figure 4.2. TEM images of the HF treated CCNFs (a) uncoiled fibers and (b) a coiled fiber

4.2.1.3 The effect of functionalization on the carbon materials

Prior to functionalization (by oxidation using nitric acid), Soxhlet extraction was performed on the CMs. This process was performed in order to remove all the polyaromatic compounds left behind in the synthesis. All the carbon materials contained polyaromatic compounds as the colour of toluene changed from colourless to a brown solution as the Soxhlet extraction preceded. The intensity of the brown solution was mostly observed after extraction of the CSs when compared to the other carbon materials.

There are two major reasons as to why functionalization of carbon materials was performed. The first reason was to improve the hydrophilic nature of the carbon materials. The as-synthesized carbon material does not dissolve/disperse in water, but they are rather observed to be suspended above the solvent. However, after oxidation the CMs could be well dispersed in water. The second reason was to introduce functional groups on the CMs in order to improve anchoring of metals onto the carbon during catalyst synthesis. Some of the potential functional groups introduced on the CMs are shown in Figure 4.3.[1] These include oxygenated groups such as the COOH, OH, OR groups etc. The degree of oxidation indicates the effect of the severity of the oxidation treatment on the CMs.

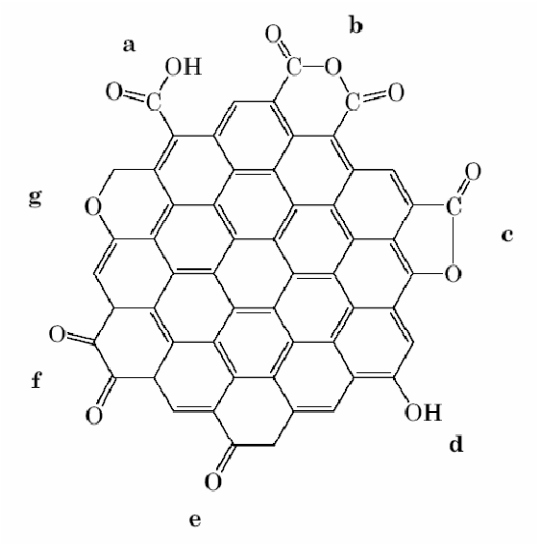

Figure 4.3. Different oxygen-containing surface groups on the carbon materials. a) carboxyl groups, b) carboxylic anhydride groups, c) lactone groups, d) phenol groups, e) carbonyl groups, f) quinone groups, g) xanthene or ether groups.[1]

The masses of the CMs produced were measured before and after functionalization using two different conditions and are shown in Tables 4.1 a and 4.1 b.

Table 4.1a: Yield of CMs remaining after reflux for 3 h at 100 ^{o}C in nitric acid

Carbon materials	**Mass before reflux (g)**	**Mass after reflux (g)**	**Yield (%)**
CNTs	1.025	0.9486	92.5
CSs	1.048	0.5670	54.1
CCNFs	1.018	0.4352	42.8

Table 4.1b: Yield of CMs remaining after reflux for 12 h at 50 ^{o}C in nitric acid

Carbon materials	**Mass before reflux (g)**	**Mass after reflux (g)**	**Yield (%)**
CNTs	1.037	0.9979	95.8
CSs	1.069	0.9699	90.7
CCNFs	1.034	0.9735	94.1

A comparison of the yields from the two functionalization modes show that there were large mass losses for CSs and CCNFs when the CMs were heated under reflux for 3 h at 100 ^{o}C (Table 4.1 a) compared to when the CMs were functionalized at 50 ^{o}C for 12 h (Table 4.1 b). Under reflux at 100 ^{o}C for 3 h the yields for CSs and CCNFs were 54.1 % and 42.8 % respectively. This suggests that CSs and CCNFs were destroyed under these conditions. This was confirmed by TEM analysis. Figure 4.4 shows the effect of functionalization at 100 ^{o}C for 3 h on the CCNFs.

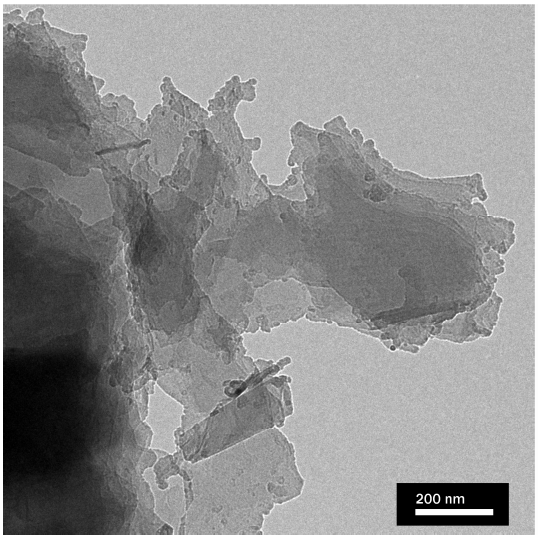

Figure 4.4. TEM image of CCNFs functionalized at 100 ^{o}C for 3 h

A prolonged or high temperature reflux induces opening of CM tips or damage to the walls of the carbons.[2] Because of this drawback, products produced after functionalization was limited to 50 ^{o}C for 12 h and these conditions were used in later studies. It is important to note that the CNTs were resistant to the harsh conditions. This confirms that the CNTs have a well defined aromatic structure that is less readily oxidized. The TEM images of the three CMs refluxed at 50 ^{o}C for 12 h are shown in Figure 4.5.

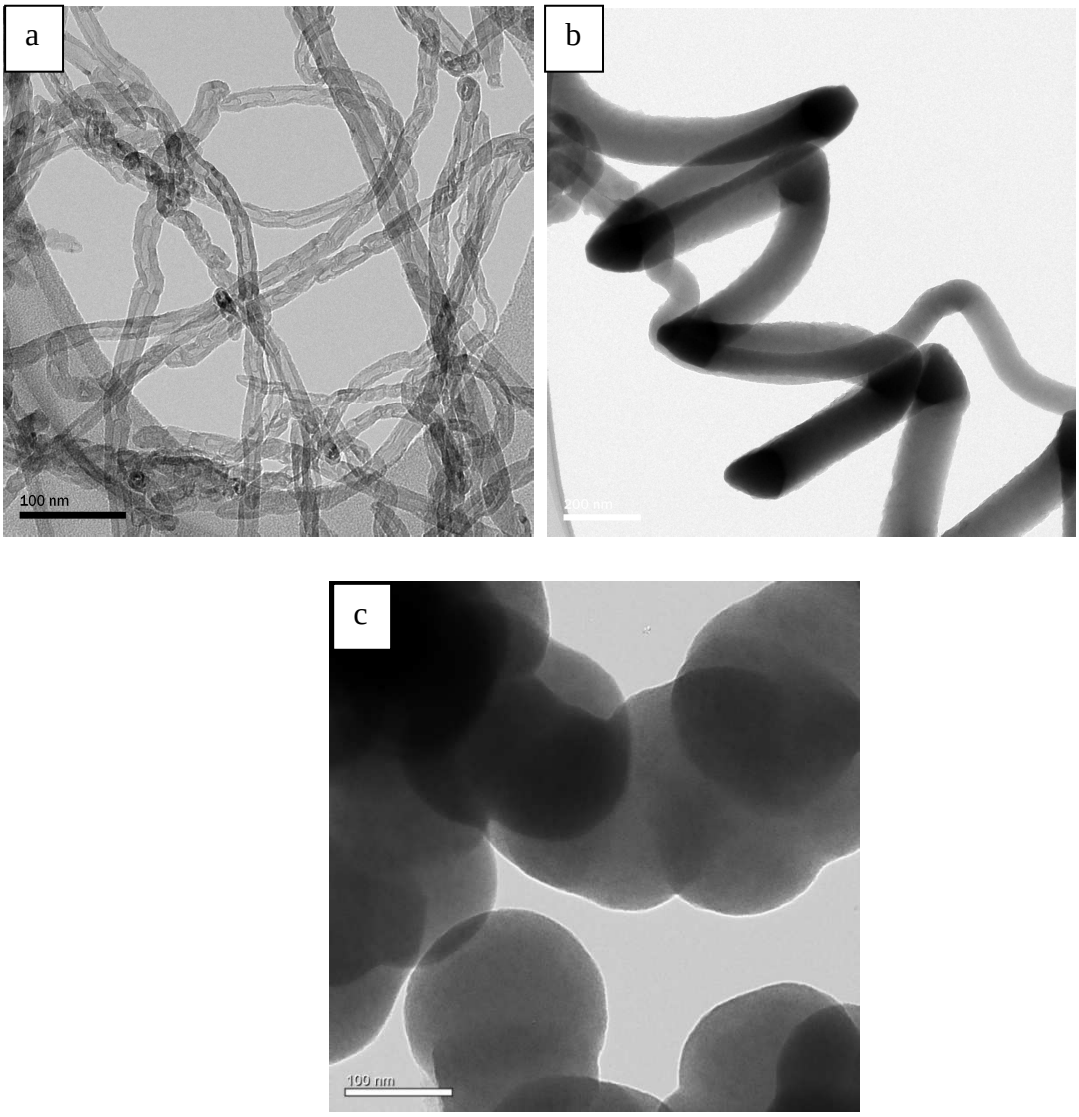

Figure 4.5. TEM images of (a) CNTs (b) CCNFs (c) CSs functionalized by reflux at 50 ^{o}C for 12 h.

A marked difference between the as-synthesized CNTs (Figure 4.1) and the functionalized CMs (Figure 4.5) can be seen. Impurities associated with the CNTs were removed by nitric acid in the functionalization process. The remains of the catalyst (Fe-Co/$CaCO_3$) used in the synthesis of the CNTs were removed from the external CNT surface. Changes on the CCNFs and CSs surfaces could not be seen by TEM.

The amount of acid groups attached to the CMs was estimated using alkalimetry and the results are shown in Table 4.2. The results show small but measurable differences for the 3 samples.

Table 4.2: Estimates of the acid groups on the carbon materials (50 ^{o}C/12 h)

Carbon materials	**Acid groups (mequi/g)**
CNTs	9.2×10^{-2}
CCNFs	8.9×10^{-2}
CSs	8.3×10^{-2}
CNTs[a]	3.4×10^{-1}

a-acid treated at 100 ^{o}C/3 h

From the alkalimetry results it is clear that functional groups were attached to all three of the CMs. CNTs functionalized at 100 ^{o}C for 3 h had more acid groups (3.4×10^{-1}) than CNTs functionalized at 50 ^{o}C for 12 h (9.2×10^{-2}). This means that the harsher the oxidation treatment, the more acid groups that can be attached.

4.2.1.4 Thermal gravimetric analysis of the carbon materials

Thermal gravimetric analysis (TGA) can be used quantitatively to evaluate the purity of the carbon materials, in particular the content of the residual metal and the degree of functionalization. The residual metal content in the carbon materials can be obtained by oxidizing the carbon materials in air. The carbon materials are converted to CO/CO_2 in air and the metal or metal oxide remains at the end of the process.[3] To confirm that TiO_2 was removed from the CCNFs, TGA analysis was performed.

Figure 4.6a show the TGA plot of the CCNFs before and after purification with HF. It can be clearly seen from the TGA plots that TiO_2 was completely removed from the carbon. The residual mass before purification was 23.62 % and after purification it went down to ca. 0 %. It was also observed that the TGA profile of the purified CCNF showed changes at around 200 ^{o}C. The mass loss between 200-300 ^{o}C is due to the presence of the acid groups. It can also be noted that both curves show a change in rate at about 400 ^{o}C suggesting two types of carbon are formed with CCNFs i.e. this could be related to the presence of the linear and coiled fibers.

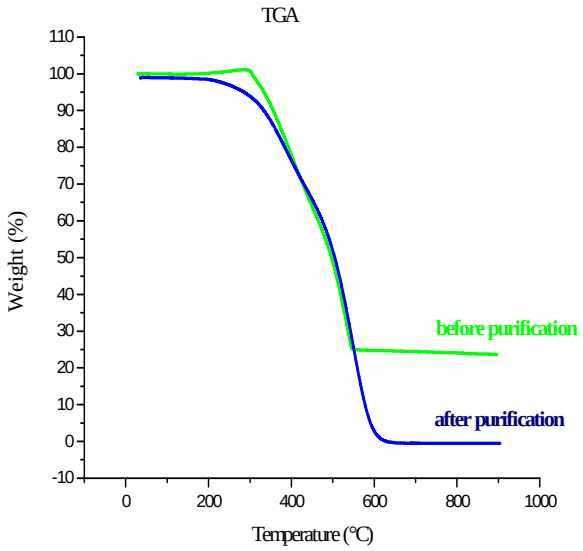

Figure 4.6a. TGA profile of CCNFs before and after purification

Functionalization of the CNTs had a dual purpose. The first was to remove the residual metal after synthesis from the CNTs and the second was to introduce functional groups. TGA was used to determine the successful removal of Fe and Co (from Fe-Co/$CaCO_3$). Figure 4.6b shows the TGA profile of the as-synthesized and functionalized CNTs. The residual mass before functionalization was 13 % which dropped to close to ca. 0 % when the CNTs were functionalized with concentrated nitric acid at 50 ^{o}C for 12 h. Therefore the majority of the impurities in the CNTs were successfully removed and the minority of the residual was Fe trapped inside the CNTs.

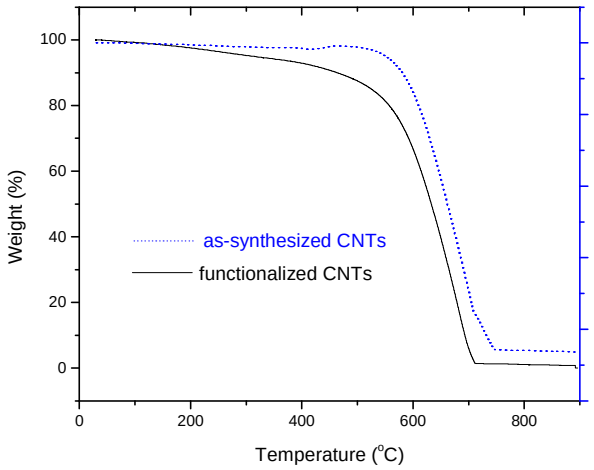

Figure 4.6b. TGA profile of the as-synthesized and functionalized CNTs

The thermal stability of the CNTs also decreased (figure 4.6 b) after purification. These observations suggest that an increase in the amount of defects created on the CNTs surface upon purification aids in the oxidation reaction. Thus, the position of the decomposition peak is affected by the amount of residual catalyst in the sample, the defect content created on the surface of the CNTs and the amount of amorphous carbon present.

The TGA profiles of CSs are presented in Figure 4.6c. The thermal stability of the functionalized CSs decreased because the functional groups added to the carbon make them more easily oxidized material.

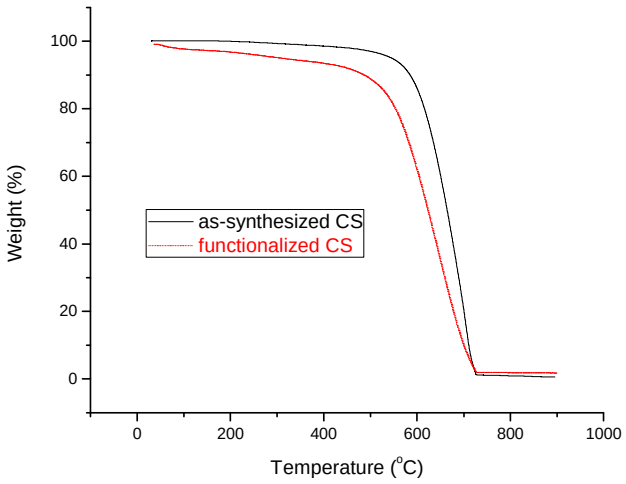

Figure 4.6c. TGA profile of the as-synthesized and functionalized CSs

4.2.1.5 Raman spectra of the carbon materials

Raman spectra of CCNFs showing the D and G bands associated with the C-C bonds are presented in Figure 4.7. In the Raman spectra, there are two prominent peaks namely the D band and the G bands that are associated with carbon materials. The D band is related to the disorder structure and attributed to the defects in the curved graphene sheet, the tube ends or amorphous carbon. The G band is related to the structural integrity of the sp^2-bonded carbon atoms in the two dimensional hexagonal lattice, indicating the presence of crystalline graphitic carbon.[4] The ratio of the intensity of these bands or the ratio of their areas provides (I_D/I_G) crucial information on the graphicity or lack of defects on the carbon materials. Table 4.3 shows that the peaks in the higher frequency region (at 1562 cm^{-1}) correspond to the G band for both the as-synthesized and functionalized CCNFs and peaks at 1435 and 1425 cm^{-1} are for the as-synthesized and functionalized CCNFs respectively.

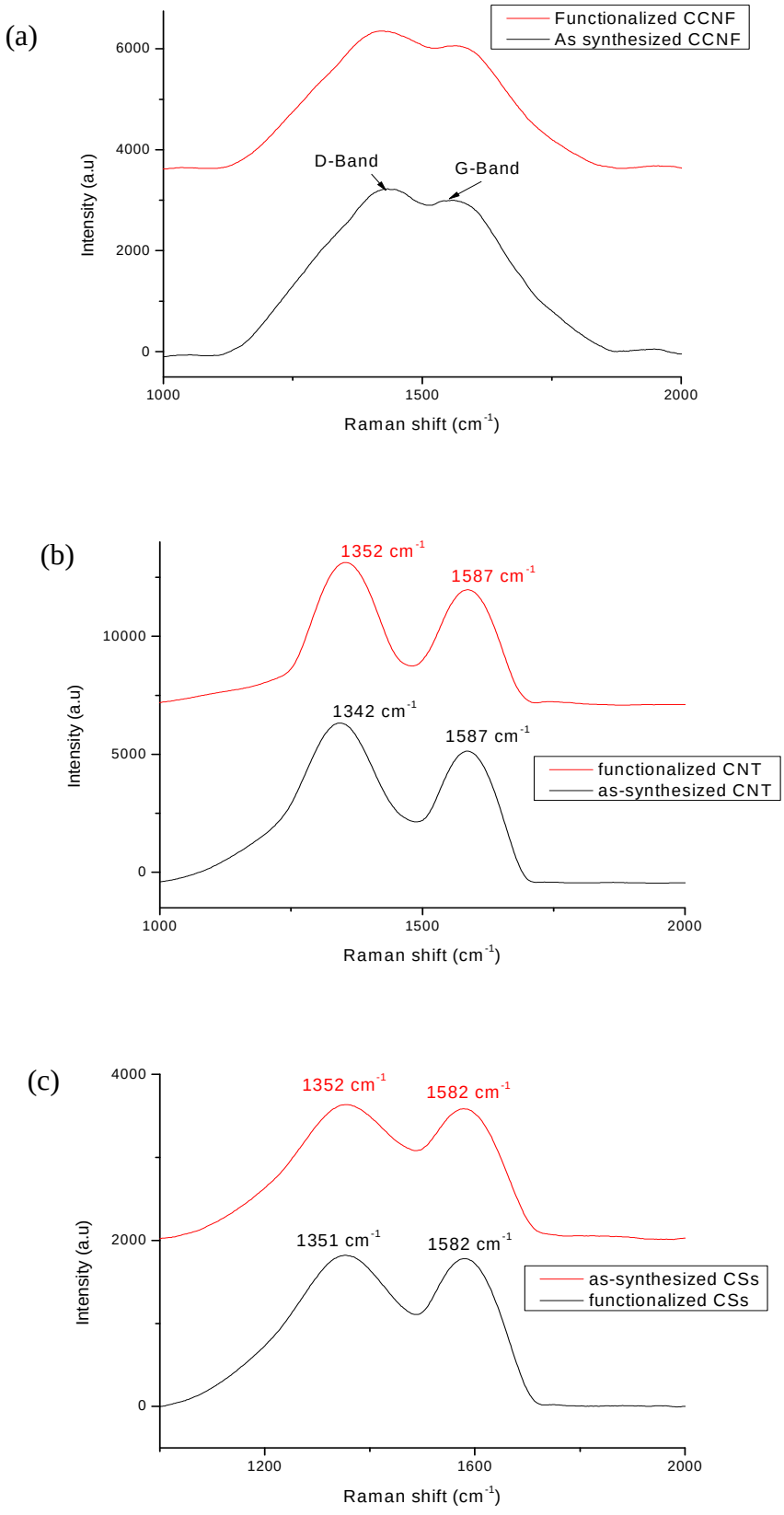

Figure 4.7. Comparison of the Raman spectra of functionalized and as-synthesized (a) CCNFs, (b) CNTs and (c) CSs.

The ratios of the D band to the G band (I_D/I_G) for the as-synthesized and functionalized CCNF were found to be 0.99 and 1.71 respectively. This indicates that functionalization of the CCNFs introduced some defects onto the materials. The Raman spectra for the CNTs and CSs were well pronounced as they have distinct D and G bands. The I_D/I_G ratios for the as-synthesized and functionalized CNTs are 2.04 and 2.51 respectively while the I_D/I_G ratios for the as-synthesized and functionalized CSs are 2.7 and 3.02 respectively. This suggests that more disorder has been created in the CSs after acid treatment.

Table 4.3: Raman data for as-synthesized and acid-treated CCNF and CNTs

Sample ID	Peak position (cm^{-1})		I_D/I_G
	D-band	G-band	
As-synthesized CCNFs	1425	1562	0.99
Functionalized CCNFs	1435	1562	1.71
As-synthesized CNTs	1342	1587	2.04
Functionalized CNTs	1352	1587	2.51
As-synthesized CSs	1352	1582	2.70
Functionalized CSs	1351	1582	3.02

4.2.1.6 Infrared spectroscopy

Infrared (IR) spectroscopy was used to determine the presence of functional groups on the CMs before and after functionalization. Figure 4.8A. shows the peaks at 1000-1100 cm^{-1} that can be attributed to C-O symmetrical stretching, at 1401 cm^{-1} to O-H bending[5] and at 1639 cm^{-1} is related to the COOH vibrational mode[6]. Comparing the IR spectra in Figure 4.8 for the three different CMs, significant differences are revealed indicating that functional groups have been attached to all the CCNFs, CSs and the CNTs but to different degrees. Two distinct peaks are observed at 1424 cm^{-1} and 1639 cm^{-1} for CCNFs. The CNTs shows the disappearance of the peak at 1398 cm^{-1}, as well as peaks at 1598 cm^{-1} and 1734 cm^{-1} (Figure 4.8B). The CSs also show differences between the functionalized and the as-synthesized materials. A peak is found at 1289 cm^{-1}. In conclusion the functionalization of carbon materials has created a change on the surfaces of the different carbon materials. However, little else can be added to the information above; it is known that quantification of the IR spectra of solid materials e.g. solid carbon materials is not easy.

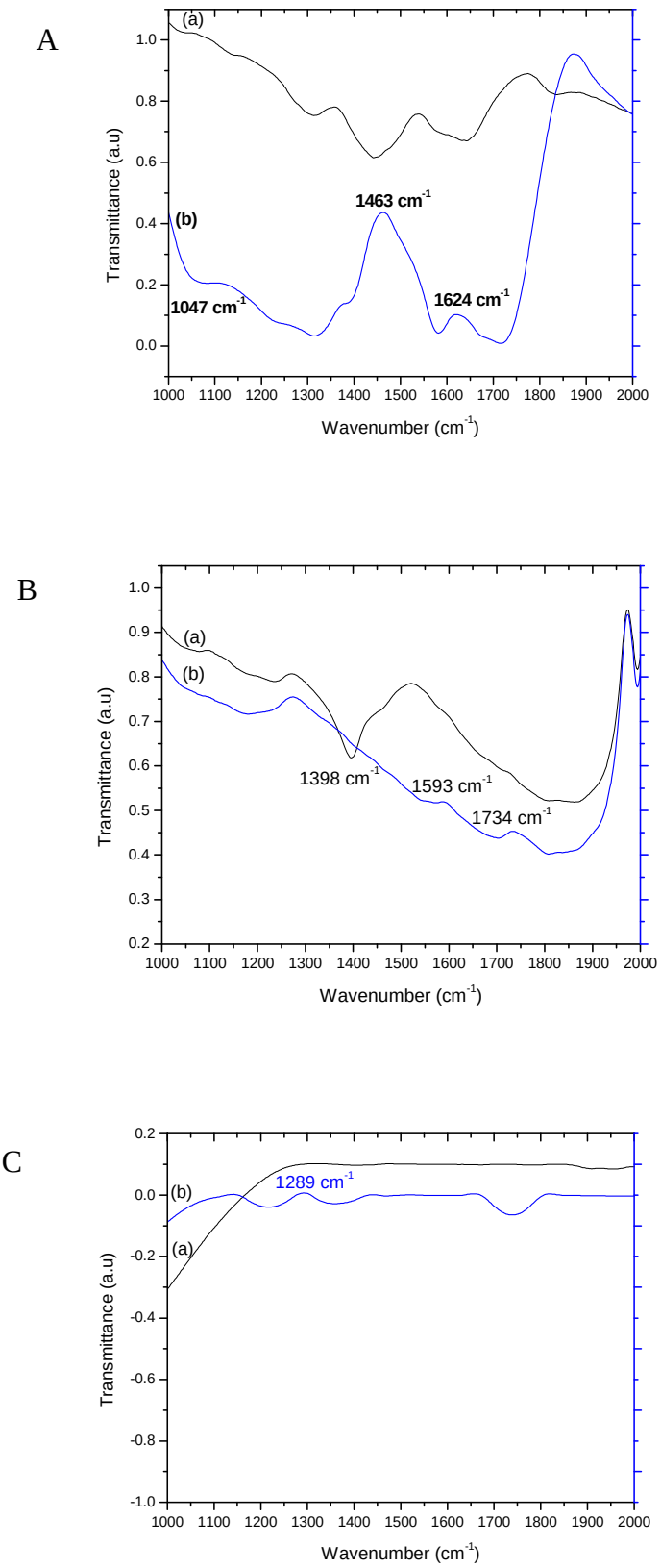

Figure 4.8. IR spectra of (A) CCNFs , (B) CNTs and (C) CSs with (a) as-synthesized (b) functionalized samples are shown in all the three figures

4.2.1.7 Surface area and pore volume measurements

Nitrogen adsorption at boiling temperature (77 K) is a technique that is used to determine the surface area of materials and to characterize their porous structure.[7] The surface area and pore volume of the catalyst supports are given in Table 4.4. The surface area and pore volume increased when the carbon materials were functionalized. This is attributed to the creation of defects by the action of acid. Both as-synthesized and functionalized CSs have low surface areas and negligible porosity (Table 4.4). The low surface area is a direct consequence of the spherical morphology, i.e. the sphere is the geometrical body with lowest exposed surface area per unit volume.[8]

Table 4.4: Surface area and pore volume of the catalyst supports

Sample ID	BET surface area[a] (m^2/g)	Pore volume (cm^3/g)
As-synthesized CCNFs	89	0.31
As-synthesized CNTs	80	0.27
As-synthesized CSs	7	0.02
CCNFs	94	0.34
CNTs	90	0.32
CSs	9	0.03
AC	688	0.41
CeO_2	76	0.40
0.5 % Pt/CCNF	113	0.41
0.5 % Pt/CNT	112	0.40
0.5 % Pt/CS	9	0.03
0.5 % Pt/AC	532	0.33
0.5 % Pt/CeO_2	71	0.28
0.5 % Pt- CeO_2/CCNF	115	0.42
Spent catalyst 0.5 % Pt-CeO_2/CCNF	115	0.41

a Error bar ± 2%

4.2.2 Characterization of ceria by TEM

Ceria was synthesized using the sol-gel method.[9] The ceria produced was characterized using TEM, in order to determine its morphology. Figure 4.9 shows the TEM image of a ceria sample. It was observed that the ceria produced was feather-like with rough edges. This property is ideal for ceria's function as a catalyst support. Mak et al[10] described the

morphology of ceria as that of a lamellar meso-structure due to the existence of “lines” on the structure of the ceria particles, as can also be seen in Figure 4.9.

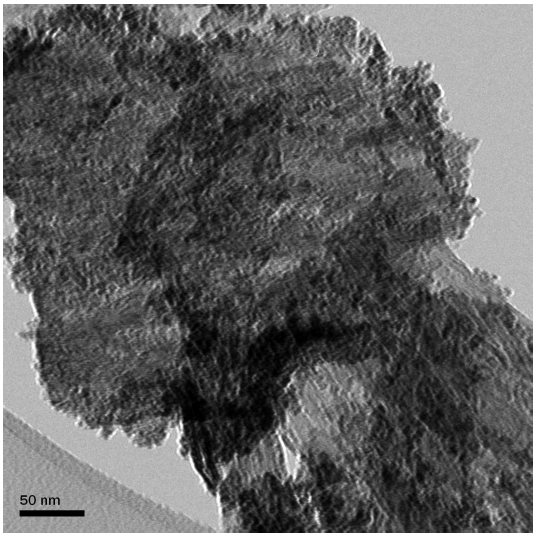

Figure 4.9. TEM image of ceria

4.2.3 Characterization of activated carbon and titania by TEM

Activated carbon (AC) and titania (Degussa P 25) were used as catalyst supports in this study. They were used as purchased without further treatment. Their morphology was characterized by TEM. Figure 4.10. shows the TEM images of AC and titania. The information that can be obtained from TEM of AC is its morphology (solid carbonaceous material); while titania possess cube like particles.

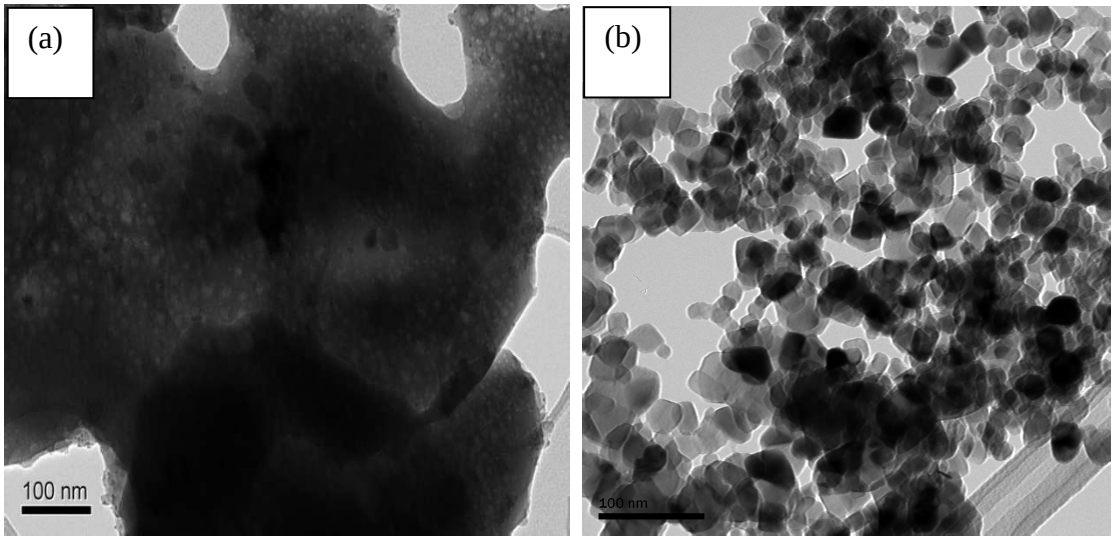

Figure 4.10. TEM images of (a) AC and (b) titania

4.3 Analysis of the Pt supported catalysts

Platinum was deposited on to the support materials using the polyol method. The synthesis method involves the reaction of hexachloroplatinic acid (Pt precursor) with the support materials in ethylene glycol (EG). When heat is supplied to EG, it decomposes to form reducing species. The reducing species (such as CH_3CHO) then reduce the metal ions to metal particles.[11]

4.3.1 Mechanism of polyol synthesis

The mechanism of polyol synthesis is illustrated in cartoon form in Figure 4.13. The carbon materials (Figure 4.11a) were first exposed to an oxidation environment where negatively charged groups are attached to the carbon (Figure 4.11b). The Pt^{4+} ions then diffused to these functional sites via electrostatic attraction to form nucleation sites (Figure 4.11c). At high temperature EG decomposes to form reducing species which in turn reduces Pt^{4+} to Pt^0. The metallic grains formed further agglomerate to form nanoparticles (Figure 4.11d).

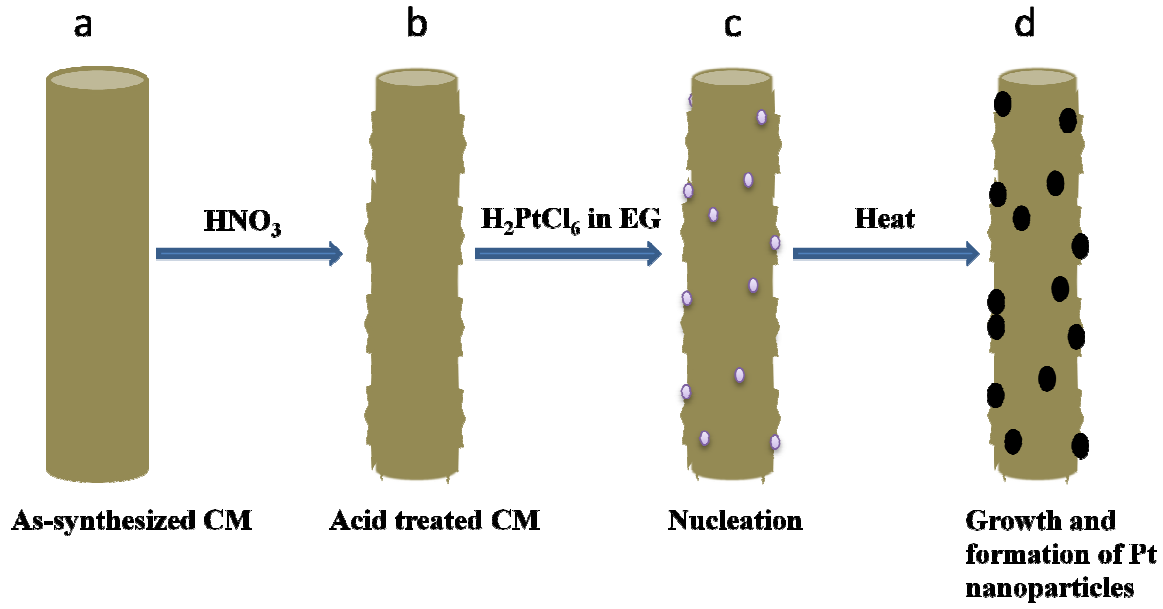

Figure 4.11. Schematic representation of the mechanism behind the polyol synthesis method

The mechanism for the deposition of Pt on other supports (ceria, AC, titania) is the same except that the reaction does not require an acid treatment step.

4.3.2 Formation of Pt: UV-vis spectroscopy

The UV-vis spectra of H_2PtCl_6 in ethylene glycol was recorded and the reduction process was monitored through measurement of the Pt absorbance at different times (Figure 4.12). The solution of a mixture of hexachloroplatinic acid, ethylene glycol and water exhibited a peak at 260 nm (Figure 4.12a). For a 0.5 % Pt loading, the solution was placed in a microwave oven for 1 minute and the solution analyzed by UV-vis spectroscopy; the peak intensity decreased (Figure 4.12b). The solution was then exposed to another 1 minute in the microwave oven. The spectrum recorded showed that the Pt peak at 260 nm disappeared completely (Figure 4.12c). Luo and Sun[12] attributed the disappearance of the Pt peak in a related study to the reduction of the $PtCl_6^{2-}$. This indicates the complete reduction of Pt^{+4} to Pt^0. Therefore 2 minutes was enough to reduce Pt ions and Pt nanoparticles in the samples under study.

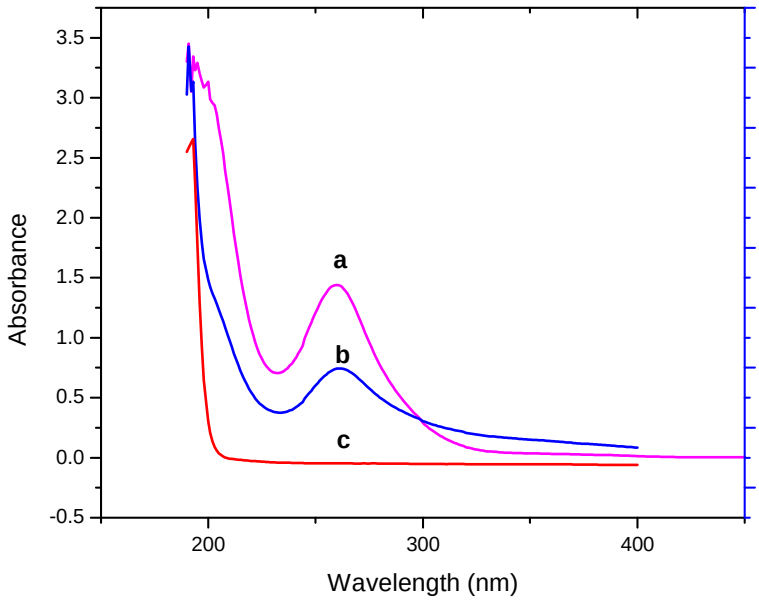

Figure 4.12. UV-vis spectra of 0.5 % loading of Pt (a) before reduction, (b) after 1 minute in the microwave oven and (c) 2 after minutes in the microwave oven.

4.4 0.5 % Pt loaded catalysts.

Platinum was loaded on the as-synthesized and functionalized carbon materials (CCNFs, CSs and CNTs), activated carbon (AC), ceria and titania. The platinum supported catalysts were

characterized by TEM. These catalysts were denoted as Pt/CCNF, Pt/CNT, Pt/CS, Pt/AC, Pt/CeO_2 and Pt/TiO_2.

4.4.1 TEM analysis for the 0.5 % Pt loaded on to the as-synthesized CMs

Figure 4.13 shows the TEM images of Pt loaded onto the as-synthesized CCNFs, CSs and CNTs. From the TEM images it can be observed that the Pt nanoparticles were well dispersed despite the occurrence of some impurities in the CCNF (Figure 4.13a). A possible explanation for the good deposition of Pt is that the materials have a highly disordered surface as shown from the TGA plot in Figure 4.6a. On the other hand the TEM images of the as-synthesized CNTs and CSs showed that Pt was barely visible. This indicates that some of the Pt nanoparticles were not adsorbed onto as-synthesized CNTs and CSs. This observation was not a surprise because the samples of the filtrates collected for Pt/CCNF, Pt/CS and Pt/CNT showed the existence of dark solutions for Pt/CS and Pt/CNT (Figure 4.14b and c). A possible explanation for this is that Pt nanoparticles (black) are in solution because the attraction between carbon and Pt is low as the carbon materials are hydrophobic in nature. An almost colourless solution for Pt/CCNF (Figure 4.14a) is observed implying that most of the Pt nanoparticles have been adsorbed onto the CCNF.

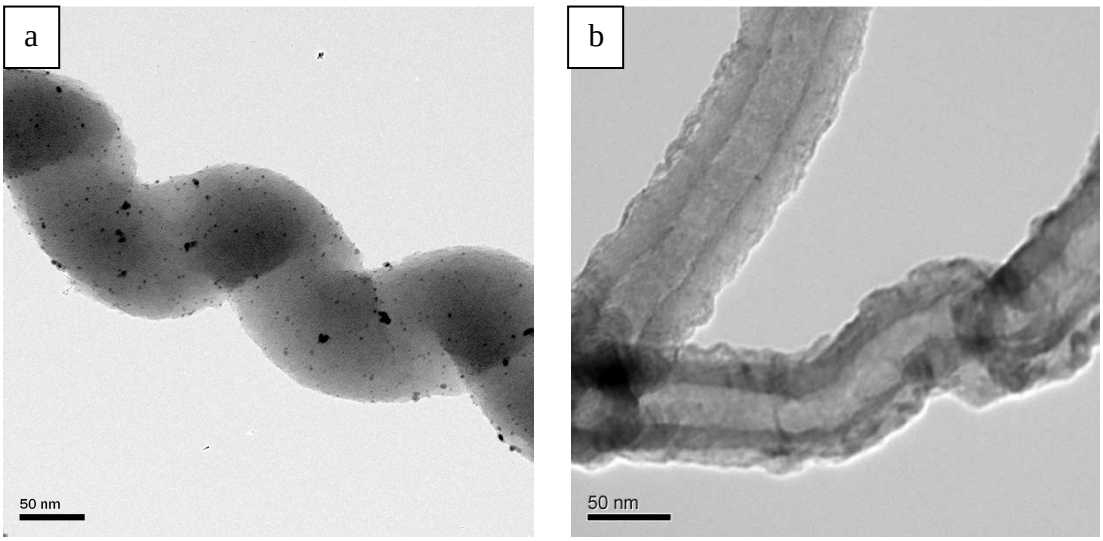

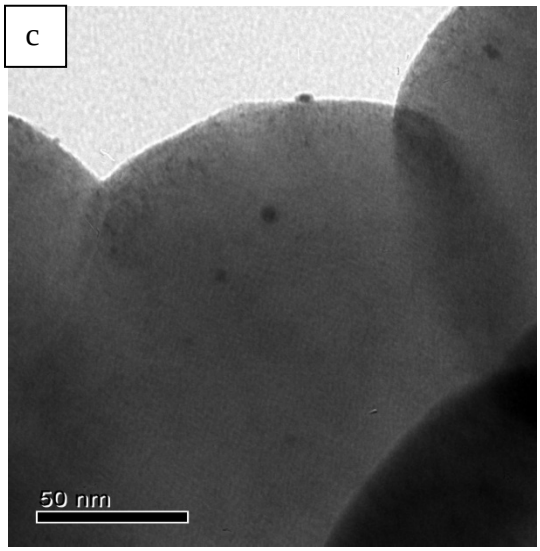

Figure 4.13. Pt loaded to the as-synthesized (a) CCNFs, (b) CNTs and (c) CSs

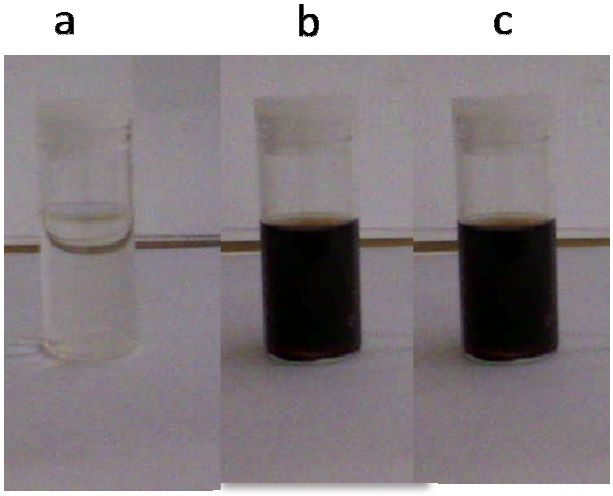

Figure 4.14. Filtrates obtained from (a) Pt/CCNF, (b) Pt/CNT and Pt/CS

4.4.2 TEM analysis for the 0.5 % Pt loaded catalysts (polyol method)

Representative TEM micrographs of 0.5 % Pt supported catalysts (and their corresponding histograms) prepared by microwave heating methods are shown in Figure 4.15. It can be observed that the different supports have different sizes of Pt. Titania has the smallest particle size of Pt particles with a mean of 1.6 nm and AC has the largest particle size of Pt, with a mean of 2.9 nm. The histograms indicate that Pt has a narrow distribution range on the various supports. A summary table with mean sizes of Pt on the various supports is presented in Table 4.5.

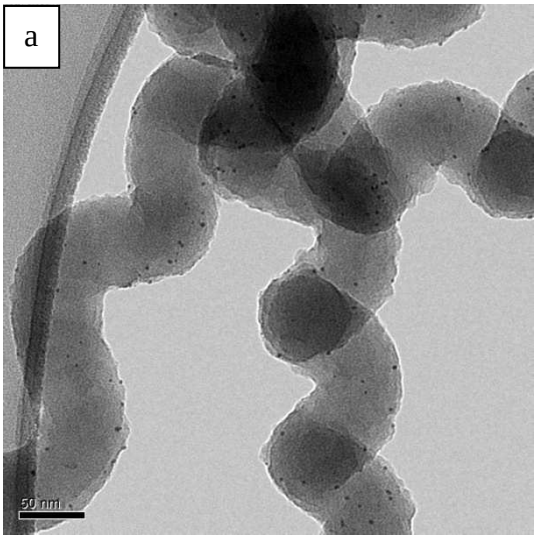
a
50 nm

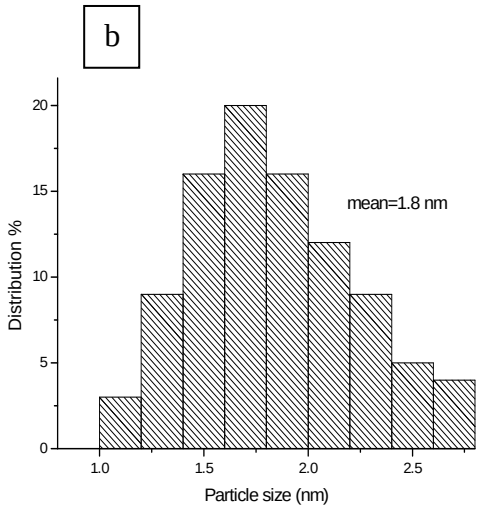
b
Distribution %
Particle size (nm)
mean=1.8 nm
0
5
10
15
20
1.0
1.5
2.0
2.5

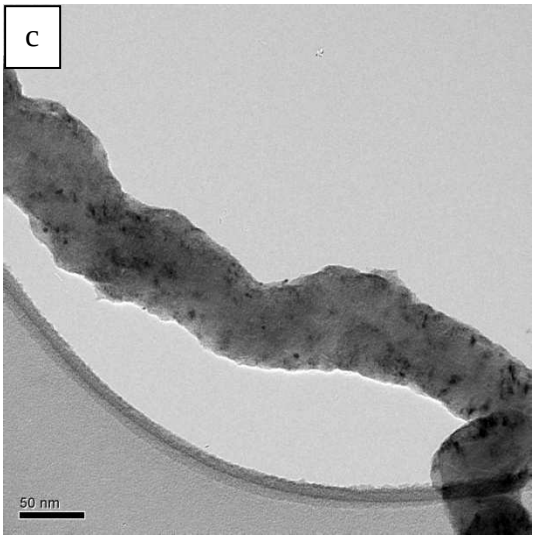
c
50 nm

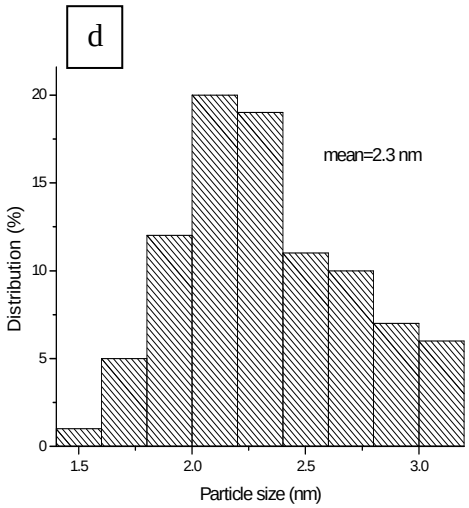
d
Distribution (%)
Particle size (nm)
mean=2.3 nm
0
5
10
15
20
1.5
2.0
2.5
3.0

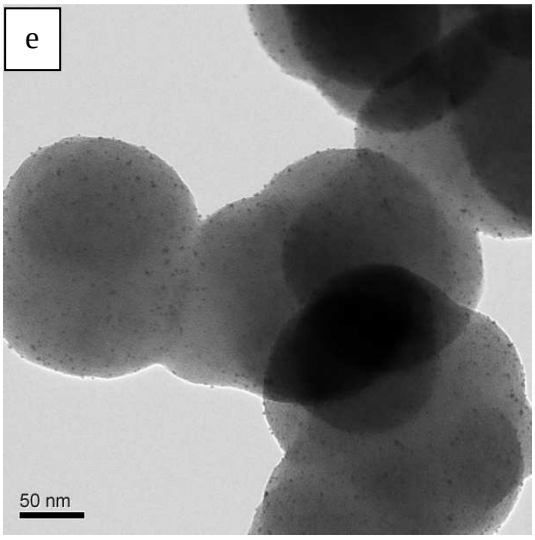
e
50 nm

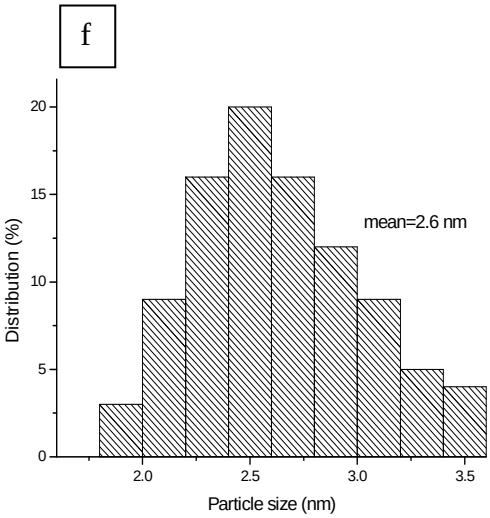
f
Distribution (%)
Particle size (nm)
mean=2.6 nm
0
5
10
15
20
2.0
2.5
3.0
3.5

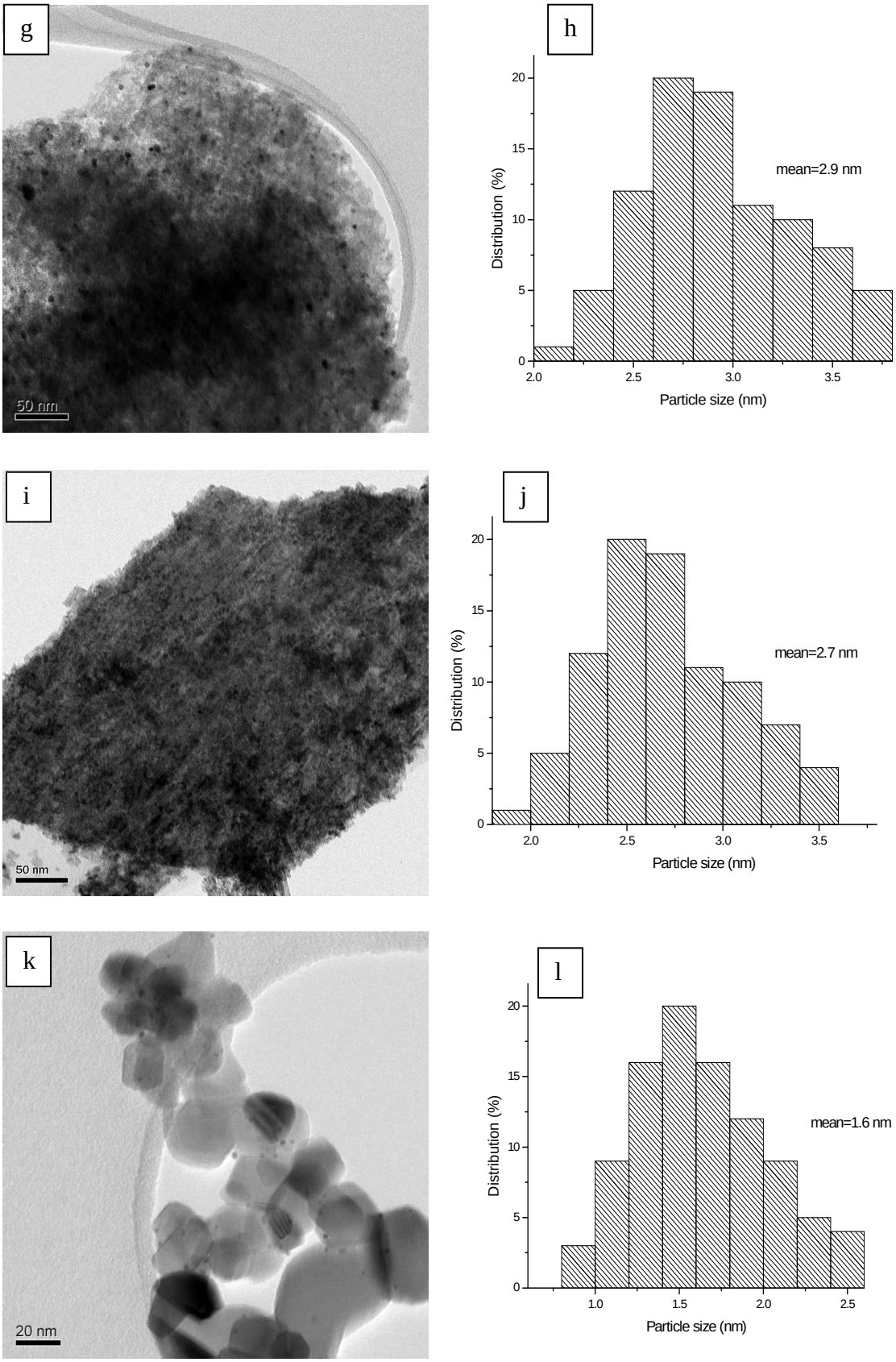

Figure 4.15. TEM images and size distributions of 0.5 % Pt supported on (a) and (b) CCNF; (c) and (d) CNT; (e) and (f) CS; (g) and (h) AC; (i) and (j) CeO_2; (k) and (l) TiO_2.

Table 4.5: Summary table of the mean particle size of catalyst with different Pt loading.

Catalyst	Mean particle size (nm)		
	0.5 % Pt loading	1 % Pt loading	5 % Pt loading
Pt/CCNF	1.8	2.5	3.8
Pt/CNT	2.3	3.0	4.3
Pt/CS	2.6	3.3	4.6
Pt/AC	2.9	3.6	6.9
Pt/CeO_2	2.7	3.4	5.0
Pt/TiO_2	1.6	2.3	3.3

Error bar= 1 %

4.4.3 Determination of presence of Pt in the catalyst.

The EDS analysis confirmed the presence of platinum in the catalyst sample 0.5 % Pt/CCNF. Figure 4.16 shows the EDS spectrum of 0.5 % Pt/CCNF. The copper that is observed in the spectrum is due to the copper grid.

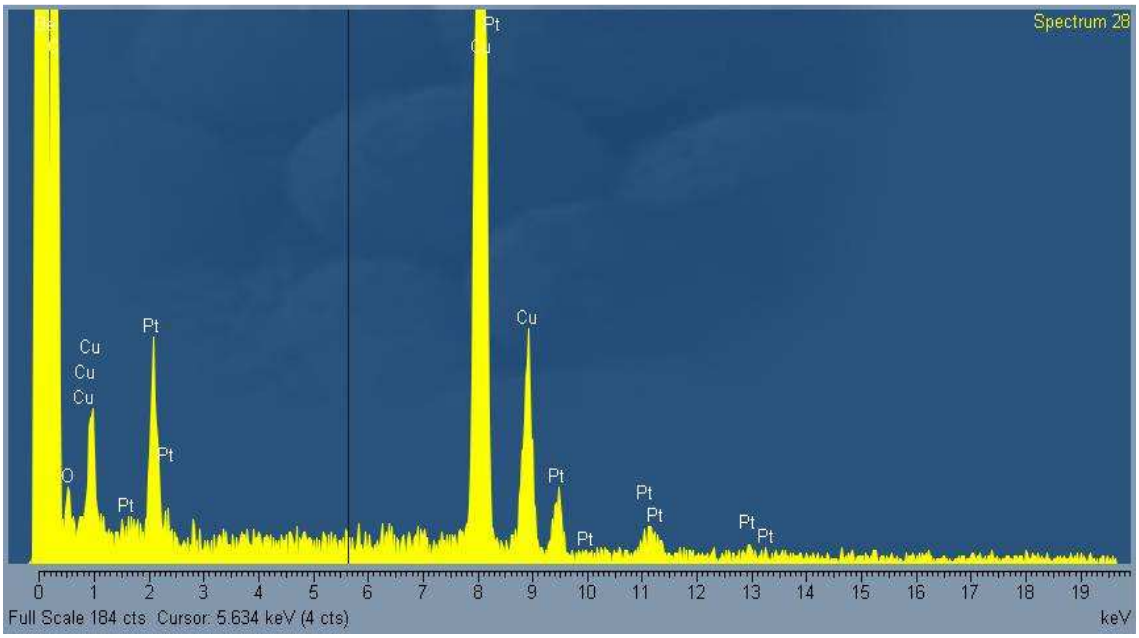

Figure 4.16. EDS spectra of Pt/CCNF

The Pt quantification was achieved by ICP AES. The results of the analysis ascertained the loading of Pt in the catalysts. Table 4.6 shows the metal loading in the catalysts and that they agree with the expected loadings. This contrast with the Pt loading on the as-synthesized CMs.

Table 4.6: Pt loading in the catalysts obtained from ICP AES analysis

Catalysts	Theoretical	Pt/CCNF	Pt/CNT	Pt/CS	Pt/AC	Pt/CeO_2	Pt/TiO_2
Pt loading (%)	0.5	0.5	0.5	0.5	0.5	0.5	0.5
Pt loading (%)	1.0	1.0	1.1	1.0	1.2	1.0	1.0
Pt loading (%)	5.0	5.1	5.0	5.0	5.1	5.1	5.0

4.4.4 Surface area and pore volume measurements of 0.5% Pt catalysts

The BET surface areas were measured for the 0.5 % Pt supported catalysts and the results are presented in Table 4.4. The BET surface areas have increased with Pt loading for CCNFs, CNTs and CSs. This is attributed to the absence of micropores which can get blocked and reduce the BET surface area. Pt/CS with low surface area and low total pore volume did not experience any appreciable change upon Pt introduction. The BET surface area of ceria and AC decreased with Pt introduction. This is attributed to a partial pore blockage by the Pt particles.

4.5 1 % Pt loaded catalysts

The Pt nanoparticles were synthesized using the microwave polyol method and Pt was successfully loaded onto five different catalyst supports (CNTs, CSs, AC, ceria and titania). Figure 4.17 shows the TEM images of the Pt supported on the different catalyst supports. The mean sizes are 2.5, 3.0, 3.3, 3.6, 3.4 and 2.3 nm for Pt supported on CCNF, CNT, CS, CeO_2, AC and titania respectively. The microwave heated polyol synthesis is hence effective in depositing small platinum particles on the support. Data are shown in Table 4.5. In all cases the Pt particle size has increased with loading.

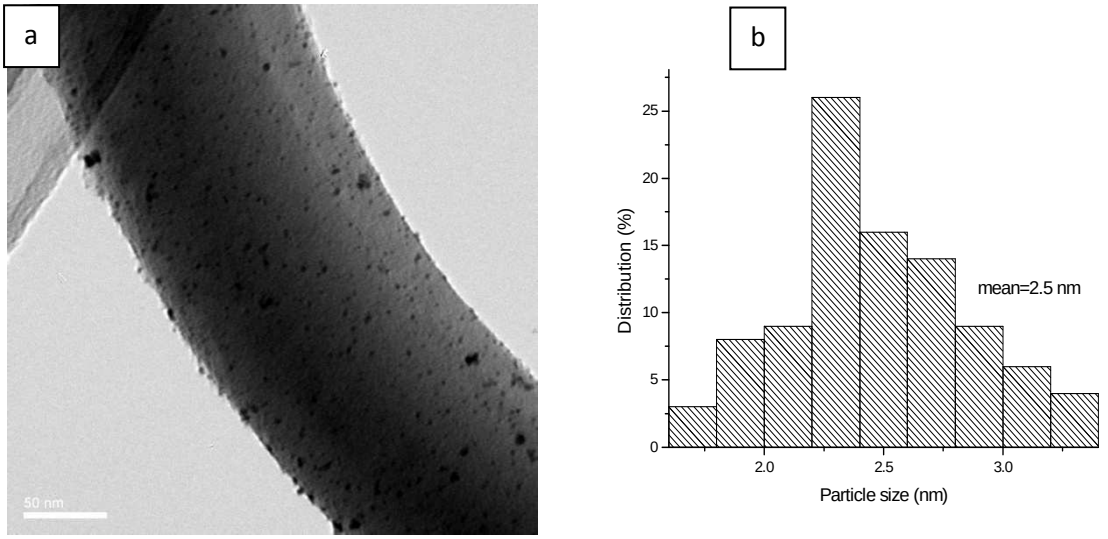

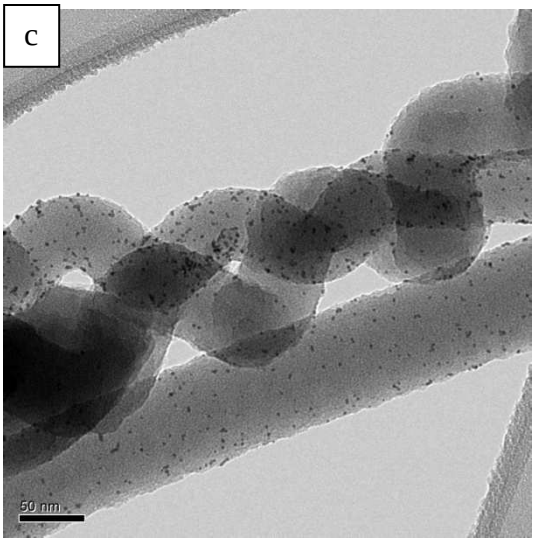
c
50 nm

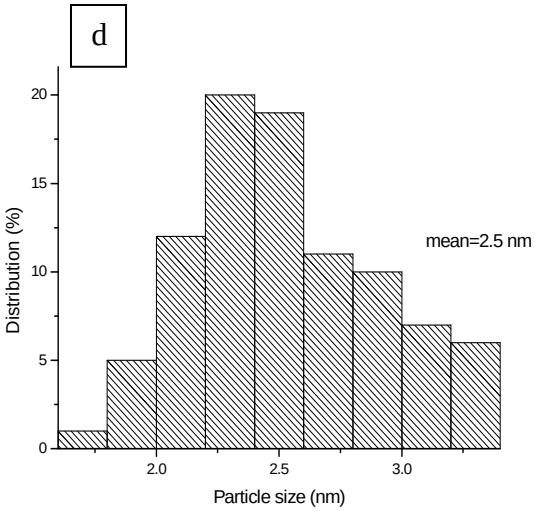
d
Distribution (%)
Particle size (nm)
mean=2.5 nm
0
5
10
15
20
2.0
2.5
3.0

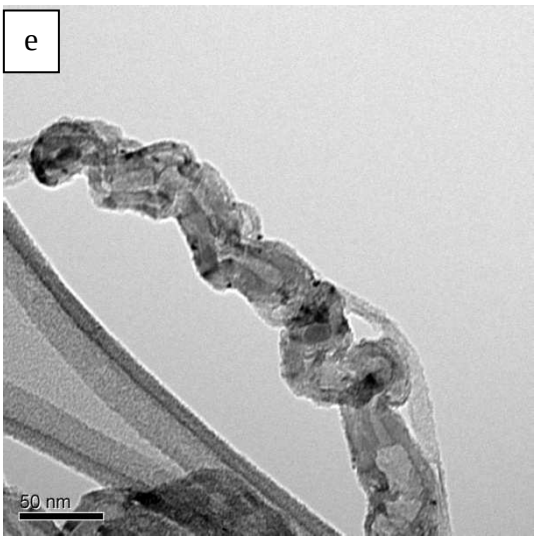
e
50 nm

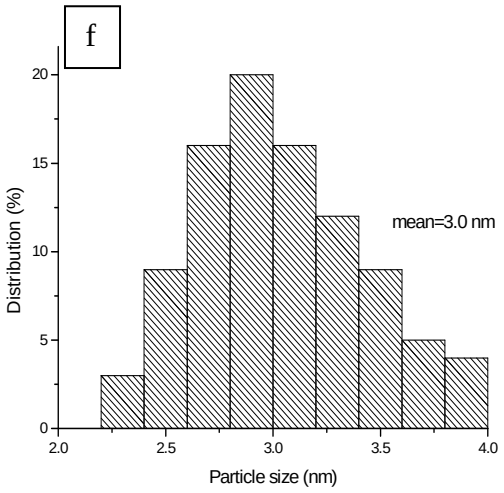
f
Distribution (%)
Particle size (nm)
mean=3.0 nm
0
5
10
15
20
2.0
2.5
3.0
3.5
4.0

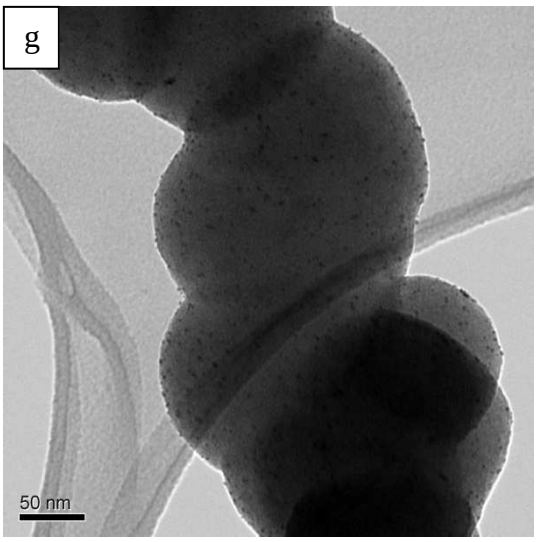
g
50 nm

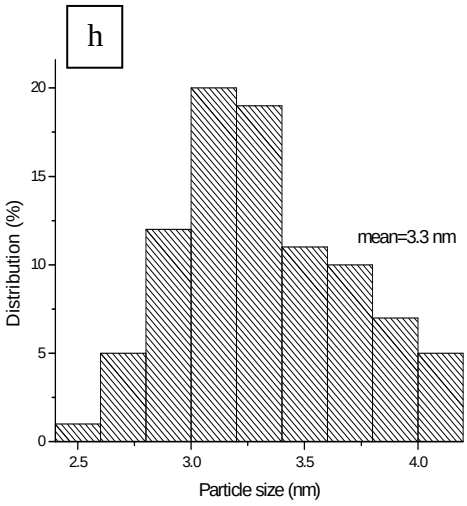
h
Distribution (%)
Particle size (nm)
mean=3.3 nm
0
5
10
15
20
2.5
3.0
3.5
4.0

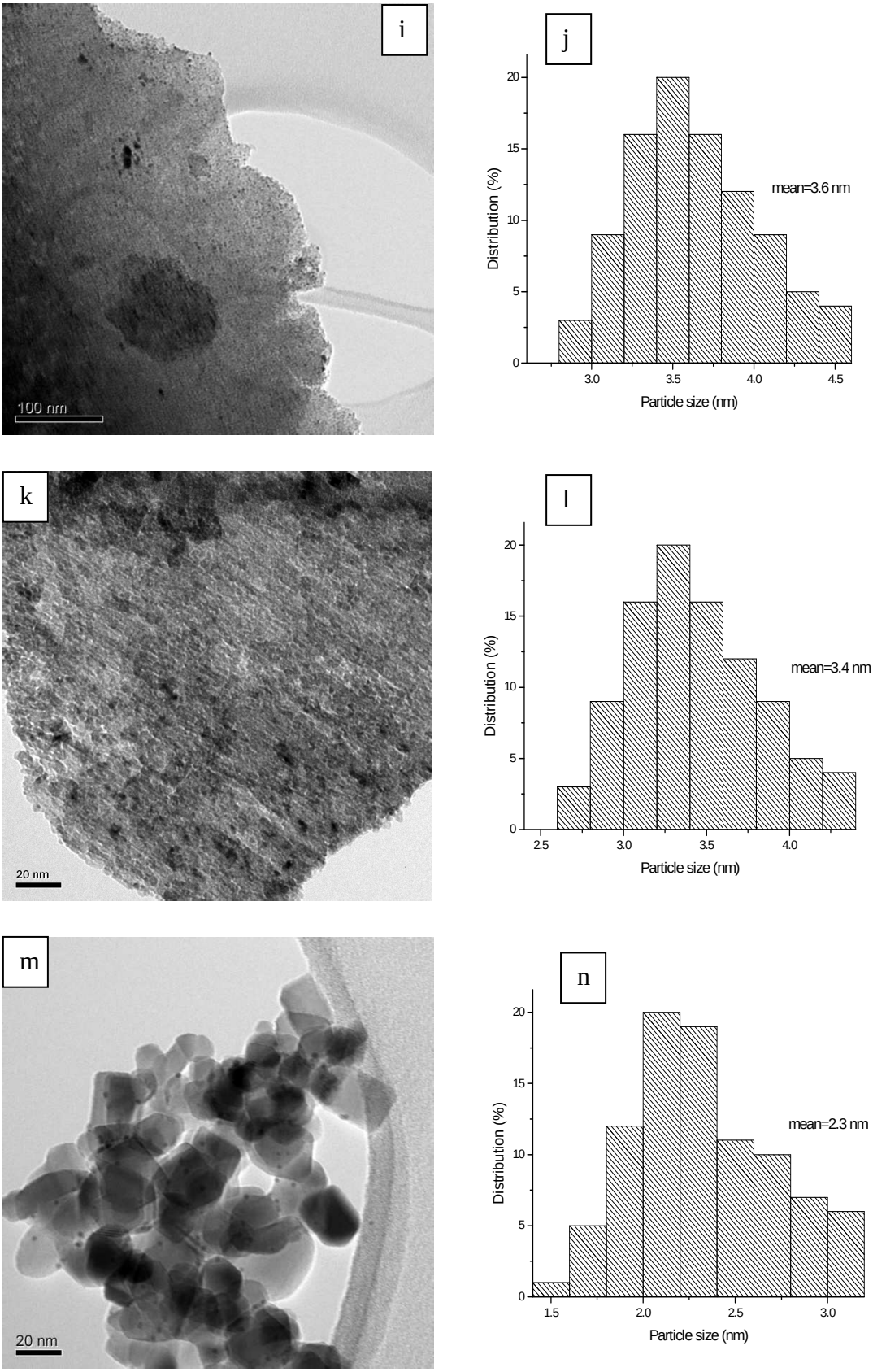

Figure 4.17. TEM images and size distributions of 1 % Pt supported on (a) and (b) CCNF prepared by conventional heating and the rest were prepared by microwave heating; (c) and (d) CCNF; (e) and (f) CNT; (g) and (h) CS; (i) and (j) AC; (k) and (l) CeO_2; (m) and (n) TiO_2.

4.5.1 Microwave versus conventional heating

Different heating methods were used to prepare 1 and 5 % loading of Pt/CCNFs. A summary of the comparison between particles formed using either microwave or conventional heating method is presented in Table 4.7. It can be seen that the conventional method and the microwave heating method both produce similar Pt size distributions. This is surprising since in the conventional method, stirring is continuous until the experiment is performed while in the microwave oven there is no stirring. Despite the lack of differences, the microwave method offers uniformity, speed, energy efficiency and implementation simplicity.[13]

Table 4.7: Comparison of the mean particle size obtained using different heating method

Heating method	Pt loading (%)	Mean particle size (nm)
Microwave	1	2.5
	5	3.8
Conventional (reflux)	1	2.5
	5	3.6

Error bar ± 0.8 nm

4.6 5 % Pt loaded catalysts

Platinum was deposited on CCNF, CNT, CS, AC, ceria and titania using the polyol method. These samples have a metal loading of 5 %. TEM micrographs of the supported Pt catalysts are presented in Figure 4.18. The corresponding histogram are also shown in Figure 4.18, they show a narrow distribution of Pt on the various supports (see also Table 4.5). The comparison of the heating methods is also given for Pt/CCNFs. The conventional heating has a mean Pt size of 3.6 nm whilst the microwave heating has a mean Pt size of 3.8 nm. In conclusion microwave heating is a better choice as it produces roughly the same size of particles as conventional heating at a faster rate with energy efficiency.

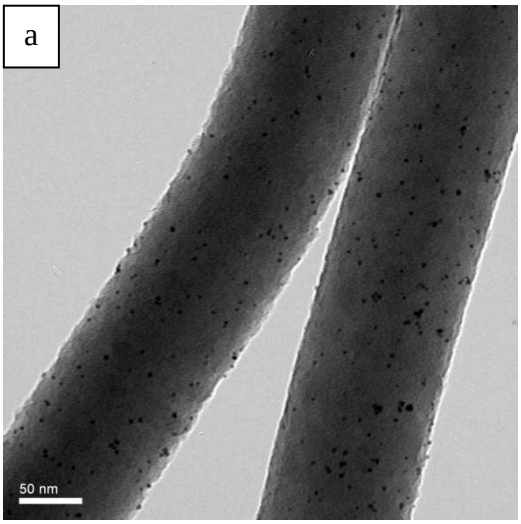
a
50 nm

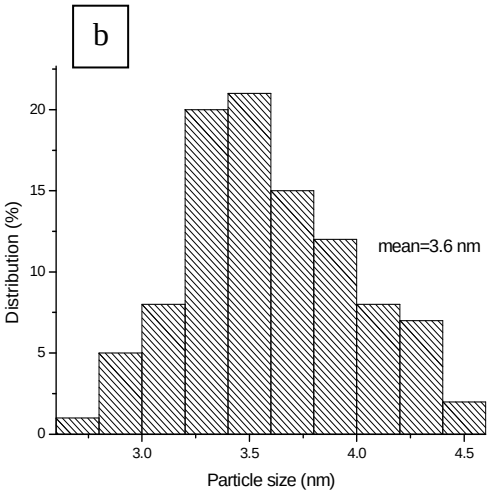
b
Distribution (%)
Particle size (nm)
mean=3.6 nm
0
5
10
15
20
3.0
3.5
4.0
4.5

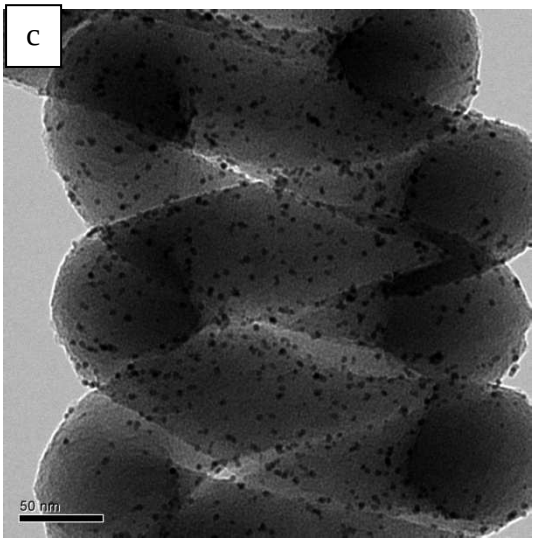
c
50 nm

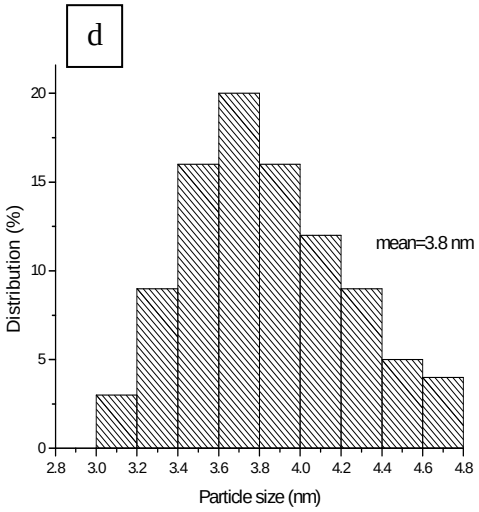
d
Distribution (%)
Particle size (nm)
mean=3.8 nm
0
5
10
15
20
2.8
3.0
3.2
3.4
3.6
3.8
4.0
4.2
4.4
4.6
4.8

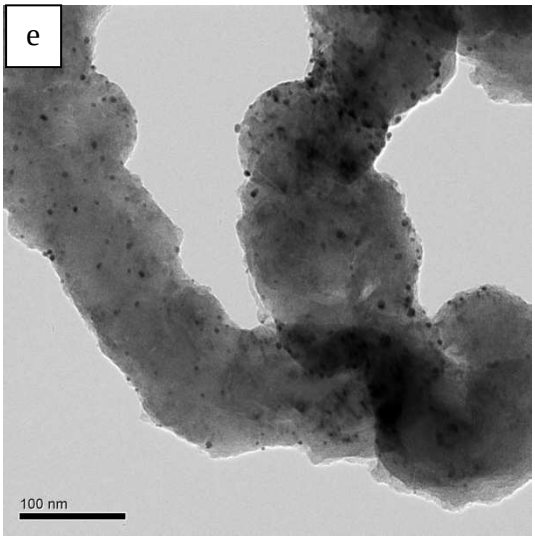
e
100 nm

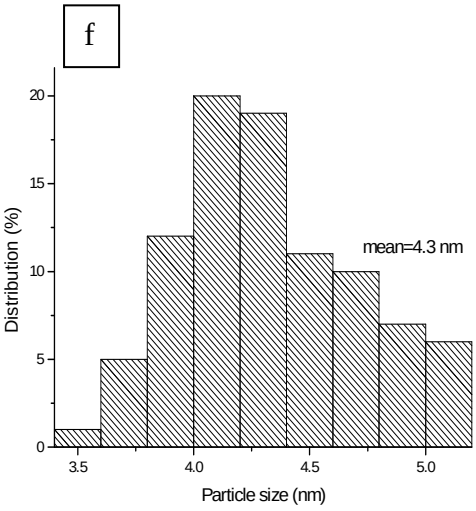
f
Distribution (%)
Particle size (nm)
mean=4.3 nm
0
5
10
15
20
3.5
4.0
4.5
5.0

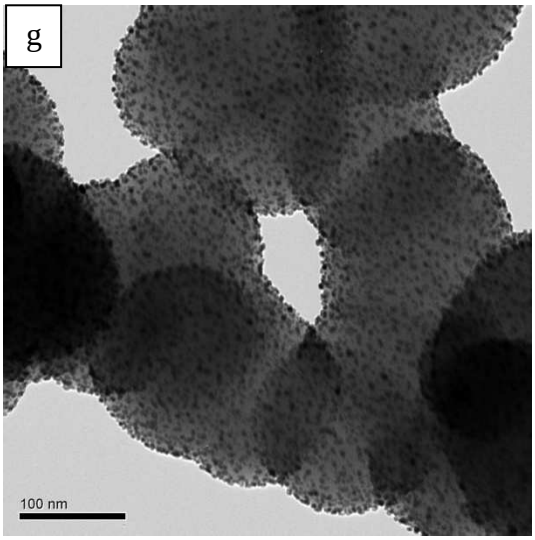
g
100 nm

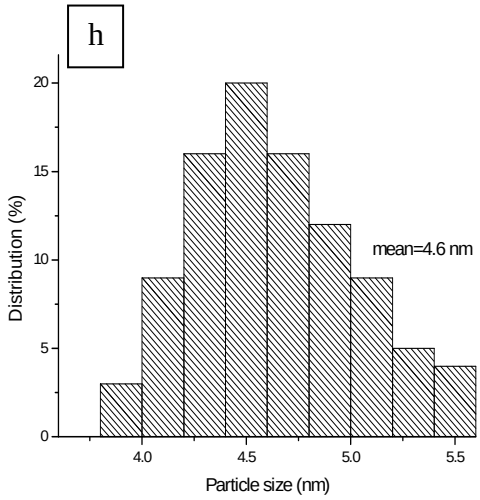
h
Distribution (%)
Particle size (nm)
mean=4.6 nm
0
5
10
15
20
4.0
4.5
5.0
5.5

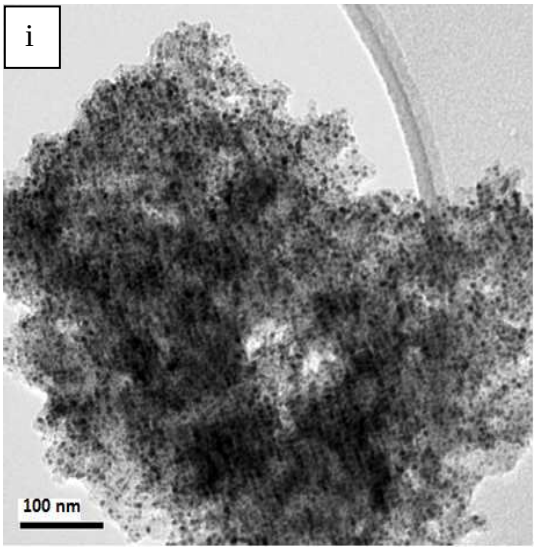
i
100 nm

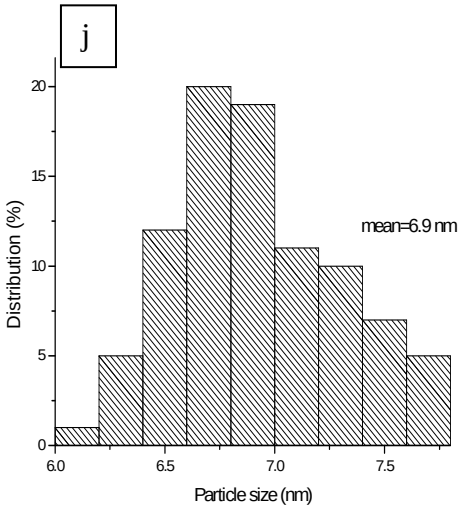
j
Distribution (%)
Particle size (nm)
mean=6.9 nm
0
5
10
15
20
6.0
6.5
7.0
7.5

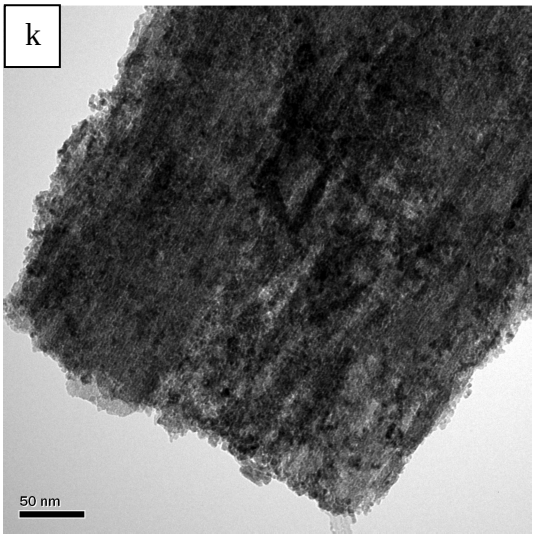
k
50 nm

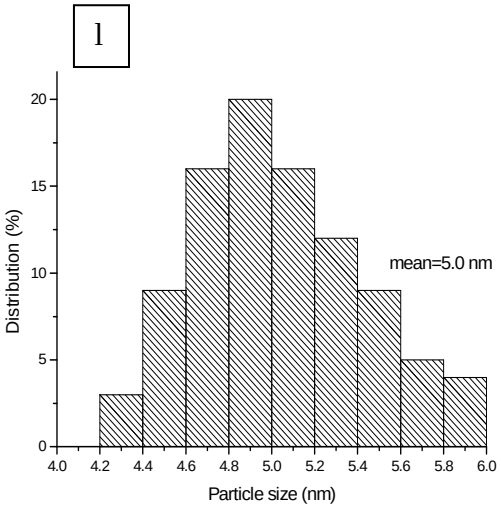
l
Distribution (%)
Particle size (nm)
mean=5.0 nm
0
5
10
15
20
4.0
4.2
4.4
4.6
4.8
5.0
5.2
5.4
5.6
5.8
6.0

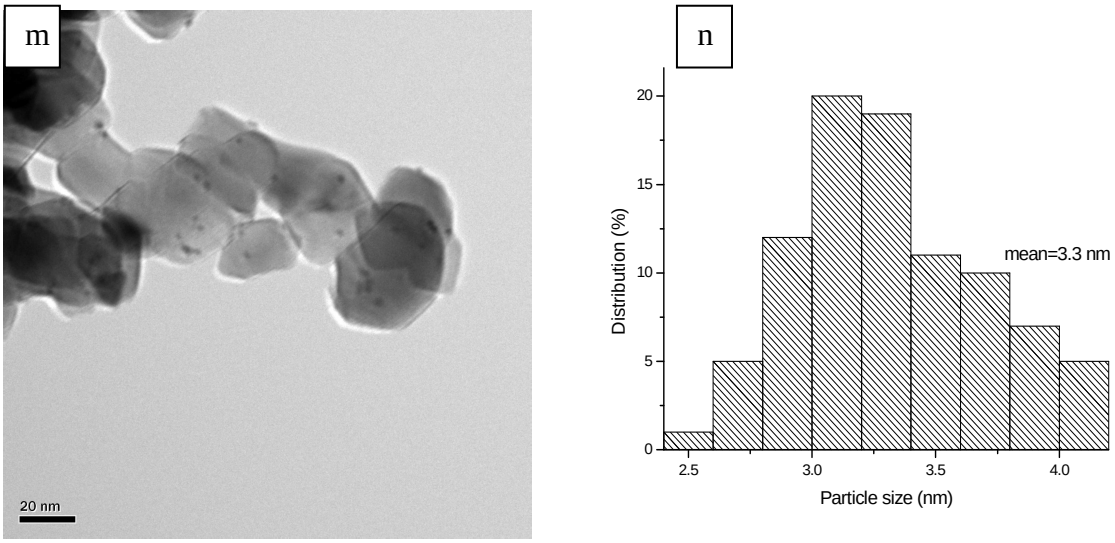

Figure 4.18. TEM images and size distributions of 5 % Pt supported on (a) and (b) CCNFs prepared by conventional heating and the rest were prepared by microwave heating; (c) and (d) CCNFs; (e) and (f) CNTs; (g) and (h) CSs; (i) and (j) AC; (k) and (l) CeO_2; (m) and (n) TiO_2.

4.6.1 Effect of loading on the particles size

There is a general trend that can be observed in Table 4.5 in terms of the relationship of particle size to metal loading i.e. an increase in metal loading results in an increase in the size of the Pt nanoparticles. The mean Pt particle size followed a similar trend, for example, 0.5 % Pt/CCNFs have a mean size of 1.8 nm while the 5 % Pt/CCNF had a mean size of 3.8 nm. Knupp et al[5] obtained a similar trend for the effect of increasing metal loading on the size of Pt particles and they suggested that it was due to the fact that when the loading is increased, agglomeration is more apparent and large particles begin to form. The mean Pt nanoparticle size thus gets larger.

4.6.2 Temperature programmed reduction

Temperature programmed reduction (TPR) analysis was done prior to any further reduction treatment to determine whether the Pt catalyst (Pt/CS, Pt/CCNF and Pt/CNT) was already in its reduced state. The TPR profiles of Pt/CS, Pt/CCNF and Pt/CNT (5 % loading) after synthesis and drying are depicted in Figure 4.19. Plomp and co-workers[14] state that the reduction of Pt occurs between 177 and 302 ^{o}C. Figure 4.19 clearly showed that there is no peak in that temperature range. This indicates that Pt on CSs, CCNFs and CNTs were successful reduced using the microwave assisted polyol synthesis. The profile at temperature above 500 ^{o}C is ascribed to the gasification of the supports. The gasification of the support

can result in the formation of methane. Methane is formed under the hydrogenation conditions when temperatures are above 427 ^{o}C.[15] At high temperature, methane could decompose to generate carbon deposits on the CCNFs. This is due to the fact that the CCNFs were synthesized at low temperature (250 ^{o}C). Thus a high temperature could result in the graphitization of the materials. TEM was used to confirm the material deposited on to the CCNF was carbon as shown in Figure 4.20.

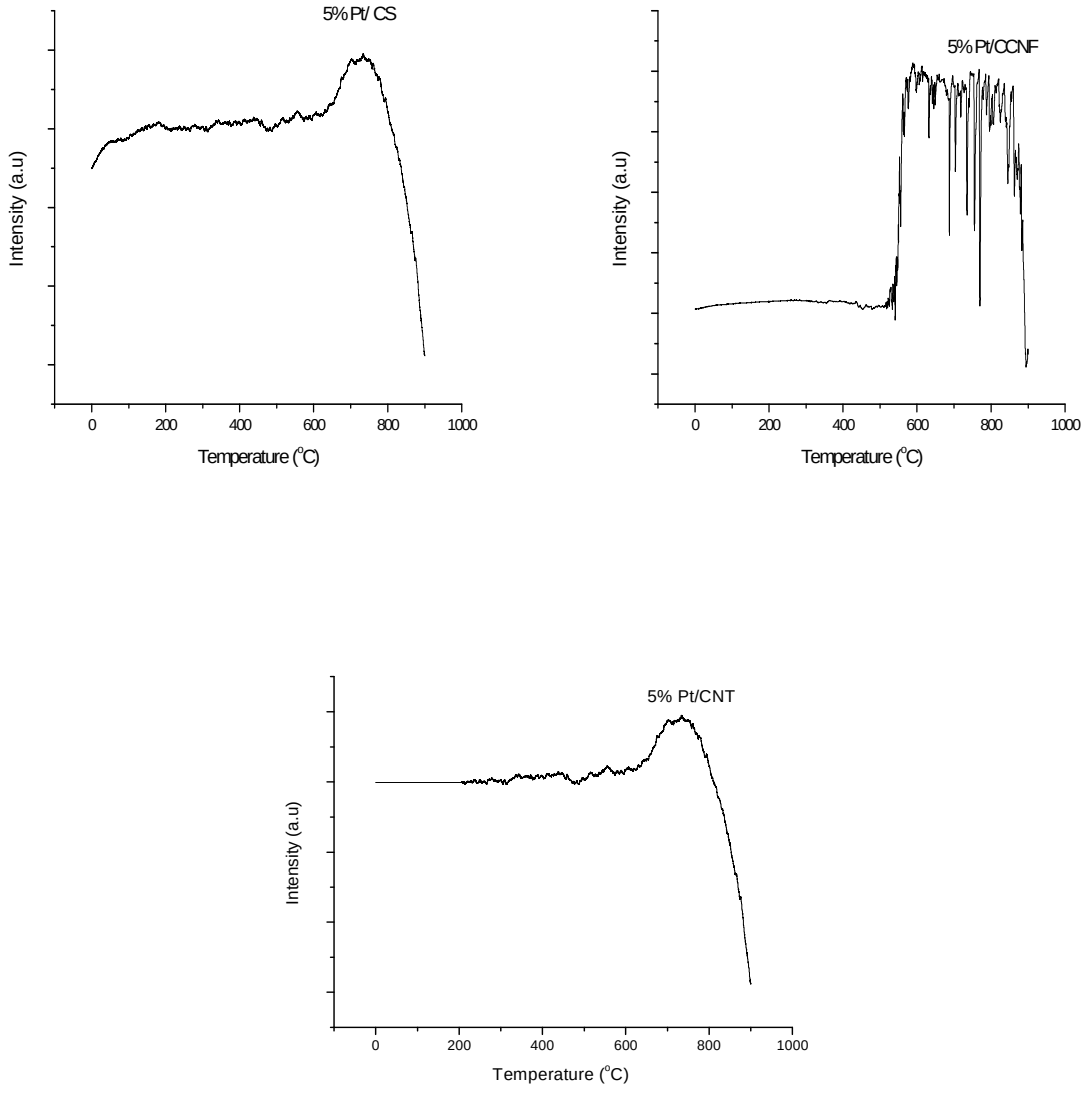

Figure 4.19. TPR profile of (a) Pt/CS, (b) Pt/CCNF and (c) Pt/CNT

From the TEM image, the morphology of the deposited carbon material seems to suggest the formation of carbon spheres which are accreted.

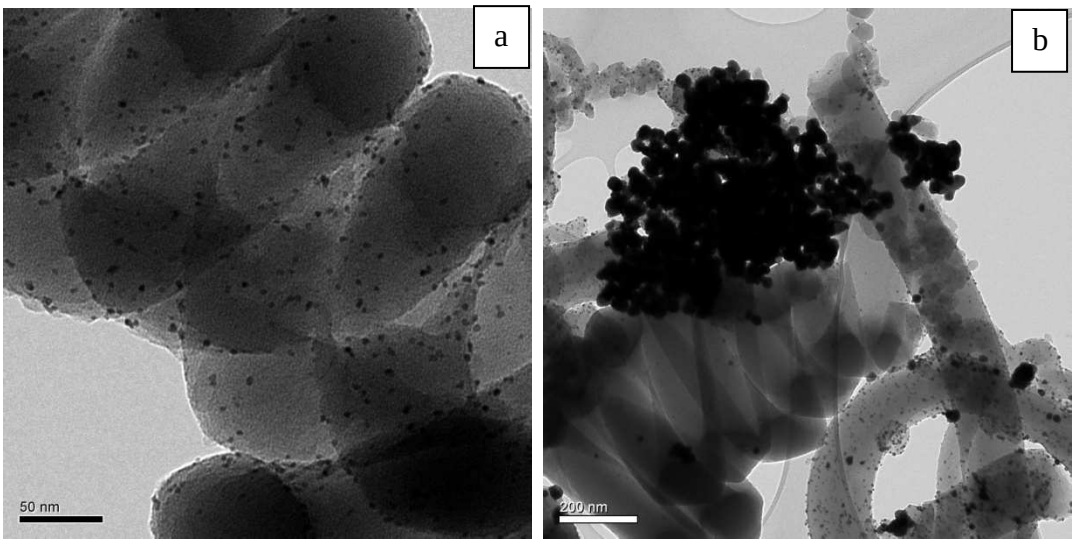

Figure 4.20. TEM image of Pt/CCNF (a) before and (b) after TPR analysis

TPR was also used to obtain information about the onset of reduction of the ceria and the Pt/CeO_2. The significance of the information is to help to control the eventual hydrogenation parameters of the catalyst. Figure 4.21 shows the TPR profiles of ceria and Pt/CeO_2. From Figure 4.20, ceria shows a peak at 475 ^oC which corresponds to the reduction of ceria particles from Ce^{4+} to Ce^{3+}. This is in agreement with studies reported by Zhang and co-workers[16] who stated that the reduction of ceria occurs at 475 ^oC. When Pt was introduced on to the surface of ceria, the reduction of ceria shifted to lower temperatures (367 ^oC). This indicates that the reduction of ceria is effectively promoted by Pt. This is attributed to the ability of Pt to activate H_2 and spill it over to the support. For catalytic purposes, the working temperature should be below 300 ^oC to avoid the effect of this CeO_2 reduction.

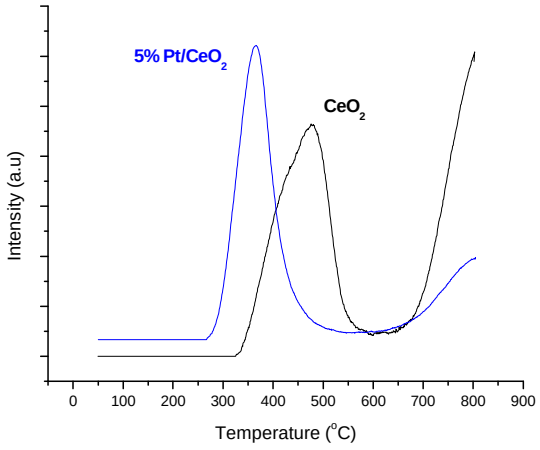

Figure 4.21. H_2-TPR profile of Pt/CeO_2 and CeO_2

4.6.3 X-ray diffraction studies on Pt supported catalysts

X-ray diffraction (XRD) was done to determine the phases in the Pt supported catalysts. XRD spectra of the standard Pt peaks are located at 39^{o} (111), 46^{o} (200), 67^{o} (220) and 81^{o} (311).[17] The peaks indicate that the Pt nanoparticles produced are face centred cubic. The XRD patterns for the CM and Pt/CM are presented in Figure 4.22.

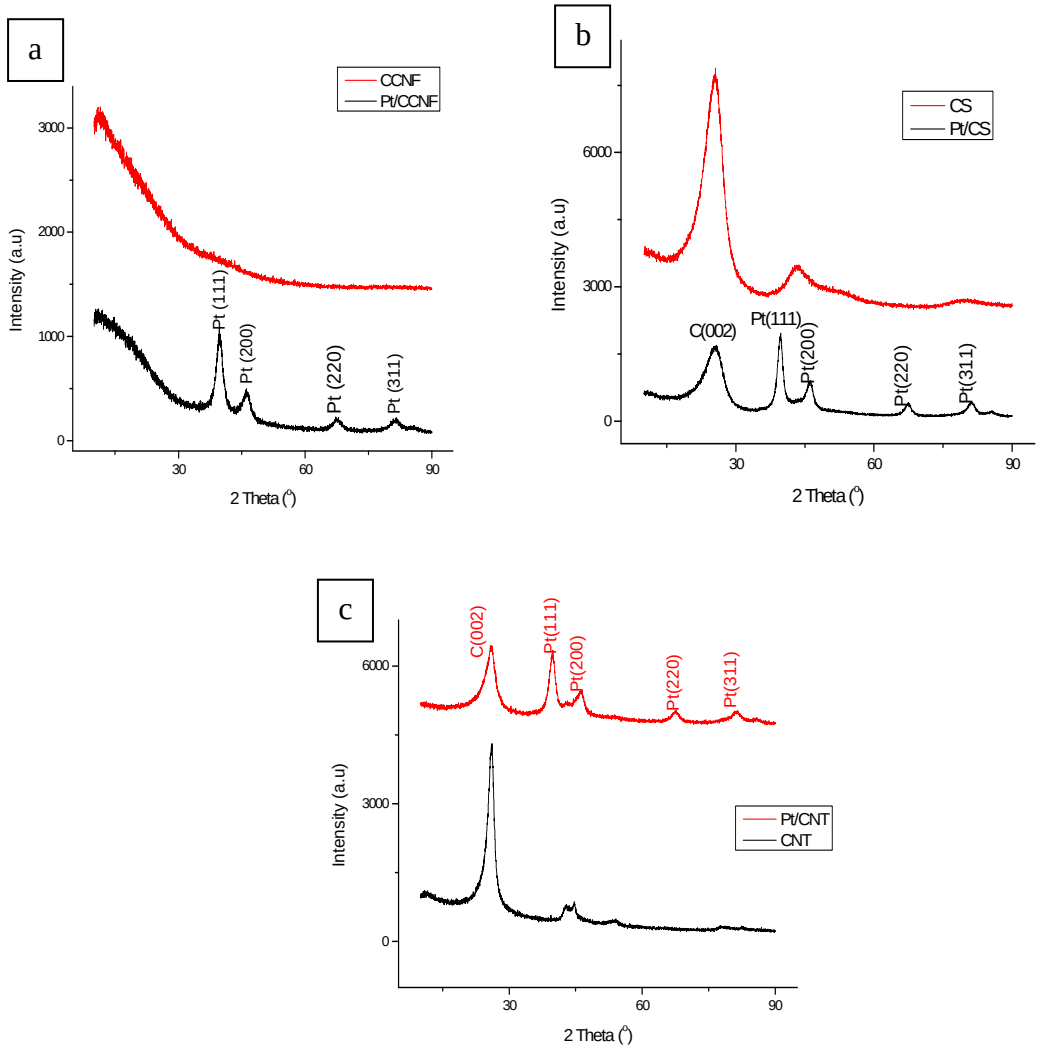

Figure 4.22. XRD patterns of (a) CCNF and Pt/CCNF, (b) CS and Pt/CS and (c) CNT and Pt/CNT

The CCNF is amorphous since it did not show a carbon graphite peak at 25.5 ^{o} (Figure 4.22a) while both CS and CNT possessed this peak at 25.5^{o} indicating that they are more crystalline. All the Pt peak positions suggest that it is crystalline with a face centred cubic structure.

XRD spectra were also recorded for AC, ceria, titania, Pt/AC, Pt/CeO_2 and Pt/TiO_2. The XRD spectra are presented on Figure 4.23.

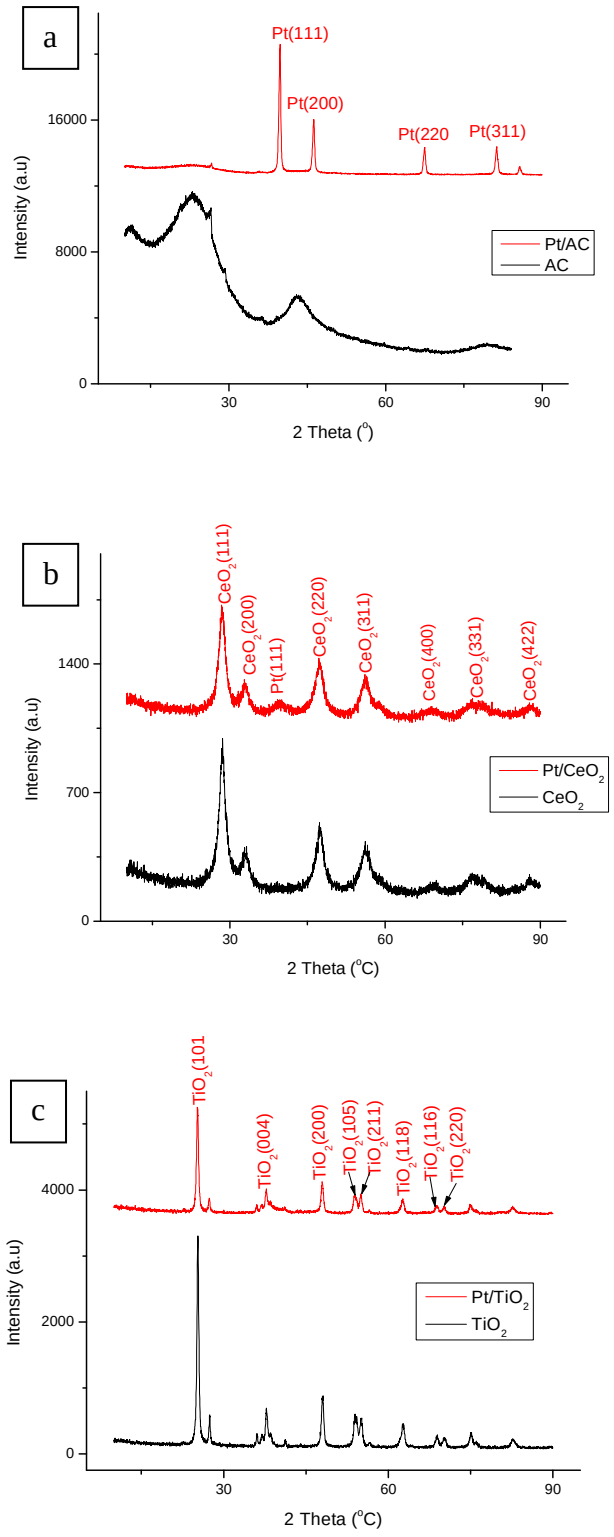

Figure 4.23. XRD patterns of (a) AC and Pt/AC, (b) CeO_2 and Pt/CeO_2 and (c) TiO_2 and Pt/TiO_2

A graphite peak is observed at around 25.5 ^{o}C in the XRD spectrum of AC (Figure 4.23a). The characteristic diffraction peaks of the face centred cubic crystalline Pt in the Pt/AC catalyst, namely (111), (200) and (220) in the region of 39^{o}, 46^{o} and 67^{o} demonstrates the presence of Pt in metallic form.[18] Ceria did not change its cubic structure in the presence of Pt. Only one peak of Pt can be observed (Figure 4.23b) at Pt(111) indicating that Pt is present in the face centred cubic crystalline in Pt/CeO_2. The XRD patterns of the Pt/TiO_2 catalyst was essentially the same as that of the TiO_2 sample (Figure 4.23c). The absence of the diffraction line of Pt for Pt/TiO_2 indicates that Pt is in a high degree of dispersion.[19]

4.6.4 Particle size from XRD

The particle sizes of 5 % Pt catalysts were calculated using the Scherrer equations. The Scherrer equation is given below:

$$L = \frac{0.9 \times \lambda}{B \times \theta}$$

where L is the average particle size, λ is the sources wavelength, B is the full width at half maximum of the peak position and θ is the angle at which the diffraction peak arises. Table 4.8 shows the particle size obtained from both TEM and XRD for the 5 % Pt loaded materials. The results of particle size from the TEM study are in agreement with what can be observed from the XRD patterns. The broad peaks on the Pt/CCNF (Figure 4.21a), indicates that the Pt particles have a small size (4.4 nm) and the narrow peaks on the Pt/AC (Figure 4.22a) indicates a big particle size (8.2 nm)

Table 4.8: Summary table of the mean particle size of catalyst with different Pt loading.

Catalyst	**Mean particle size (nm) for 5 % Pt loaded on supports**	
	TEM	**XRD**
Pt/CCNF	3.8	4.1
Pt/CNT	4.3	4.5
Pt/CS	4.6	4.9
Pt/AC	6.9	8.2
Pt/CeO_2	5.0	5.3
Pt/TiO_2	3.3	-

Error bar= 1 %

4.7 Ceria supported on carbon materials

A Pt-CeO_2/CM catalyst was made in two steps. The first step entailed depositing ceria on to carbon materials and the second step was the addition of Pt to CeO_2/CM. The synthesis method involves the reduction of cerium nitrate using ethylene glycol as a solvent and reducing agent, while sodium acetate was used as the stabilizing agent. Ceria particles were deposited on the CM with loadings of 5 % and 10 %. The TEM images for the CeO_2/CM are shown in Figure 4.24. Ceria particles are well distributed on the CCNF, CS and CNT surfaces as shown in Figure 4.24. This indicates that the polyol method of synthesis is quite good for ceria deposition. The average particle size of ceria particles on CeO_2/CCNF is 4.8 nm, CeO_2/CNT is 5.3 nm and CeO_2/CS is 5.5 nm.

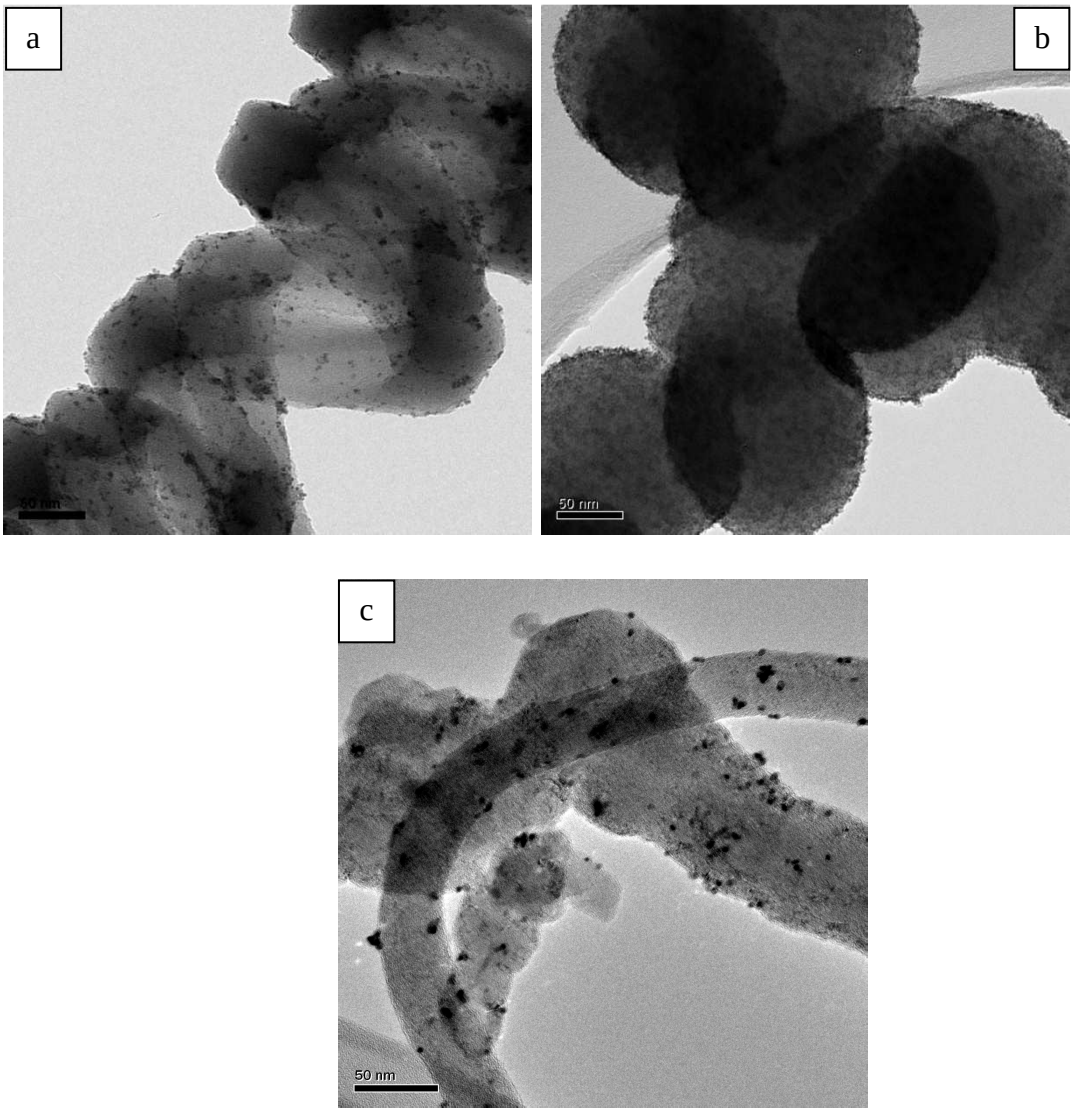

Figure 4.24. TEM images of (a) CeO_2/CCNF, (b) CeO_2/CS and (c) CeO_2/CNT

The percentage of ceria loaded on to the carbon materials was confirmed by TGA. Figure 4.25 shows the TGA profiles of CCNFs loaded with 5 % and 10 % ceria. The residual amounts of ceria were 5.2 % and 10.3 % respectively. The loading of ceria on the CNTs and CSs are presented in Table 4.9. The loading of ceria was successfully determined and the values are very close to the expected loadings.

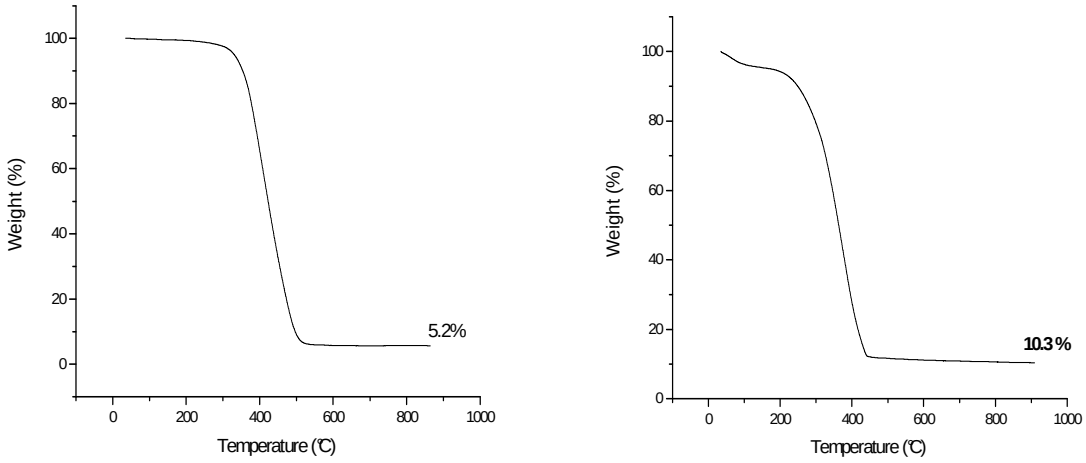

Figure 4.25. TGA profile of 5 % and 10 % loading of ceria on CCNF.

Table 4.9: Ceria loading obtained using TGA

Material	Residual amount of ceria (%)	
	Theoretical	**Experimental**
CeO_2/CS	5.0	5.1
	10.0	10.2
CeO_2/CNT	5.0	5.0
	10.0	10.1

4.7.1 XRD profile of ceria supported on carbon materials

The XRD technique was used to confirm the presence of ceria in the carbon materials and also to check if it retained the fluorite structure. The peaks in the region 28.5^o (111), 32.9^o (200) and 56.3^o (311) can be indexed for CeO_2 with a fluorite structure.[18] Figure 4.26 shows the XRD patterns of ceria and ceria supported on carbon materials. It can be clearly seen that there is no shift in any of the diffraction peaks of ceria at all compositions indicating that

carbon materials have no effect on the crystallographic orientations of ceria particles. Because of the nature of CCNFs, the peaks of ceria are not well pronounced. In conclusion, ceria was successful deposited on the carbon materials and it was in its fluorite structure.

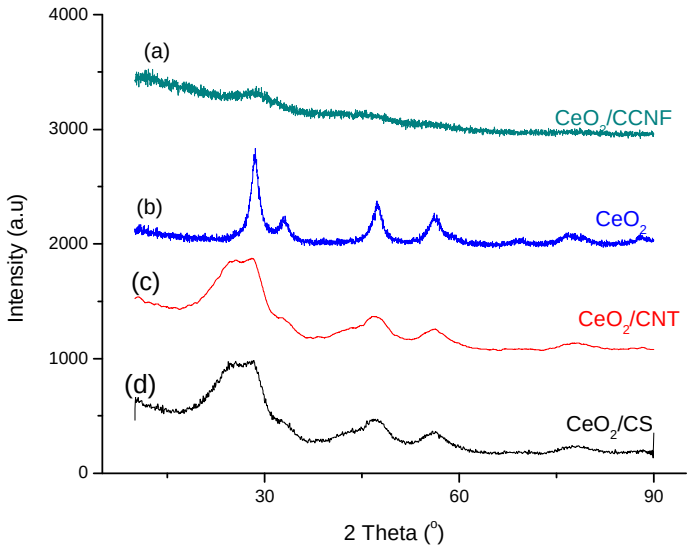

Figure 4.26. XRD patterns of (a) CeO_2/CCNF, (b) CeO_2, (c) CeO_2/CNT and (d) CeO_2/CS

4.7.2 Platinum deposited onto CeO_2/CM

Platinum (0.5 %) was deposited onto the CeO_2/CM using the polyol method. The platinum precursor (H_2PtCl_6) was reduced with ethylene glycol at temperatures of 160 ^oC and the Pt nanoparticles formed were deposited onto the support (CeO_2/CM). TEM analysis was used to determine the morphology of Pt-CeO_2/CM catalyst formed. Figure 4.27 shows the TEM images of the 0.5% Pt-CeO_2/CM catalysts.

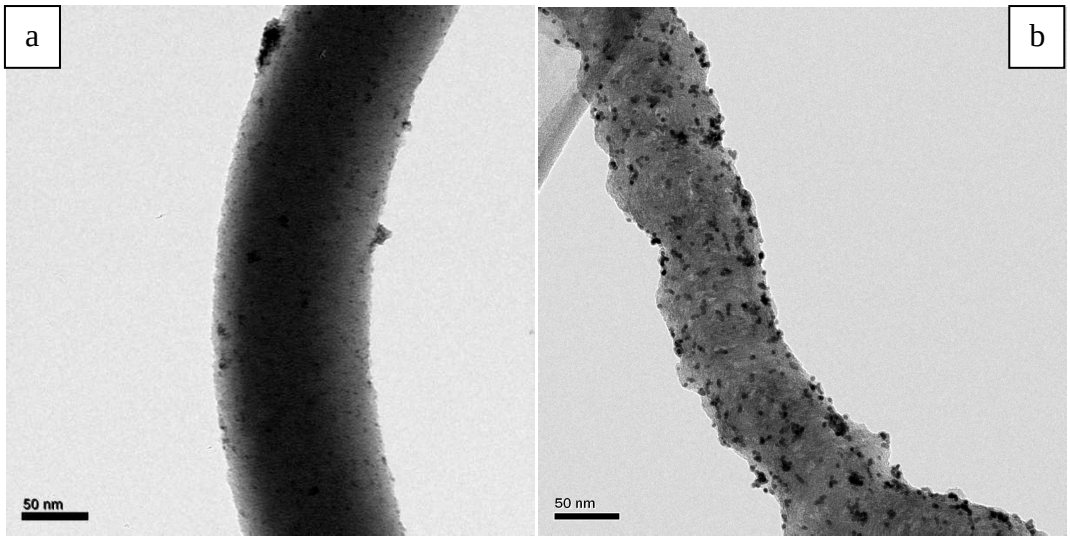

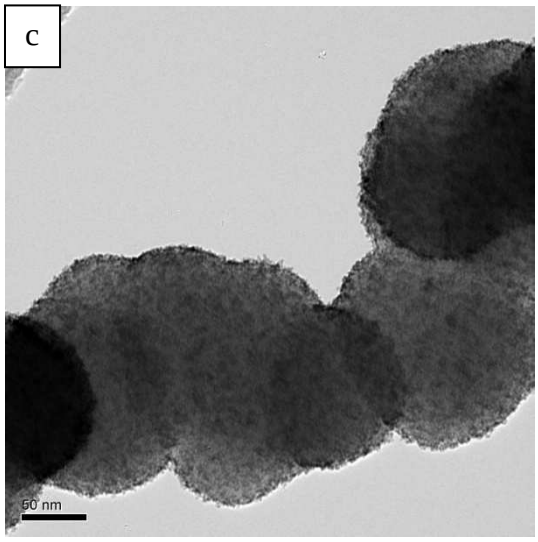

Figure 4.27. TEM images of (a) Pt-CeO_2/CCNF (b) Pt-CeO_2/CNT and (c) Pt-CeO_2/CS

It can clearly be seen from Figure 4.26 that ceria is well distributed across the entire surface of CCNFs, CNTs and CSs though it is difficult to locate the Pt nanoparticles. EDS was used to show that Pt was present in the catalysts. Figure 4.28 shows the EDS spectrum of Pt/CCNF

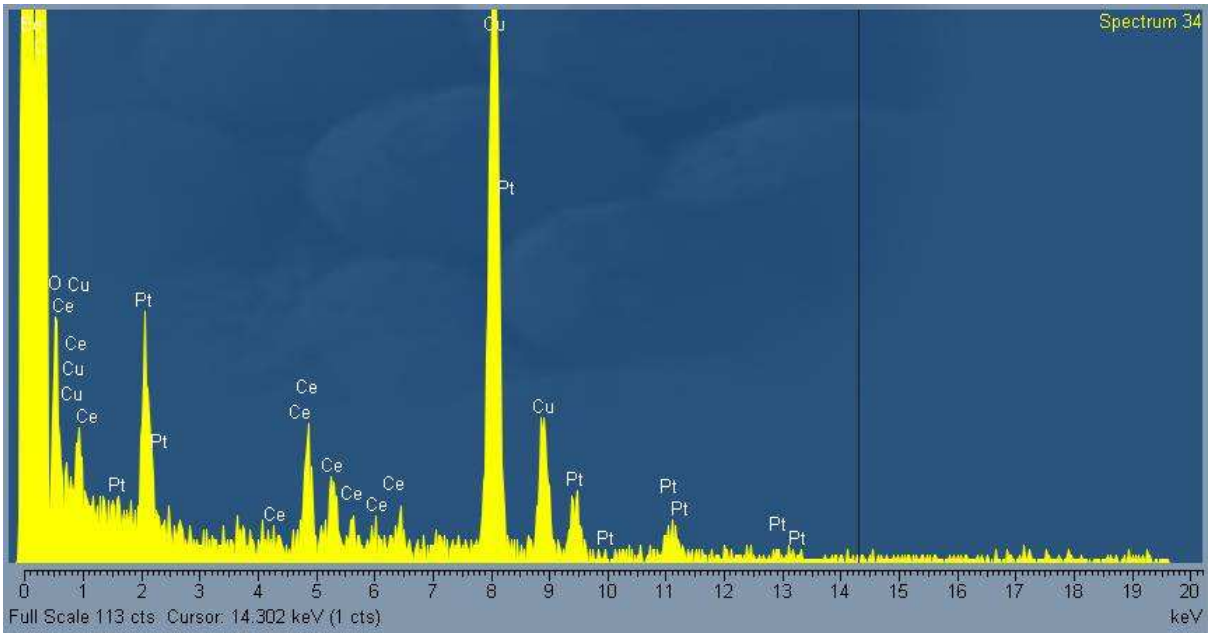

Figure 4.28. EDS spectra of Pt-CeO_2/CCNF

The copper that is observed in the spectrum is due to the copper grid. Pt quantification was achieved by ICP AES. The results are shown in Table 4.10.

Table 4.10: Pt loading in the catalysts

Catalyst	Pt loading (%)[a]
Pt- CeO_2/CCNF	0.50
Pt- CeO_2/CNT	0.50
Pt- CeO_2/CS	0.51

[a] theoretical= 0.5 % Pt

4.8 Catalytic activity

The hydrogenation of ethylene over the Pt catalyst supported on carbon materials (CNTs, CCNFs, CSs and AC), oxides (TiO_2 and CeO_2) and CeO_2/CM was performed at 30 ^oC. The hydrogenation activity was first tested on the supports to check the inertness of the supports. The results of the experiments showed that all the supports showed no activity for the hydrogenation of ethylene.

4.8.1 Effect of functionalization

The activity of the as-synthesized CCNF and the functionalized CCNF loaded with 1 % Pt was tested for the hydrogenation of ethylene and the results are presented on Figure 4.29. The functionalized CCNF gave a 100 % conversion indicating that all the ethylene was converted to ethane while the conversion (67 %) of the as-synthesized CCNF decreased with time on stream as shown in Figure 4.29a. Characterization of the spent catalyst by TEM revealed that the as-synthesized CCNFs sintered rapidly. Figure 4.30a show the TEM image of the spent catalyst (Pt supported on as-synthesized CCNF). There is evidence of Pt agglomerates which are located at the curves of the CCNFs.

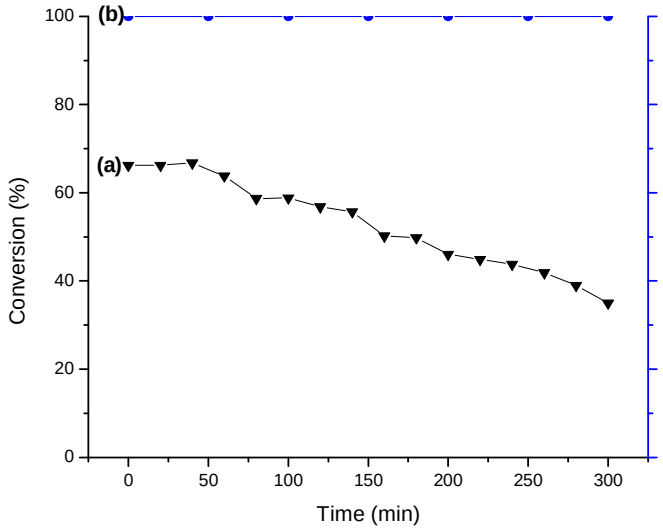

Figure 4.29. Ethylene conversion over Pt supported on (a) as-synthesized CCNFs and (b) functionalized CCNFs at 30 ^{o}C. [H_2/C_2H_4 = 2; flow rate = 100 mL/min; catalyst mass = 0.1 g]

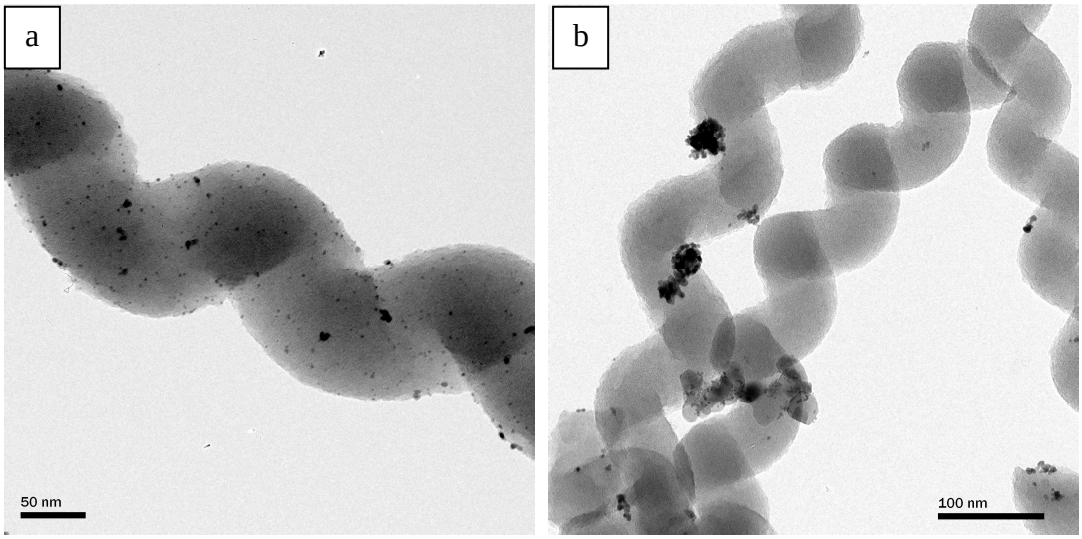

Figure 4.30a. TEM images of the Pt/as-synthesized CCNFs (a) before and (b) after hydrogenation of ethylene

The possible explanation for the rapid sintering of the Pt on the as-synthesized CCNFs relates to the lack of strong anchoring of the Pt on the as-synthesized CCNFs. As a result the Pt nanoparticles move freely and then aggregate. The view about no strong anchoring is supported by reports from Yang et al[20], who indicated that the as-synthesized CNTs do not possess a large quantity of functional groups on their surface. There was no observable TEM change on the size of the Pt particles on the spent catalyst of Pt/functionalized CCNFs (Figure 4.30b).

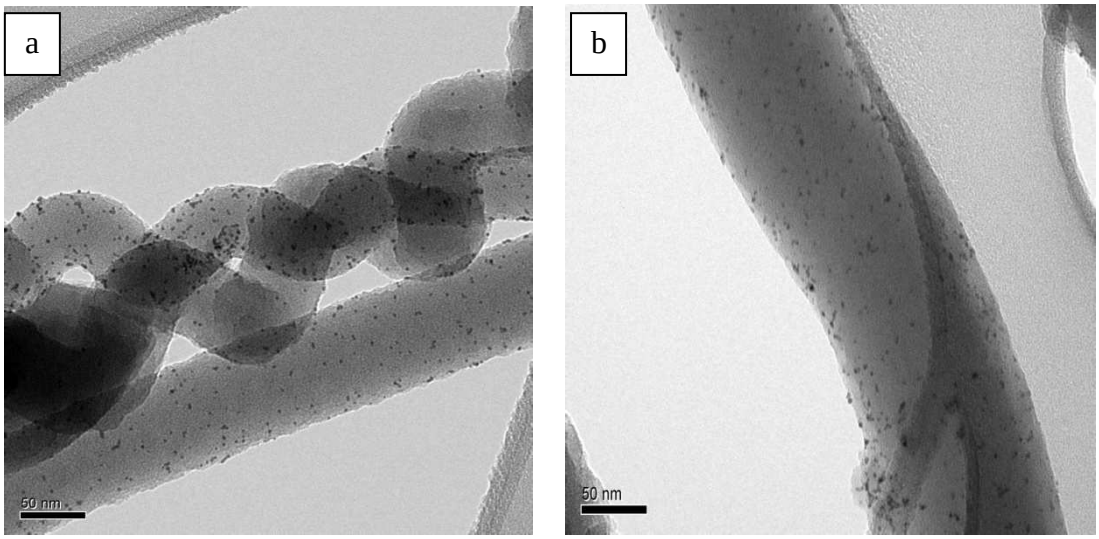

Figure 4.30b. TEM images of (a) before and (b) after hydrogenation of ethylene using Pt/functionalized CCNF

The initial and final activity of Pt supported on the as-synthesized CNT and CS is shown on the Table 4.11.

Table 4.11: Conversion rates of the 1 % Pt supported for the as-synthesized and functionalized CNTs and CSs in 300 mins

Catalyst	**Conversion (%)**	
	Initial	**Final**
Pt on as-synthesized CNT	22	0
Pt on functionalized CNT	100	100
Pt on as-synthesized CS	31	0
Pt on functionalized CS	100	100

The low initial activity for both Pt supported on as-synthesized CNTs and CSs is attributed to poor deposition of Pt during synthesis (see Figure 4.13). This was caused by lack of anchoring sites on the surface of CNTs and CSs. The conversion decreased to zero in 300 mins due to sintering. When there is no strong anchoring of Pt nanoparticles, they easily move and agglomerate. The decrease in conversion can also be due to metal leaching. In conclusion functionalization of carbon materials is crucial as it leads to strong anchoring of the active Pt phase.

4.8.2 Effect of metal loading

A series of Pt/CCNF catalysts were prepared with different Pt loadings (0.5, 1, 5 %). Figure 4.31 shows the ethylene conversion as a function of time for the Pt/CCNF catalysts. The 5 % Pt loaded catalyst showed 100 % conversion for the entire catalytic reaction. The 1 % loaded Pt catalyst gave a 100 % conversion for 3500 mins and then it began to decrease. The activity of 0.5 % Pt/CCNF catalyst was the lowest with a 80 % initial conversion. Generally the higher the loading implies more catalyst particles to interact with the reactants and thus the 5 % Pt loaded material has the highest activity as compared to the 1 % and 0.5 % Pt loaded CCNFs. The deactivation of the reaction as time increased might be due to coke deposition or sintering. The smaller the particles (0.5 % Pt) the more easily they can be covered with the coke.

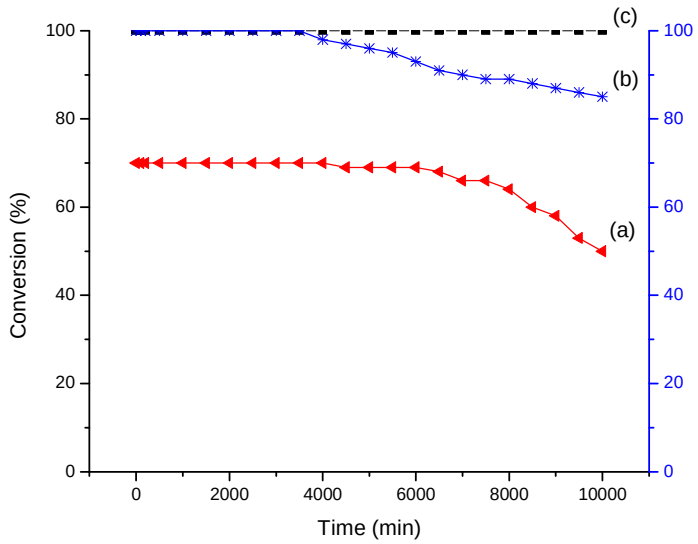

Figure 4.31. Effect of Pt loading on the conversion of ethylene, (a) 0.5 %, (b) 1 %, (c) 5 % [H_2/C_2H_4 = 2; flow rate = 100 mL/min; catalyst mass = 0.1 g]

The same trend was observed with Pt/CNT and Pt/CS catalysts; increasing Pt loading resulted in an increase in the rate of hydrogenation. Table 4.12 shows the conversion of ethylene to ethane using different Pt/CNT and Pt/CS catalysts. In both catalysts, the 5 % Pt loading remain unaltered for the duration of the experiment. The decrease in metal loading resulted in decrease in the activity this was attributed to a small amount of Pt particles that get in contact with the reactants.

Table 4.12: Conversion of ethylene using different loadings of Pt on CNTs and CSs

Catalyst	Pt loading (%)	Conversion (%)	
		Initial	Final
Pt/CNT	5	100	100
	1	100	81
	0.5	68	50
Pt/CS	5	100	100
	1	100	78
	0.5	65	43

4.8.3 Effects of increasing the ratio of H_2:C_2H_4

The ratio of H_2 to C_2H_4 was increased to 5:1 and the results are shown in Table 4.13.

Table 4.13: Effect of increasing flow rate of H_2:C_2H_4. ($H_2/C_2H_4 = 5$)

Conversion (%)		
0.5 % Pt/CCNF	**0.5 % Pt/CNT**	**0.5 % Pt/CS**
100	100	100

Increasing the flow of hydrogen caused an increase in the stability of the reaction. (Figure 4.30, and Table 4.13). This was explained by Neurock and Mei[21], who reported that when the partial pressure of hydrogen is greater than that of ethylene, the rate of decomposition of ethylene is slower than ethylene hydrogenation. This leads to a very slow rate of formation of ethylidyne and CH_x intermediates which hinders the hydrogenation of ethylene and therefore the stability of the reaction.

4.9 Effect of catalyst supports

A range of supports (Pt/CCNF, Pt/CNT, Pt/CS, Pt/AC, Pt/CeO_2 and Pt/TiO_2) were used for the hydrogenation of ethylene. The results of the experiment are depicted in Figure 4.32.

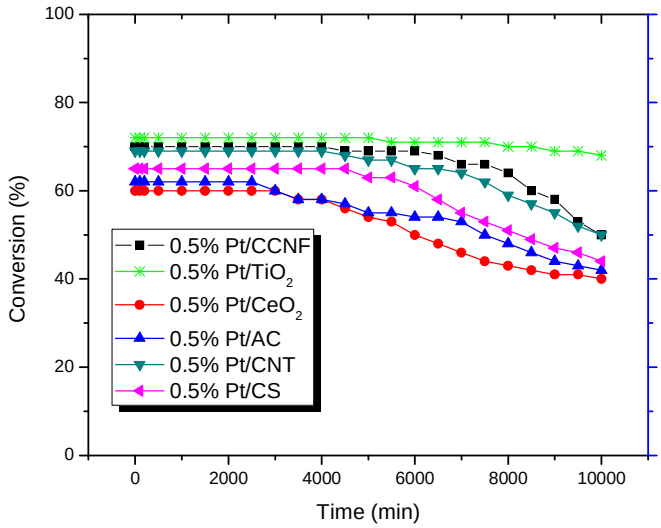

Figure 4.32. Effects of the supports on the conversion of ethylene. [H_2/C_2H_4 = 2; Flow rate = 100 mL/min; Catalyst mass = 0.1 g]

It can be observed from Figure 4.32 that titania was the best support. Pt/TiO_2 had an initial activity of 72 % whilst Pt/CCNF (70 %), Pt/CNT (68 %), Pt/CS (65 %), Pt/AC (62 %), Pt/CeO_2 (60 %). These activities are good considering that only 0.5 % loading of Pt is being used. Another interesting feature that can be obtained from Figure 4.32, is that it takes a lot of time for the catalyst to start to deactivate. Deactivation starts at ca. 3000 mins for Pt/CeO_2 and Pt/AC whilst Pt/CCNF, Pt/CNT and Pt/CS extend up to ca. 4000 mins. The high activity of Pt/TiO_2 can be attributed to the small particle sizes of Pt formed on its surface (Table 4.4) and also the high dispersion noted from the XRD data. Amongst the carbon materials, the CCNFs was the best support. This can be explained in terms of the size of Pt nanoparticles. The small particle size of Pt leads to an enhancement of its catalytic properties[22] as large fractions of the active metal atoms are on the surface and thus are accessible to reactant molecules and available for catalysis.[23] The Pt supported on carbon materials (CCNFs, CNTs, CSs) had a higher rate of reaction than ceria and AC because they possess mesopores which are suitable for catalytic reactions. The relatively lower activity of Pt/AC can be attributed to the existence of micropores. Bitter,[24] reported that microporosity hampers fast diffusion of reactants and products to and from active sites making these less productive. The stability of the Pt supported catalysts can be attributed to strong anchoring of the Pt nanoparticles on the different supports. In other words the method of depositing Pt on the support (polyol method) was effective in ensuring that Pt is firmly held on the support. The deactivation which

occurred may be a result of sintering as well as the formation of carbon deposits which in turn block the active sites of Pt.

4.9.1 Effect of adding ceria on the Pt/CM catalyst

Ceria (5 %) was added to the Pt/CM to make Pt-CeO_2/CM. This was done in order to improve the surface area of the active phase. When the surface area of the active phase increases, the rate of reaction will also increase. The results for the hydrogenation of ethylene using Pt-CeO_2/CM catalyst are presented in Figure 4.33. The addition of 5 % ceria onto Pt/CM caused an increase in the rate of reaction. Figure 4.33 shows that when ceria is added to the CCNFs it gives a have higher activity that when ceria is absent. This was due to a ceria effect.

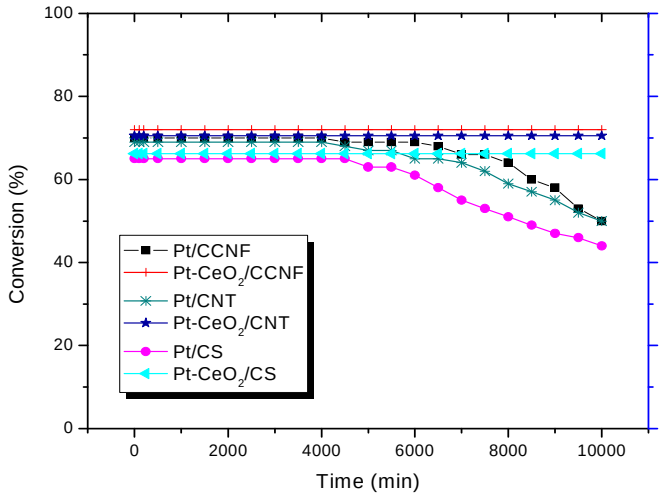

Figure 4.33. Effect of adding ceria to the Pt/CM catalyst. [H_2/C_2H_4 = 2; flow rate = 100 mL/min; catalyst mass = 0.1 g]

The catalysts were stable for the entire hydrogenation reaction. The stability of the ceria based catalyst was also attributed to the fact that ceria suppresses the sintering of the active metal[25] and also preserves the catalyst surface area[26]. The catalyst surface area of the 0.5 % Pt-CeO_2/CCNF and the BET surface area (Table 4.4) did not change on the spent catalyst. The proposed mechanism of suppressed sintering of Pt particles is shown in Figure 4.34. The ceria particles are thought to be situated between the Pt nanoparticles. It is therefore difficult for the Pt nanoparticles to agglomerate. The TEM image in Figure 4.35 shows the 0.5 % Pt-CeO_2/CCNF catalyst in which Pt is situated between the ceria particles. Figure 4.35 shows that both ceria and Pt particles are on the surface of CCNF.

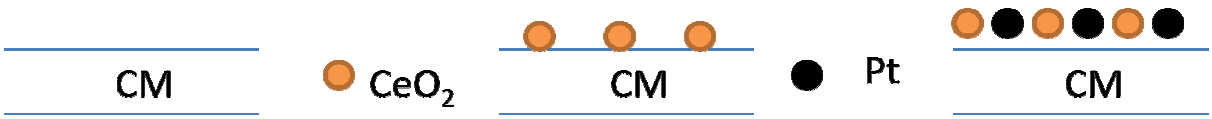

Figure 4.34. Cartoon showing a possible mechanism for suppression of Pt sintering. (CM stands for the carbon materials, CeO_2 represent ceria particles and Pt represents platinum particles)

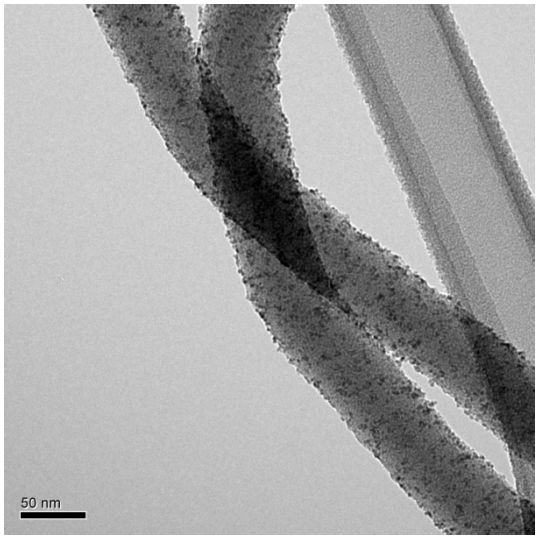

Figure 4.35. TEM image of Pt-CeO_2/CCNF

4.9.2 Effect of temperature

Figure 4.36 displays the effect of temperature on the activity of a 0.5 % Pt/CCNF catalyst. The temperature increase caused a small increase in the initial rate of reaction. A reaction temperature of 30 ^oC for the hydrogenation of ethylene over Pt/CCNF catalyst gave results indicative of a moderately stable catalyst. The final rate of reaction at a temperature of 100 ^oC was low, presumably due to a sintering effect which is more pronounced at high temperatures. Mondal reported the same results for a Pd/CNT catalyst used in the hydrogenation of ethylene. The decrease in activity was due to sintering and loss of Pd surface area which resulted in formation of larger Pd particles.[26] TEM analysis was used to characterize the spent Pt/CCNF catalyst (reaction temperature: 100 ^oC). Figure 4.37 shows the TEM image of the spent catalyst. It was observed that the particles have increased in size. Only the results for Pt/CCNF catalyst are shown in this study. In future work the Pt/CNT and Pt/CS will be investigated. CNTs[27] and CSs[28] have been studied as catalyst supports by Mondal et al using Pd.

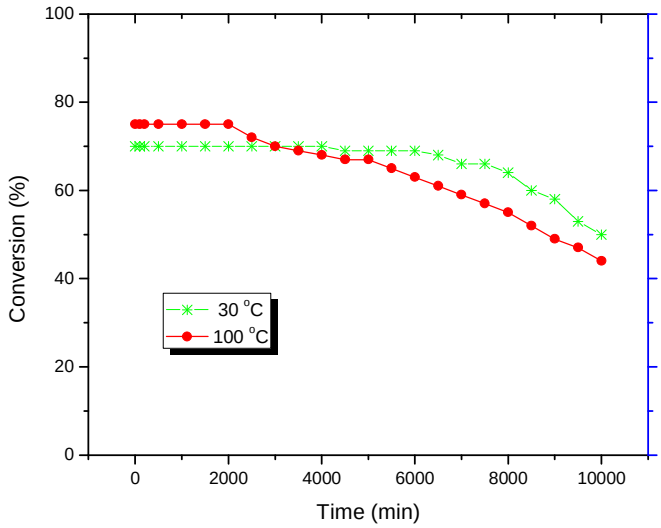

Figure 4.36. Effect of temperature on ethylene conversion over 0.5 % Pt/CCNF. [H_2/C_2H_4 = 2; flow rate = 100 mL/min; catalyst mass = 0.1 g]

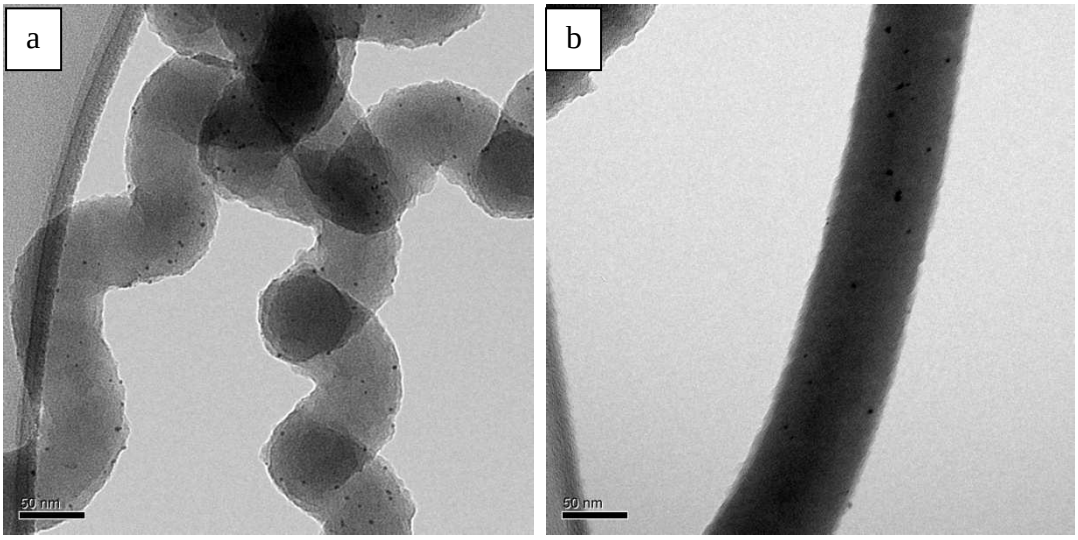

Figure 4.37. TEM image of (a) before and (b) after hydrogenation of ethylene

4.9.3 Effect of ceria loading

Figure 4.38 shows the effect of different ceria loadings on the hydrogenation activity for Pt supported on CCNFs. An increase in ceria loading did not result in an increased rate of reaction. The 1 % Pt-10 % CeO_2/CCNF catalyst showed ca. 70 % conversion of ethylene up to 3030 minutes and then the activity began to decrease. This might be due to Pt particles interacting with CeO_2 and not the CCNFs. If the Pt nanoparticles are on the surface of ceria it may be easy for them to agglomerate as they are free to move. The TEM image shown in

Figure 4.39 indicates the well distributed ceria particles on the CCNFs and Pt on the surface of ceria.

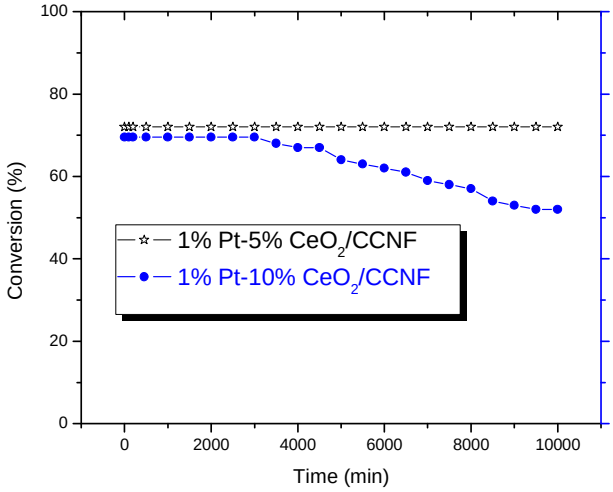

Figure 4.38. Effect of ceria loading. . [H_2/C_2H_4 = 2; flow rate = 100 mL/min; catalyst mass = 0.1 g]

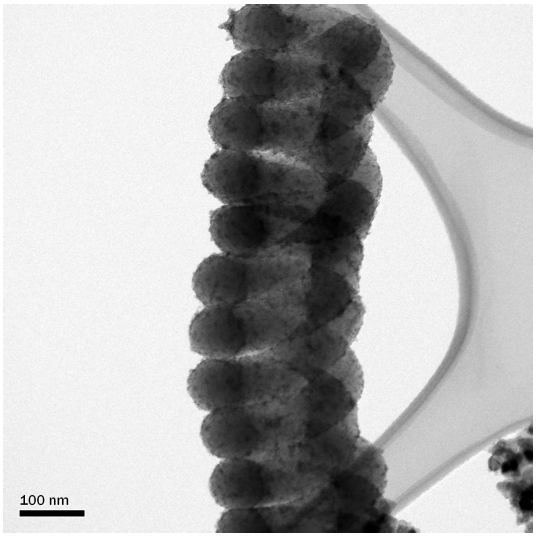

Figure 4.39. TEM image of 1 % Pt-10 % CeO_2/CCNF

In conclusion, functionalization of carbon materials is an important methodology used to improve the anchoring of Pt nanoparticles. The polyol method was very effective in depositing Pt on to the support materials as the Pt nanoparticles formed were well dispersed with a narrow size distribution. The effects of the catalyst supports were studied using the hydrogenation of ethylene as a test reaction. The addition of ceria to Pt/CM catalyst proved to be effective in enhancing of stability and activity of the hydrogenation reaction.

References

1. T. G. Ros, A. J. van Dillen, J. W. Geus, D. C. Koningsberger, J. Eur. Chem. 8 (2002) 1151-1162
2. P. Serp, J. Fugueiredo, Carbon Materials for Catalysis, Wiley, USA, (2009) 132-538
3. A.R. Harutyunyan, B.K. Pradhan, J. Chang, G. Chen, P.C. Eklund, J. Phys. Chem. B 106 (2002) 8671-8675
4. S. Z. Mortazavi, A. J. Novinrooz, A. Reyhani, S. Mirershadi, Cent. Eur. J. Phy. 8 (2010) 940-946
5. S. L. Knupp, W. Li, O. Paschos, T. M. Murray, J. Snyder, P. Haldar, Carbon 46 (2008) 1276-1284
6. J. Wei, J. Ding, X. Zhang, D. Wu, Z. Wang, J. Luo, K. Wang, Mater. Lett. 59 (2005) 322– 325
7. G. Leofanti, M. Padovan, G. Tozzola, B. Venturelli, Catalysis Today 41 (1998) 207-219
8. A. Nieto-Marquez, S. Gil, A. Romero, J. Valverde, S. Gomez-Quero, M. Keane, Appl. Catal. A: General 363 (2009) 188-198
9. S. Monyanon, S. Pongstabodee, A. Luengnaruemitchai, J. Pow. Sour. 163 (2006) 547-554
10. A. C. Mak, C. Yu, J. C. Yu, Z. Zhang, C. Ho, Nano Res. 1 (2008) 474 482
11. X. Li, W. Chen, J. Zhao, W. Xing, Z. Xu, Carbon 43 (2005) 2168–2174
12. Y. Luo, X. Sun, Mater. Lett. 61 (2007) 2015–2017
13. J, Zhao, P. Wang, W. Chen, R. Liu, X. Li, Q. Nie, J. Pow. Sour. 160 (2006) 563-569
14. A. Plomp, T. Schubert, U. Storr, K. P. de Jong, J. H. Bitter, Top Catal. 52 (2009) 424–430
15. F. Rodríguez-Reinoso, Carbon 36 (1998) 159-175
16. Y. Zhang, Z. Wang, J. Zhou, J. Liu, K. Cen, Inte. J. Hydrogen Energy 33 (2008) 602 – 607
17. W. Zhang, J. Chen, G. F. Swiegers, Z. Ma, G. G. Wallace, Nanoscale 2 (2010) 282-286
18. J. Zhao, W. Chen, Y. Zheng, Mater. Chem. Phys. 113 (2009) 591-595
19. C. Zhang, H. He, K. Tanaka, Appl. Catal. B 65 (2006) 37–43
20. S. H. Yang, W. H. Shin, J. W. Lee, S. Y. Kim, S. I. Woo, J. Kang, J. Phys. Chem. B 110 (2005) 13941-13946

21. M. Neurock, D. Mei, Topics in Catalysis, 20 (2002) 5-23
22. C. B. Hwang, Y. S. Fu, Y. L. Lu, S. W. Jang, P. T. Chou, C. R. Wang, S. J. Yu, J. Catal. 195 (2000) 336-341
23. C. W. Chen, T. Serizawa, M. Akashi, Chem. Mater. 11 (1999) 1381-1389
24. J. H. Bitter, J. Mater. Chem. 20 (2010) 7312–7321
25. http://openlearn.open.ac.uk/mod/oucontent/view.php?id=398548&section=1.4.6 (accessed 4 February 2011)
26. G. Rao, B. G. Mishra, Bull. Catal. Soc. India 2 (2003) 122-134
27. http://152.106.6.200:8080/dspace/bitstream/10210/2536/11/Chapter%209%20-%20CNTs%20in%20Catalysis.pdf (accessed 4 February 2011)
28. K. C. Mondal, L. M. Cele, M. J. Witcomb, N. J. Coville, Catal. Com. 9 (2008) 494-498

CHAPTER FIVE

CONCLUSIONS

5.1 Introduction

The first objective of this study was to synthesize carbon materials (CNTs, CCNFs and CSs) and ceria. The carbon materials (CM) were made by the chemical vapour deposition method (CVD) while ceria was made by the sol-gel method. The second objective was to deposit Pt on the carbon materials (including activated carbon (AC)), oxides (ceria and titania) and CeO_2-CMs. The third and last objective was to test the various Pt supported catalyst for the hydrogenation of ethylene. The characterization techniques employed in the study included the use the following: TEM, TGA, BET, Raman spectroscopy, XRD, EDS, TPR, IR spectroscopy, UV-vis spectroscopy and ICP-AES. The study was successfully conducted and the following conclusions were drawn from the results.

5.2.1 Carbon materials

The TEM images revealed that the carbon materials were successfully produced using the CVD methods. For the carbon materials, acetylene was used as the carbon source and the catalysts employed were 5 % Fe-Co/$CaCO_3$ (for CNT synthesis), 5 % Cu/TiO_2 (for CCNF synthesis) and no catalyst (for the CS synthesis).

The as-synthesized carbon materials contained some impurities. The impurities in the CCNFs were removed using hydrofluoric acid. The polyaromatic compounds in the carbon materials were removed using the Soxhlet extraction technique. Further removal of impurities was carried out during the functionalization of the carbon materials. Nitric acid was used to functionalize the carbon materials in order to introduce hydroxyl and carboxyl groups onto the carbon materials' surfaces. The success of the functionalization was confirmed by alkalimetry titration and IR spectroscopy data.

Analysis of the as-synthesized and functionalized carbon materials using Raman spectroscopy showed the presence of disorder in the materials whilst TGA showed the successful removal of impurities in the carbon materials.

5.2.2 Ceria

Ceria was successfully synthesized using the sol-gel method. The ceria synthesis was confirmed using TEM and TPR results. TEM showed the morphology of the ceria whilst TPR studies showed the temperature at which it reduces, which confirmed the ceria particles had been prepared.

5.2.3 Titania and activated carbon

Titania and activated carbon (AC) were obtained from Sigma-Aldrich and used without further purification. TEM image analysis confirmed the morphology of titania and AC.

5.3 Deposition of platinum

A microwave assisted polyol method was used to deposit Pt on to the various supports. The synthesis was successfully monitored using UV-vis spectroscopy; the disappearance of the peak at 260 nm in the spectrum indicated the formation of Pt nanoparticles. TEM images showed that the Pt nanoparticles were uniform in size and well dispersed. The presence of Pt and Ce were confirmed using EDS and metal loading was confirmed using ICP-AES (and TGA for the carbon materials). It was found that all the catalysts displayed the diffraction patterns of the Pt fcc structure. TPR was used to confirm that Pt was reduced fully as there was no peak in the profile between 177 and 302 ^{o}C, typical of Pt in a high oxidation state.

Increasing the Pt loading on a fixed surface area of a support material resulted in an increase in the particle sizes. This was due to the agglomeration of the Pt nanoparticles. BET surface area analysis showed two trends. The first was that the BET surface area increased when Pt metal was loaded on the carbon materials (CCNF, CNT and CS). The second was that the BET surface area decreased when Pt was deposited on ceria and AC.

5.4 Hydrogenation activities of the Pt supported catalysts

The effect of functionalization of the carbon materials was investigated and it was found that the functionalized carbon materials had a higher rate of reaction than the as-synthesized carbon materials. This was attributed to strong anchoring of Pt on the functionalized carbon materials.

The hydrogenation activity increased with increased Pt metal loading. This is because when the loading has been increased, there are more Pt nanoparticles that are available to react with the reactants. The other possible reason is that the large particles produced by the high metal loading are less prone to sintering than the smaller particles obtained at low metal loadings.

It was found that increasing the ratio of hydrogen to ethylene in the reactant stream resulted in an increase in the rate of reaction. This was attributed to the fact that at high hydrogen concentration, the rate of formation of carbon deposit is slow and the rate of hydrogenation is high. No carbon deposits are thus expected on the Pt catalyst particles.

Titania was the best catalyst support in terms of activity results. This was attributed to the small particle size of platinum that was obtained on the titania surface. The small particle size indicates that a large fraction of active Pt atoms are on the surface and thus accessible to reactant molecules and available for hydrogenation reactions. Amongst the carbon materials, CCNF had the highest activity. This was related to the Pt particle sizes which were slightly smaller than found on the other carbon materials. Pt/AC had the least activity. This could be related to the presence of micropores, which limit the rate of diffusion of reactants to and from the active phase.

The addition of ceria onto Pt/CM caused an increase in the rate of the ethylene hydrogenation reaction. The ethylene conversions of ceria based catalysts were higher than the Pt/CM catalysts. This was attributed to the role that was played by ceria of preserving the surface area of Pt as well as suppressing the sintering of Pt nanoparticles. However, when the CeO_2 content was too high (10 %) the hydrogenation activity decreased.

It was found that temperature increased the rate of reaction but at high temperatures, the activity continually decreased. This again relates to sintering effects that are enhanced at high temperature.

5.5 Recommendations for future work

Since the Pt-CeO_2/CM catalyst was effective for the hydrogenation of ethylene, it will be good to test it for higher alkenes such as propene so that we can gain more information about the enhancement of catalytic activity brought about by ceria.

Platinum is a good oxidation catalyst. It can catalyse the oxidation of CO to CO_2. A high CO conversion occurs at high temperatures. So for the future work, it will be fascinating to work with Pt-CeO_2/CM catalysts in the carbon monoxide oxidation reaction and establish whether temperature can be lowered and still maintain a high activity for oxidation reactions.

Replacing Pt with other platinum group metals (Pd, Ru, Rh and Os) in Pt-CeO_2/CM. The aim of the project will be to find out if ceria can maintain the enhancement of catalytic activity as well as to compare the different catalysts in the hydrogenation of ethylene.